6-24-2019

Character and Genesis of Indium Mineralization, East Kemptville, Nova Scotia

Jason Willson
University of Windsor

Character and Genesis of Indium Mineralization, East Kemptville, Nova Scotia

By

Jason Willson

A Thesis

Submitted to the Faculty of Graduate Studies
through the School of the Environment
in Partial Fulfillment of the Requirements for
the Degree of Master of Science
at the University of Windsor

Windsor, Ontario, Canada

2019

Character and Genesis of Indium Mineralization, East Kemptville, Nova Scotia

by

Jason Willson

APPROVED BY:

_____

C. Macdonald
Department of Chemistry and Biochemistry

_____

J. Gagnon
School of the Environment

_____

I. Samson, Advisor
School of the Environment

June 24, 2019

Declaration of Originality

I hereby certify that I am the sole author of this thesis and that no part of this thesis has been published or submitted for publication.

I certify that, to the best of my knowledge, my thesis does not infringe upon anyone's copyright nor violate any proprietary rights and that any ideas, techniques, quotations, or any other material from the work of other people included in my thesis, published or otherwise, are fully acknowledged in accordance with the standard referencing practices. Furthermore, to the extent that I have included copyrighted material that surpasses the bounds of fair dealing within the meaning of the Canada Copyright Act, I certify that I have obtained a written permission from the copyright owner(s) to include such material(s) in my thesis and have included copies of such copyright clearances to my appendix.

I declare that this is a true copy of my thesis, including any final revisions, as approved by my thesis committee and the Graduate Studies office, and that this thesis has not been submitted for a higher degree to any other University or Institution.

Abstract

The East Kemptville deposit is a Sn-polymetallic greisen deposit that is a known host of indium mineralization, an important element in high-technology applications. Indium mineralization occurs primarily as a minor or trace element in sulfide minerals, with sphalerite and chalcopyrite being the most abundant of these. These indium-bearing sulfides are associated with greisen and quartz-sulfide vein mineralization in the Main and Baby zones. It has been previously proposed that these two different mineralization styles are related to different paragenetic events, with the quartz-sulfide vein mineralization being further subdivided into two broad temporal events. Mineral textures and mineral chemistry of indium-bearing sulfides indicate that the concentrations of indium are similar between the two main mineralization styles and the two ore zones. The compositional similarity among indium-bearing sulfides and lack of any temporal or spatial differences in the composition of the sulfide minerals, indicates that the fluids responsible for indium enrichment formed from a common fluid source and under relatively constant physicochemical conditions. Mineral geothermometry indicates a temperature range of 230 to 275 °C for sphalerite-stannite mineralization. Sulfur isotope data from secondary ion mass spectroscopy ($\delta^{34}S$ = 2.1-7.9 ‰; spatial resolution of 5-15 μm) represent a larger range of values compared to mineral separates (δ34S = 4.9-7.0 ‰) and suggest that a magmatic fluid interacted with the surrounding metasedimentary country rocks. Differences in gangue mineralogy reflect the nature of the local wallrocks, which indicates that the mineralizing fluids equilibrated with the wallrocks and that the system was partially rock buffered. In addition to the indium-bearing mineralization, East Kemptville also contains a late indium-poor breccia. The characteristics of indium mineralization at the nearby Duck Pond deposit are similar to those of East Kemptville, suggesting a similar genesis.

Acknowledgements

I would like to acknowledge everyone who provided the help and support I needed to complete this thesis. First and foremost, I would like to thank my supervisor Dr. Iain Samson for providing the opportunity and guidance in this thesis. I would also like to thank Dr. Dan Kontak from Laurentian University for providing his insight about the East Kemptville deposit and his helpful suggestions. Special thanks go to Bill Mercer and Avalon Advanced Materials for their in-kind contributions, assistance with field work, and logistical support. I would also like to thank Dr. Joel Gagnon of the University of Windsor for all his scientific advice regarding laser ablation inductively coupled mass spectrometry. Thanks also goes to Dr. Graham Layne of Memorial University for his services and technical advice regarding the sulfur isotope analyses. I acknowledge the staff at the University of Windsor and in particular Melissa Price, for all their gracious help and support. Thanks, is given to all my fellow colleagues that have assisted me along the way. Lastly, thanks to everyone who provided the much-needed encouragement during my time at the University of Windsor.

Table of Contents

List of Tables

List of Figures

List of Electronic Appendices

Appendix A: Major- and minor-element composition (EPMA) of select oxide and sulfide minerals from the East Kemptville and Duck Pond deposits.

Appendix B: Major- and minor-element composition (EDS) of select oxide and sulfide minerals from the East Kemptville and Duck Pond deposits.

Appendix C: Minor- and trace-element composition (LA-ICP-MS) of select oxide and sulfide minerals from the East Kemptville and Duck Pond deposits.

Appendix D: Sulfur isotope composition (EA-IRMS) of sulfide mineral separates from the East Kemptville and Duck Pond deposits.

Appendix E: In situ sulfur isotope composition (SIMS) of sulfide minerals from the East Kemptville and Duck Pond deposits.

List of Abbreviations

DLC = Davis Lake Complex

BSE = Backscattered electron image

BDL = Below detection limit

EA-IR-MS = Element analyzer coupled isotope-ratio mass spectroscopy

EKEDFZ = East Kemptville-East Dalhousie Fault Zone

EKLG = East Kemptville leucogranite

EPMA = electron probe microanalysis

LA-ICP-MS = laser ablation inductively-coupled plasma mass spectroscopy

LILE = large-ion lithophile elements

REE = rare-earth elements

SEM-EDS = scanning electron microscopy-energy dispersive spectroscopy

SIMS = secondary ion mass spectrometry

SMB = South Mountain Batholith

V-CDT - Vienna Canyon Diablo Troilite

Chapter 1

Introduction

The reasons for the enrichment of indium in hydrothermal mineral deposits are currently not well understood, such that these deposits have become a recent focus of research, largely as a result of the increased use of indium in a number of high-technology applications (e.g. photovoltaics, liquid crystal displays, and semiconductors). Indium has been primary recovered as a byproduct from base-metal sulfide deposits, such as the Kidd Creek volcanogenic massive sulfide deposit, which produced 50 t of indium annually (Schartz-Schampera, 2014). Large indium resources also occur in Sn-polymetallic deposits, which include greisen-type, Sn-polymetallic vein, Sn-W porphyry, epithermal, stratabound, and skarn deposits. An example in eastern Canada is the Mount Pleasant Sn-W-Mo-Bi-In deposit, in New Brunswick, with an estimated 1246 t of contained indium (Werner et al., 2017).

The most common indium-rich minerals in Sn-polymetallic deposits are roquesite ($CuInS_2$) and sakuraiite $(Cu,Zn,Fe)_3(In,Sn)S_4$), although these have only been observed in trace quantities. In all hydrothermal deposit types, indium most often occurs as a trace or minor element in sulfide minerals, the most important being sphalerite, chalcopyrite, and stannite (in order of decreasing economic importance; Sinclair, 2014). Lesser amounts of indium can also occur in cassiterite (Pavola et al., 2015). The concentration of indium in sulfide minerals can be highly variable in a given mineral deposit. For example, Murakami & Ishihara (2012) reported indium concentrations between 0.00 and 9.65 wt.% in sphalerite from the Potosi Sn-Cu deposit, Bolivia, and Sinclair et al. (2006) reported indium concentrations in sphalerite ranging from <0.01 to 6.90 wt.% for the Mount Pleasant deposit, Canada. In these studies, the authors did not provide any insights into the cause of this variation. In other Sn-polymetallic deposits (e.g. Toyoha, Pingüino, Hämmerlein; Ohta, 1991; Lopez et al., 2014; Bauer et al., 2017) temporal variations in indium enrichment have been observed. This indicates that a further understanding of temporal variations and physicochemical conditions in these systems is crucial for understanding indium enrichment.

The fluids responsible for Sn-polymetallic mineralization have been characterized as magmatically derived fluids with a component of externally derived fluids (Bodnar et al., 2014). Unfortunately, the relative roles of magmatic and external fluids in indium enrichment have not yet been constrained. At Mount Pleasant, Sinclair et al. (2006) suggested that the indium-mineralizing fluids were magmatic and that the deposition was due to cooling and dilution by meteoric waters. However, targeted studies that examined fluid chemistry and the isotopic character of indium-enriched and -devoid stages in these deposits are still required. The most direct method is to analyze the fluid directly (i.e., fluid inclusion analysis), although the effectiveness of this method relies on evidence that the analyzed fluid inclusions are primary in origin and that they reflect the fluid of interest. Indirect methods (i.e., stable isotopes, minor- and trace-element mineral chemistry) have been useful in constraining the source of metals and the chemical evolution of hydrothermal fluids (e.g., Pfaff et al., 2011; Reich et al., 2012; Gagnevin et al., 2014).

The East Kemptville Sn-Zn-Cu-In-Ag deposit is located in the Canadian Appalachians in southwest Nova Scotia, Canada. The deposit is a granitoid-related greisen, with an estimated 1236 t of contained indium, making it one of the largest undeveloped indium deposits in North America (Werner et al., 2017). Previous research on the East Kemptville deposit has largely focused on understanding the processes responsible for Sn mineralization (Richardson, 1988; Kontak, 1994; Halter et al., 1995; 1996; 1998), with few studies on the sulfide mineralization (Kontak, 1990a; 1993). This previous research concluded that sulfide mineralization occurs in several paragenetic stages, however, the relationship with the associated indium mineralization is unknown. Additionally, the spatial coverage of these earlier studies was limited to an individual ore zone.

An important aspect of this study is to characterize the mineralogical distribution of indium at East Kemptville in order to assess if there are spatial and temporal variations in indium mineralization. This is addressed through a detailed mineralogical study of the different ore zones, and integrates mineral textures coupled with mineral chemistry. The physicochemical conditions and chemical evolution of the hydrothermal fluids responsible for mineralization are characterized using mineral geothermometry and trace-element mineral chemistry. Sulfur isotopes are used to characterize the fluids source responsible

for mineralization. This contribution is the first comprehensive study on the nature and genesis of indium mineralization in the East Kemptville deposit. Additionally, the results from this study are compared with other deposits to examine the relationship between East Kemptville and other indium-bearing Sn-polymetallic deposits.

Chapter 2

Geologic Framework of the East Kemptville Deposit

2.1 Geologic Setting

The East Kemptville deposit is located in the Meguma terrane of the northern segment of the Appalachian orogen and is hosted within the Davis Lake Complex (DLC), an 800 km^2, internally zoned, granitic pluton of the late Devonian (ca. 375 Ma) South Mountain Batholith (SMB) (Dostal & Chatterjee, 1995). The DLC consists of biotite leucomonzogranites, muscovite-biotite leuocomonzogranites, and topaz-muscovite leucogranites (Dostal & Chatterjee, 1995) that intruded the Meguma metasedimentary rocks of the Ediacaran to Ordovician Halifax and Goldenville groups (White, 2010; Fig. 2.1). The deposit is hosted by the most evolved granitic phase of the DLC, the East Kemptville leucogranite (EKLG), which is considered to be a product of fluid-melt fractionation of the DLC (Dostal & Chatterjee, 1995). The EKLG is a fluorine-rich, topaz- and muscovite-bearing granite that contains local occurrences of stockscheider-type pegmatites and miaroles (Kontak, 1990). The geochemical signature of the EKLG is characterized by depleted whole-rock ∑REE, LILE enrichment (K, Cs, Rb, Li, F, B), and a low Nb/Ta ratio (~2-3), compared with other phases of the DLC and SMB (Kontak, 1990b; Kontak et al., 2001). The age of the EKLG is inferred to be similar to the DLC, which has been dated at ca. 375 $\pm$ 3 Ma by Pb-Pb isotope methods (Chatterjee & Cormier, 1991; Dostal & Chatterjee, 1995). The EKLG was emplaced along the East Kemptville-East Dalhousie Fault Zone (EKEDFZ), a large fault zone that extends along the length of the SMB (Horne, 1992; 2006). This fault zone has had a prolonged history of movement that is recorded by tectono-thermal resetting of the Rb-Sr and K-Ar systems (Kontak et al., 1995). The southwest Nova Scotia tin domain corresponds to the western portion of the EKEFZ, a 70 by 10 km linear belt of Sn-polymetallic and precious-metal occurrences (Fig. 1) (Chaterjee, 1983). Two periods of Sn-polymetallic mineralization are recorded in the domain, i) an earlier (ca. 380 Ma) event and, ii) a later (Ca. 360 Ma) event (Kontak et al., 2013). The former is restricted to the most easterly portion of the tin domain and consists of the East Kemptville deposit and the spatially related Duck Pond vein- and stratabound polymetallic tin deposit. The younger Sn-polymetallic occurrences are found west of the

East Kemptville deposit and consists of the Gardeners Meadow, Dominique, and Clayton Hill occurrences.

2.2 Deposit Geology

2.2.1 East Kemptville

The East Kemptville deposit consists of greisen-related mineralization and late quartz-sulfide veins that occur in two zones of mineralization: The Main and Baby zones (Fig. 2.2). Together, these two zones make up the historic geological reserve of 66.1 Mt of 0.155 wt.% Sn (John, 1983). Recent work by Avalon Advanced Materials has shown that In grades are up to 85 ppm (Gowans et al., 2018). In both zones, the mineralization is hosted by the EKLG, with mineralization located close to the contact between the EKLG and the country rocks (Halter et al., 1996). Mineralization in both zones is spatially associated with a major sub-vertical fault zone that form part of the EKEDFZ and comprises a variety of Sn, Zn, Cu, Ag, and In-bearing minerals. Despite the similarities in metal suites between the two zones, they differ in their size, ore grades, structural character, and mineralization styles.

The Main Zone was the focus of historic mining efforts and is characterized by lower ore grades and a greater ore tonnage than the Baby Zone. Mineralization in the Main Zone is structurally controlled, with mineralization concentrated in several NE-trending greisen-bodies that are parallel to the NE structural trend. Mineralization typically occurs in quartz ± topaz veins and associated greisen selvages (a.k.a. greisen-bordered veins, zoned greisen veins). In this thesis, the veins will be referred to as “greisen veins” and the selvages as greisen selvages. The combined vein-selvage package is generally less than 2 m wide, and can exceed 20 m in strike length and 15 m in depth (Fig. 2.3a) (Richardson, 1988). Adjacent to the fracture or vein, the wallrock has been progressively altered from quartz-muscovite greisen to quartz-topaz greisen. Greisen alteration can also occur as ‘massive‘ greisens, which comprise large bodies (at least 7 m wide, and 50 m long) that have been pervasively altered to quartz-topaz greisen with minor amounts of quartz-muscovite greisen. These massive greisens occur proximal to fault zones (Fig. 2.3b) (Richardson, 1988). Massive greisens differ from greisen selvages in that they do not contain veins with associated symmetrical greisen selvages. In the Main Zone, massive greisens are thought to represent

a high-density of coalescing greisen veins and selvages, however, these textural relationships are not well preserved (Halter et al., 1996). Most of the Sn and base-metal sulfide mineralization is associated with quartz-topaz greisens as disseminated mineralization, with lesser amounts of mineralization occurring in the quartz-muscovite alteration (Richardson, 1988; Halter et al.,1996).

The Baby Zone is characterized by higher metal grades but contains a lower tonnage than the Main Zone. The Baby Zone is contained in an elliptical, pipe-like cupola that is centered on the NE-trending fault zone. Disseminated mineralization occurs in massive greisens, with minor amounts of mineralization in greisen veins and selvages. The massive greisens are similar to those in the Main Zone, except that greisen development does not appear to have occurred along fault zones (Bickerton et al., 2017). A feature of the Baby Zone that is absent from the Main Zone is the presence of a magmatic-hydrothermal breccia at the granite-metasedimentary country rock contact. This breccia consists of a lower magmatic breccia that exhibits clasts of metasedimentary rocks in a matrix of quartz-phyric granite with variable amounts of sericite alteration. A less abundant type of breccia that occurs higher in the pipe consists of a hydrothermal clast-supported crackle breccia with metasedimentary rock clasts, and a matrix of quartz and muscovite. Mineralized portions of this breccia are rare and volumetrically small, and, where present, comprise sulfides in a quartz-fluorite matrix (Fig. 2.3c).

Sulfide minerals occur in greisens and in the quartz-sulfide veins that cross-cut the greisens and host granite, with the greisen-hosted sulfides thought to be paragentically earlier than the quartz-sulfide veins and genetically related to greisen event (Fig. 2.3d; Richardson, 1988; Kontak, 1994). These quartz-sulfide veins are found in both zones of the deposit and have a dominant NE-trend (Kontak, 1994). Richardson (1988) proposed that two temporally distinct types of quartz-sulfide vein are present: i) an early set that contains fluorite, and ii) a later set that contains phosphate minerals (apatite and triplite). Quartz-sulfide veins are post-dated by barren quartz-phosphate and quartz-dickite veins, and by joint planes filled with zeolites, phosphates, and carbonates.

2.2.2 Duck Pond

The Duck Pond deposit is located 2 km west of the East Kemptville deposit, within the East Kemptville Shear Zone, and consists of both stratabound and vein-hosted mineralization. The deposit is hosted in the basal unit of the Cunard Formation within the Halifax Group (pers. comm. D. Kontak, 2019). The metals of economic interest in the Duck Pond deposit consist of Sn, Cu, Zn, and In. The style of mineralization correlates with host rock, with pelites typically containing vein-hosted mineralization and psammites generally containing disseminated mineralization (Fig. 2.3e, f). Tin mineralization is associated with chloritic alteration, whereas base-metal sulfides occur in rocks affected by chloritic, alkalic, and argillic alteration (Pitre & Richardson, 1989; Kontak et al., 1990). Despite their proximity and similar ore-element suites, there are notable differences between the Duck Pond and East Kemptville deposits. Duck Pond is absent of F-bearing minerals which are abundant in the East Kemptville deposit.

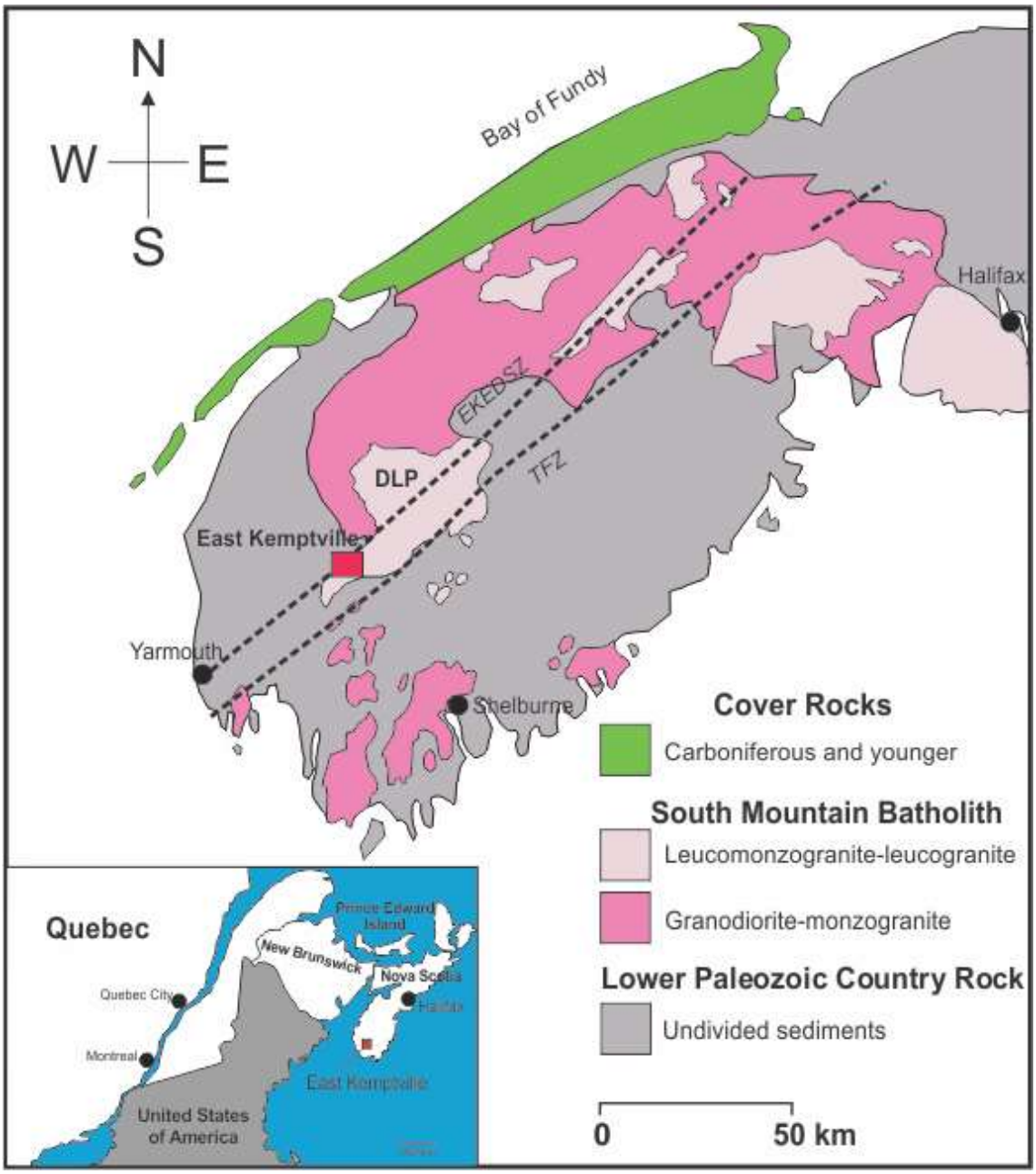

Figure 2.1 Simplified geologic map of south western Nova Scotia showing the South Mountain Batholith modified after MacDonald (1992) & White (2010). *DLC*- Davis Lake Complex, *EKEDFZ* – East Kemptville-East Dalhousie Fault Zone, *TFZ*- Tobeatic Fault Zone

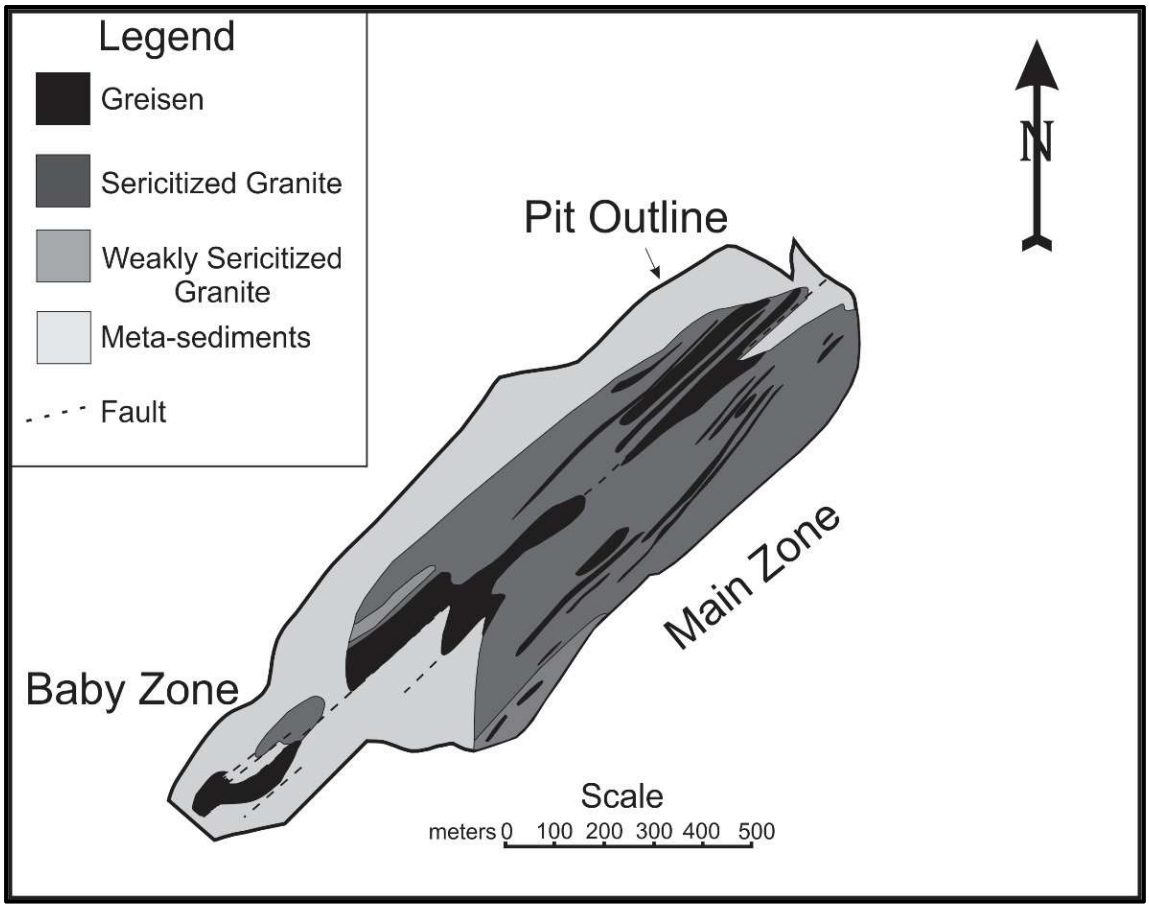

Figure 2.2 The 94-m plan view geologic map of the East Kemptville Deposit. Modified after Halter et al. (1996).

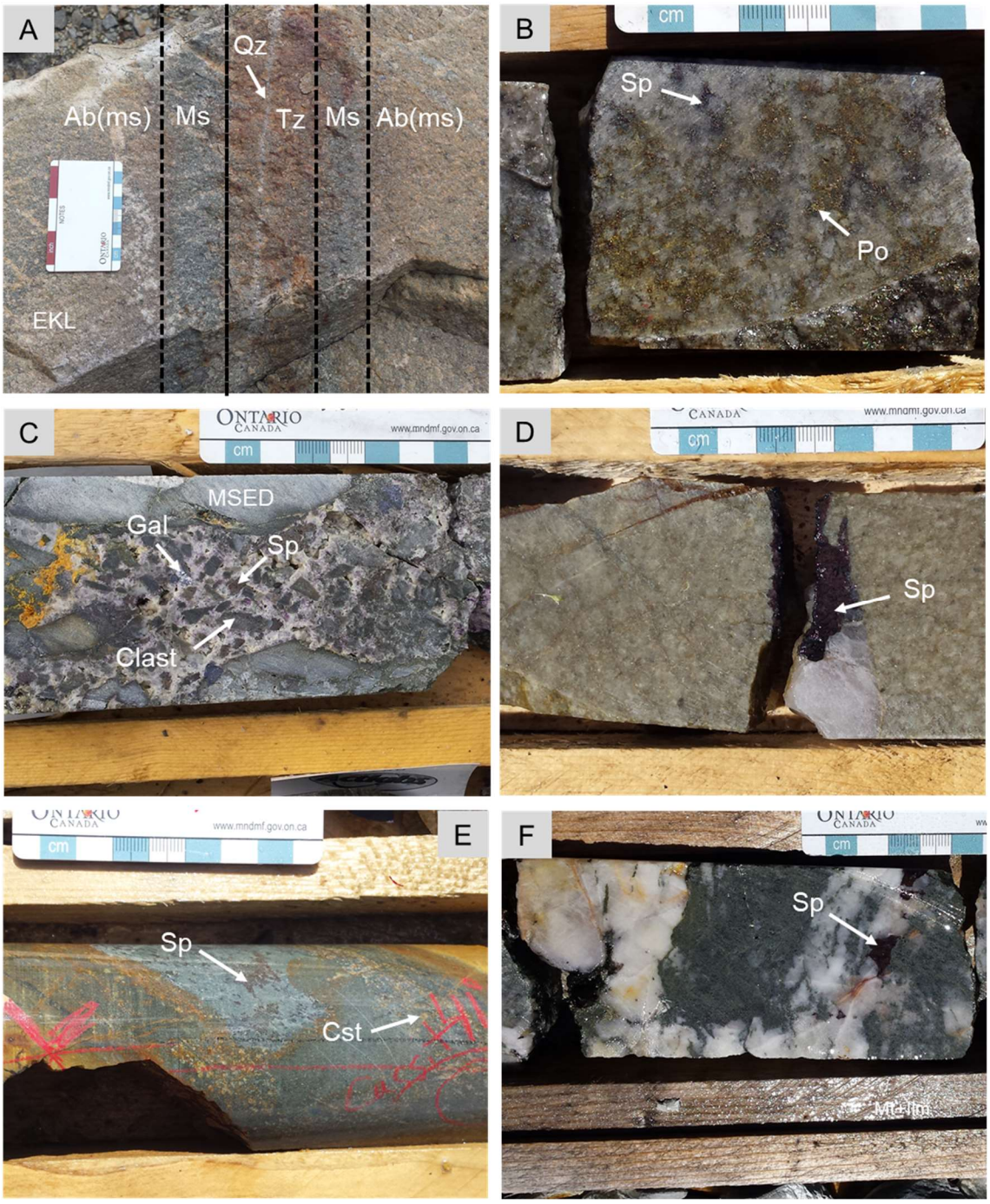

Figure 2.3 Field and drill core photos of the different mineralization styles from the East Kemptville and Duck Pond deposits. (A). A greisen-bordered vein hosted in an albite-muscovite altered granite (B). Drill core of a quartz-topaz massive greisen with fine-grained disseminated sulfide mineralization. (C). Drill core of a quartz-sulfide vein comprised of quartz and sphalerite that crosscuts an albite altered granite. (D) Drill core of a mineralized hydrothermal breccia comprising of a quartz-fluorite matrix and sulfide clasts. (E) Drill core of a stratabound-hosted mineralization of the Duck Pond deposit in a chlorite altered (rock). (F) Drill core of quartz vein hosted sulfide mineralization of the

Duck Pond deposit. EKL = East Kemptville Leucogranite, Ab(ms) = albite-muscovite alteration, Ms = muscovite alteration, Tz = topaz alteration, Qz = quartz, Sp = sphalerite, Po = pyrrhotite, Cst = cassiterite.

Chapter 3
Methods

3.1 Sampling

Representative samples of the different mineralization styles of the East Kemptville and Duck Pond deposit were collected from twenty-one and three drill holes, respectively. A total of one hundred and forty-seven polished thin sections were used for petrographic investigation and microanalysis; sixty-five from Main Zone rocks, seventy-two from Baby Zone rocks, and ten from the Duck Pond rocks.

3.2 Electron Probe Microanalysis (EPMA)

Electron probe microanalysis (EPMA) was conducted on cassiterite and sulfide minerals from seventy samples (745 analyses) using a JEOL JXA-8530F field-emission electron microprobe, located at the Earth and Planetary Materials Analysis laboratory located at the University of Western Ontario, Canada. The operating conditions included a 25 kV accelerating voltage, 60 nA beam current, and a 1 μm beam diameter. Peak counting times were 30 s for Fe, Zn, S, Cd, Sn, and Cu followed by 15 s of background collection, whereas, for In and Ag, peak counting times were 60 s with 30 s of background. Standards used were sphalerite (Zn), pyrite (Fe, S), chalcopyrite (Cu), cadmium metal (Cd), rhodonite (Mn), indium phosphate (In), cassiterite and tin alloy (Sn), and silver metal (Ag). Interference from the Sn-Lη line on the In-Lα line was corrected by determining the contribution (intensity) of the Sn-Lη line from a pure Sn standard. A similar approach was undertaken to correct the interference of Cd-Lα on the Ag-Lα peak using a Cd metal standard.

3.3 Scanning Electron Microscopy-Energy Dispersive X-ray Spectroscopy (SEM-EDS)

A scanning electron microscope fitted with back-scattered electron (BSE) and energy-dispersive X ray detectors was used for imaging (BSE), mineral identification (EDS), and semi-quantitative mineral chemistry (EDS). Analyses were conducted on a FEI Quanta 200 FEG SEM with an EDAX Octane SDD EDS detector, located at the Advanced Microscopy and Materials Characterization Lab at the University of Windsor. The SEM was operated

in high vacuum mode using a 15 kV accelerating voltage, 30 nA beam current, and a 1.5 μm beam diameter, with peak counting times of 30 s.

3.4 Laser-Ablation Inductively-Coupled Plasma Mass Spectroscopy (LA-ICP-MS)

Trace-element microanalysis of oxide and sulfide minerals was achieved using laser-ablation inductively-coupled plasma mass spectroscopy (LA-ICP-MS) for four (14 analyses) and thirty-four samples (158 analyses), respectively. Polished thin sections (30 μm thick) were used for the laser-ablation traverses. Analyses were performed using a PhotonMachines 193 nm short pulse width Analyte Excite excimer laser ablation system coupled with an Agilent 7900 fast-scanning quadrupole mass spectrometer, located at the Element and Heavy Isotope Analytical Laboratory at the University of Windsor. The laser operating conditions consisted of a 25 μm beam width, 35 % energy at 4.1 mJ, 25 Hz repetition rate, and 5 μm/s raster rate. Tuning of the ICP-MS was performed daily to maximize sensitivity, while minimizing the production of molecular oxides and doubly charged ion species. Each analysis consisted of an initial 30 s measurement of the gas background with the laser turned off to determine background element concentrations. After each analysis, a minimum of 15 s gas blank was used to monitor effective washout. Data reduction was performed using Iolite software (Paton et al., 2011) and utilized the approaches outlined by Longerich et al. (1996). Data was integrated to best reflect the signal from the mineral host and any visible mineral inclusions were avoided.

The MASS-1 synthetic polymetal sulfide standard reference material (Wilson et al, 2002) was used as the primary external calibration standard for sulfide minerals, and the GSE-1G synthetic basaltic glass standard reference material (Jochum et al., 2005) was used as the primary external calibration standard for oxide minerals. For both oxide and sulfide minerals, the NIST-610 synthetic glass standard reference material was used in addition to the primary reference material to enable quantification of elements not present in the primary external calibration standard, and as a quality control standard. For sulfide minerals, the following masses were measured, with their respective average limit of detection (LOD) reported in parts per million (in parentheses): ^{29}Si (960), ^{34}S (630), ^{44}Ca (79), ^{54}Fe (380), ^{55}Mn (0.55), ^{57}Fe ,^{59}Co (0.04), ^{60} Ni (0.20), ^{63}Cu (0.20), ^{66}Zn (1.3), ^{67}Zn (2.9), ^{69}Ga (0.03), ^{73}Ge (0.3), ^{74}Ge (0.2), ^{75}As (2.5), ^{78}Se (12.3), ^{109}Ag(0.02), ^{111}Cd (0.3),

^{113}Cd (0.2), ^{113}In (0.3), ^{115}In (0.01),^{115}Sn (0.5),^{120}Sn (0.2), ^{121}Sb (0.1), ^{208}Pb (0.04), ^{209}Bi (<0.01). For oxide minerals the follow masses were measured: ^{29}Si (110), ^{34}S (20), ^{44}Ca (11), ^{45}Sc (0.1), ^{48}Ti (0.1), ^{54}Fe (30), ^{55}Mn (0.1), ^{57}Fe (3.6), ^{63}Cu (0.02), ^{66}Zn (0.1),^{89}Y (<0.01), ^{93}Nb (<0.01), ^{111}Cd (0.02), ^{113}Cd (0.03),^{113}In (0.04), ^{115}In (<0.01), ^{115}Sn (1.33), ^{117}Sn (0.2), ^{120}Sn (0.1), ^{181}Ta (0.1), ^{184}W (<0.01),^{208}Pb (0.01), ^{238}U (<0.01). Results that were below the limit of detection were estimated and reported as 0.5x the LOD, with negative values reported as 0. Interferences between ^{115}In and ^{115}Sn, and between ^{113}Cd and ^{113}In, were corrected using the procedure outlined by Pavlova et al. (2015). In minerals where indium occurs in trace concentrations, values were only obtained using LA-ICP-MS, whereas EPMA and LA-ICP-MS were used to obtain indium concentrations where they were above the EPMA detection limit. The argide interference between ^{115}In and ^{75}As^{40}Ar was assessed by comparing the concentrations of ^{115}In and ^{113}In, which exhibited negligible differences for most sulfide minerals in this study, except for arsenopyrite where the argide interference accounted for ~ 4 ppm of ~ 46.1 wt.% As. The interference on ^{74}Ge from ^{40}Ar^{34}S and ^{58}Ni^{16}O were assessed by comparing the concentrations of Ge by ^{74}Ge with ^{73}Ge and it was determined to be negligible for most sulfides in this study, with the exception of arsenopyrite.

Iron concentrations determined by EPMA were used as the internal standard for sphalerite. Stoichiometric Fe concentrations were used as the internal standard for chalcopyrite (30.4 wt.%), arsenopyrite (34.3 wt.%), pyrrhotite (60.0 wt.%), and pyrite (46.55 wt.%); these values are consistent with EDS and EPMA measurements. Stoichiometric element concentrations were also used as the internal standards for cassiterite (87.0 wt.% Sn) and wolframite (60.0 wt.% W), which are again consistent with EPMA and EDS analyses.

3.5 QEMSCAN®

Automated SEM-based image analysis of fourteen polished thin sections was conducted using QEMSCAN® at the Advanced Mineralogy Facility at SGS Canada in Lakefield, Ontario. The QEMSCAN® analysis utilized an EVO 430 scanning-electron microscope equipped with four energy dispersive X-ray spectrometers. Data processing was performed using iDiscover software. The operating conditions of the SEM consisted of a 25 kV accelerating voltage and a 5 nA beam current. The instrument was operated using Field

Scan measurement mode. Field scans consist of spatially resolved X-ray rasters for a 1600 µm by 2300 µm area, with a measurement resolution of 14.5 µm. Each measurement is classified into mineral phases based on the X-ray spectral data and backscattered-electron intensities. The accuracy of mineral classifications was verified using optical microscopy.

3.6 Sulfur Isotopes

3.6.1 Elemental Analyzer Coupled-Isotope Ratio Mass Spectroscopy (EA-IRMS)

The sulfur isotopic compositions ($\delta^{34}S$) of thirty-seven sulfide mineral concentrates were analyzed using an Elementar isotopic cube element analyzer (EA) coupled with a ThermoDeltaplus XP isotope-ratio mass spectrometer (IR-MS) located at the G.G Hatch Laboratory at the University of Ottawa. Samples were prepared by either hand-picking mineral separates or by in situ micro-drilling of drill-core samples. The resultant separates were checked for purity using a binocular stereo microscope. Powdered samples (0.09-0.31 mg) were mixed with a minimum of twice the sample weight of WO_3 and placed in a tin capsule prior to combustion. Each sample was then combusted at 1,800 °C in the EA to release SO_2 gas. The SO_2 was transported by a He carrier gas into a gas chromatography (GC) column to purify the SO_2 from other gases (e.g., CO_2). The purified SO_2 was then carried into the IR-MS, which measured the $^{34}S/^{32}S$ ratio. Results were then corrected using a calibration derived from standard materials. Analytical precision (1 σ) calculated from replicate standard analysis is ± 0.3 ‰. All sulfur isotopic values are reported in standard delta notation in per mil (‰) relative to the Vienna Canyon Diablo Troilite (V-CDT) standard.

3.6.2 Secondary Ion Mass Spectrometry (SIMS)

In situ sulfur isotopic composition ($\delta^{34}S$) of sulfides from nine samples (59 analyses) were obtained at the MAF-IIC Microanalysis Facility at Memorial University using a Cameca IMS 4f Secondary Ion Mass Spectrometer (SIMS). Samples were prepared by mounting small rock slabs or mineral grains into a 25.4 mm round epoxy puck. Samples were finely polished (0.25 µm) and coated with 300 Å of Au to prevent primary charging under ion-bombardment. The SIMS operating conditions consisted of a primary ion microbeam of 350-1150 pA of Cs^+, with a 10 KeV potential, and a 5-15 µm diameter spot size. The Cs current was varied depending on the sulfide mineral, the size of the crystal, and the nature

of the surrounding matrix to the analyzed crystal. To remove any potential contaminants from the polished surface, the analysis area was pre-sputtered for 120 s with a 25 μm square raster. Standards used were: B95 66 (sphalerite; $\delta^{34}S$: 2.2 ‰), Norilsk (chalcopyrite; $\delta^{34}S$: 2.2 ‰), PoW (pyrrhotite; $\delta^{34}S$: 3.0 ‰), and UL9B (pyrite; $\delta^{34}S$: 16.3 ‰). The isotopic composition ($\delta^{34}S$) was determined for multiple sulfide minerals and grains in each sample. The analytical precision (1σ) calculated from replicate standard analysis include: sphalerite (± 0.5 ‰), chalcopyrite (± 0.3 ‰), pyrrhotite (± 0.5 ‰), pyrite (± 0.3 ‰). All sulfur isotopic values are reported in standard delta notation in per mil (‰) relative to the Vienna Canyon Diablo Troilite (V-CDT) standard.

Chapter 4

Results

4.1 Ore Mineralogy, Textural Variations, and Paragenesis

4.1.1 East Kemptville

4.1.1.1 Greisens

The primary Sn mineralization at East Kemptville is associated with two morphological sub-types of greisens: i) massive greisens and ii) greisen veins and selvages. The abundant minerals in the greisens are quartz, muscovite, and topaz, and these minerals occur in varying proportions in different greisens. Greisens can also be subdivided into five types according to the most abundant mineral(s) present: i) quartz-muscovite, ii) quartz-topaz, iii) muscovite, iv) topaz, and v) quartz. Cassiterite occurs in two varieties, a coarse-grained (0.5-3 cm) and a fine-grained (400-800 μm) variety. The coarse crystals are euhedral, exhibit oscillatory zoning and twinning (Fig. 4.1a), and occur in greisen veins or in muscovite-rich greisens. The fine-grained crystals are subhedral to anhedral, exhibit weak zonation, are pale in color (Fig. 4.1b), and occur in all types of both massive greisens and greisen selvages. The fine-grained cassiterite typically shares planar grain boundaries with quartz, topaz, and muscovite. Topaz occurs in quartz-topaz and topaz greisens; crystals are typically subhedral to euhedral that are typically fine- to medium-grained (200-600 μm; Fig. 4.1c). Muscovite occurs in quartz-muscovite and muscovite greisens as medium- to coarse-grained crystals (400-1200 μm) and as fine-grained aggregates (Fig 4.1d). Tourmaline is rare and occurs as euhedral to subhedral crystals and, where present, is intergrown with topaz (Fig. 4.1e). Although earlier studies (e.g., Richardson, 1989; Kontak, 1994) did not identify tourmaline in the EKLG, tourmaline was observed in massive greisen samples from the Baby Zone in this study. Recent work by Sedge et al. (2015) also identified tourmaline (elbaite-schorl solid solution) associated with greisens from the southern part of the Main Zone.

Wolframite is much less abundant than cassiterite in both massive greisens and in greisen selvages. It is typically fine- to medium-grained (100-400 μm), occurs as tabular crystals,

and forms discrete grains or aggregates, that can share planar grain boundaries with cassiterite (Fig. 4.1f). A volumetrically insignificant portion of greisen veins are wolframite-rich, in which the wolframite crystals are coarse-grained and euhedral (0.5-3 cm). Arsenopyrite primarily occurs in greisen veins, but also occurs to a lesser degree in the greisen selvages. It occurs as coarse-grained (0.5-1 cm), euhedral to subhedral crystals in aggregates that typically contain cassiterite ± wolframite (Fig 4.2a). Arsenopyrite-bearing greisen veins are most abundant at the metasedimentary rock-granite contact in the Main Zone. Arsenopyrite is rarely present in massive greisens, where it typically occurs as discrete crystals.

The base-metal sulfides minerals, sphalerite, chalcopyrite, pyrrhotite, and stannite occur in greisen veins and selvages, and in massive greisens. Disseminated sulfides occur in all mineralogical subtypes of greisen but are typically more abundant in topaz greisens and quartz-topaz greisens, with lesser amounts associated with muscovite and quartz-muscovite greisens (Table 4.1). Base-metal sulfides in all morphological greisen types typically exhibit infill textures, occurring as fracture fill in veins that crosscut cassiterite, arsenopyrite, wolframite, and topaz, and as open-space fillings in vugs (Fig. 4.2a, b, c). These various sulfides uncommonly exhibit disequilibrium textures with muscovite, topaz, and cassiterite (Fig. 4.2d). In all greisen types, base-metal sulfides typically occur together and form a mosaic texture, sharing smooth, rounded grain boundaries (Fig. 4.2e). Sulfides can exhibit triple junctions in monomineralic aggregates (Fig. 4.2f). Although uncommon, sphalerite can contain disseminated, rounded inclusions of chalcopyrite and/or pyrrhotite (Fig 4.3a). Chalcopyrite inclusions can also occur along fracture planes in sphalerite. Chalcopyrite typically contains inclusions of sphalerite and/or stannite (Fig. 4.3b). Stannite is not abundant and generally occurs as small grains (< 50 μm), primarily in contact with sphalerite, but can share grain boundaries with chalcopyrite. Stannite associated with sphalerite generally occurs as euhedral overgrowths on sphalerite, and rarely as intergrowths with sphalerite (Fig. 4.3c). Native bismuth and galena are rare and generally occur intergrown with each other and in association with pyrrhotite, chalcopyrite, sphalerite, and fluorite. Quartz and minor to trace amounts of fluorite typically occur intergrown with the base-metal sulfides. Fluorite, which can be zoned, typically occurs at

the grain boundaries of quartz and/or topaz and exhibits disequilibrium textures with the topaz (Fig. 4.2c). Chlorite and clay minerals are rare and occur intergrown with muscovite or as a replacement of muscovite. Triplite was recognized in a greisen-vein in a single sample observed from the Main Zone.

In Cu-rich assemblages where chalcopyrite is the dominant sulfide, an unnamed Zn-In mineral occurs in association with sphalerite and stannite. The unnamed Zn-In mineral was first documented by Ohta (1989) and has a chemistry that is intermediate between sphalerite and roquesite, however, the crystal structure of the mineral has not been defined. This mineral is optically similar to sphalerite in reflected light but is lighter grey in appearance and has very weak pleochroism. In this assemblage, the Zn-In mineral is most often found at the interface between sphalerite and stannite. The Zn-In mineral rims large sphalerite crystals and then is itself rimmed by stannite (Fig. 4.3d). Stannite may be absent from the assemblage, with the Zn-In mineral occurring as a rim with sphalerite. Pyrite is typically present in all greisen types but is less abundant in greisens from the Baby Zone. Pyrite exhibits disequilibrium textures with pyrrhotite; it shares irregular boundaries with pyrrhotite and typically contains inclusions of base-metal sulfides that exhibit cuspate boundaries (Fig 4.3e). Pyrite rarely occurs as discrete euhedral crystals, typically does not contain mineral inclusions, and can exhibit zoning in BSE images (Fig. 4.3f). In some samples, albeit rarely, carbonate and pyrite can be intergrown. Marcasite is less common than pyrite and, when in contact with pyrrhotite and pyrite, has irregular, disequilibrium boundaries with these other Fe-sulfides (Fig. 4.3e). In samples proximal to fault-zones, quartz exhibits variable degrees of recrystallization, represented by deformation lamellae and subgrain development. Pyrrhotite can also exhibit deformation twins and in areas of strong deformation, C-S fabrics are present.

4.1.1.2 Quartz-Sulfide Veins

Quartz-sulfide veins cross-cut massive greisens, greisen veins and selvages, unaltered EKL, and the adjacent metasedimentary rocks. Two types of veins are present in outcrop, boulders, and drill-core: i) coarse-grained veins, and ii) fibre veins. Coarse-grained veins are generally 1 to 3 cm in width, although wider veins (> 5 cm) were observed in boulders.

These veins can be planar or sinuous, exhibit sharp to diffusive wallrock contacts, and contain euhedral to subhedral quartz crystals. Fibre veins are generally thin (< 1 cm in width), exhibit syntaxial and antitaxial fabrics, and typically occur as en-echelon veins. Both these vein types lack alteration envelopes and are characterized by a similar mineralogy. Sulfides in both vein types are similar and predominantly consist of sphalerite, with lesser amounts of chalcopyrite, pyrrhotite, and pyrite. Where present, chalcopyrite and pyrrhotite typically exhibit smooth, rounded boundaries with sphalerite (Fig. 4.4a). Stannite is rare and forms partial rims on sphalerite. Pyrite occurs in the veins, primarily in the Main Zone, occurs as euhedral crystals, and can contain round inclusions of pyrrhotite, sphalerite, or chalcopyrite (4.4b). No primary indium minerals were identified in the quartz-sulfide veins.

Other minerals in the quartz-sulfide veins comprise variable proportions of fluorite, siderite, apatite, triplite, and albite. Triplite occurs as 1 to 10 mm sized subhedral crystals, in both coarse-grained and fibre veins and was only observed in veins from the Main Zone. These phosphate veins were mainly observed in EKLG that has undergone low degrees of alteration. Apatite occurs as 1 to 5 mm euhedral crystals, and has a similar distribution to triplite, although it was rarely observed in veins in the Baby zone. Where both minerals are present they exhibit disequilibrium boundaries (Fig. 4.4c). Albite was only observed in a single vein that cross-cut albitite wall-rock in the Baby Zone. Siderite occurs as euhedral grains associated with pyrite, along fractures in base-metal sulfides and apatite, and shows disequilibrium textures with apatite and triplite (Fig. 4.4d).

4.1.1.2 Hydrothermal Breccia

The hydrothermal breccia consists of metasedimentary rock clasts, which have undergone pervasive muscovite alteration, in a matrix of quartz and fluorite. Sulfides comprise sphalerite with lesser galena and chalcopyrite. Sphalerite typically occurs as elongate crystals and exhibits irregular and discontinuous zoning under plane-polarized light (dark red to yellow in color; Fig. 4.4e) and in BSE images (dark grey to light grey). Chalcopyrite also exhibits irregular zoning in BSE images (Fig. 4.4f). Chlorite has replaced muscovite in the matrix and on the rims of clasts. Quartz is generally polygonal and subhedral.

4.1.2 Duck Pond

Cassiterite at Duck Pond occurs in chlorite-altered rocks, in both psammites and pelites. The nature of the chlorite alteration varies depending on the nature of the hostrock: in psammites it occurs as pervasive, disseminated alteration, and in pelites it occurs as vein selvages. Cassiterite is generally medium- to fine-grained and can be classified into three types based on crystal habit: i) equant crystals, which are pale in color and exhibit poorly defined growth zonation, ii) acicular crystals, which are darker in color than the equant variety, and lack zoning, and iii) aggregates of fine-grained cassiterite that are generally pale in color (Fig. 4.5a,b). The various subtypes of cassiterite typically occur together, with some samples containing all three subtypes.

Disseminated sulfides, which consist of sphalerite, pyrite, and lesser amounts of chalcopyrite, are associated with alkalic and chlorite alteration. Stannite, pyrrhotite, and bornite are rare. Pitre and Richardson (1989) described an alkalic alteration that is characterized by relict plagioclase, muscovite, and quartz, which are intergrown with sulfide minerals (Fig. 4.5c). Chlorite alteration is characterized by abundant chlorite and lesser amounts of garnet, and by sulfides, which occur interstitial to, as inclusions in, or in fractures in garnet and as intergrowths with chlorite (Fig. 4.5d). Quartz-sulfide veins also occur at Duck Pond, and consist predominantly of sphalerite, which occurs with trace to minor pyrite and chlorite. For a more comprehensive description of the Duck Pond deposit see Pitre and Richardson (1989).

4.2 Mineral Chemistry

Oxide minerals from massive greisens, greisen veins and greisen selvages were analyzed by EPMA, EDS, and LA-ICP-MS to determine their major-, minor-, and trace-element chemistry. Sulfides from massive greisens, greisen veins, and greisen selvages, quartz-sulfide veins, and the hydrothermal breccia from the East Kemptville deposit, as well as sulfides from Duck Pond, were analyzed by EPMA and LA-ICP-MS to determine their major-, minor-, and trace-element composition. Complete EPMA, EDS, and LA-ICP-MS chemical analyses are provided in Appendices A, B, and C, respectively. Representative LA-ICP-MS spectra data are illustrated in Fig. 4.7 and Fig. 4.11 for oxides and sulfides, respectively.

4.2.1 Cassiterite

Cassiterite major-element chemistry was determined for six samples (42 analyses) from East Kemptville and one sample (2 analysis) from Duck Pond using both EPMA and EDS. Most cassiterite from both deposits contains low concentrations of Fe and only a few analyses indicate Fe concentrations greater than 1 wt.% for East Kemptville. Minor- and trace-element chemistry of cassiterite from the East Kemptville deposit (Fig. 4.6a) was determined for three samples (8 analyses) using LA-ICP-MS. Titanium, Fe, Nb, Ta, and W concentrations range from 100s to 1000s of ppm, with Sc concentrations in the 10s of ppm range. Zinc and U occur in concentrations of 1 to 10s of ppm, whereas Yb, Cd, and Pb occur in concentrations of less than 1 ppm. Concentrations of Cu are highly variable, ranging from <1 to 100s of ppm. Indium was detected in all analyses, and ranges in concentration from 1.0 to 23.6 ppm (Fig 4.6a). LA-ICP-MS spectra of cassiterite are characterized by smooth signals with low count variability. The exceptions are Mn, Cu, Zn, Y, Cd, and Pb, which are characterized by more significant variability (noise), as illustrated by Mn, Cu, and Pb signals in Figure 4.7a; the counts for these elements commonly co-vary. Indium generally covaries with Fe, W, and, to a lesser extent, Nb in LA-ICP-MS spectra, but these elements do not covary with Cu and Zn (Fig. 4.7a). The highest concentrations of indium are present in the coarse cassiterite variety from greisen veins that exhibits oscillatory zoning.

4.2.2 Wolframite

The major-element chemistry of wolframite-group minerals was determined for two samples (17 analyses) from the East Kemptville deposit using EDS. These data show that the wolframite at East Kemptville is ferberite, but with significant and variable Mn contents; atomic Fe/(Fe+Mn) ratios range from 0.53 to 0.86. Minor- and trace-element chemistry (Fig. 4.6b) was determined from five analyses from two samples. Niobium concentrations are in the 1000s of ppm, whereas Ti, Fe, Ta, and W range from 100s to 1000s of ppm. Yttrium and U range from several to 10s of ppm, and Cu, Cd, and Pb occur in concentrations of less than 1 ppm. Indium concentrations in wolframite range from 3.2 to 14.8 ppm (Fig 4.6b). LA-ICP-MS spectra of wolframite are characterized by smooth signals with low count variability for Sc, Mn, Zn, Fe, and In. Cadmium, Pb, and, to a lesser extent, Cu are characterized by more significant variability (noise), as illustrated by Pb in

Figure 3.7b. Indium was detected in all wolframite crystals analyzed and is homogeneously distributed through the crystals, as indicated by smooth, flat-lying signals in laser ablation spectra (Fig. 4.7b). Tin, Ta, and to a lesser extent Nb generally covary in LA-ICP-MS spectra (Fig. 4.7b).

4.2.3 Arsenopyrite

Arsenopyrite from East Kemptville contains an average (± 1σ) of 33.1 ± 1.0 wt.% Fe, whereas stoichiometric arsenopyrite contains 34.3 wt.% Fe. Arsenopyrite trace-element chemistry (Fig. 4.7c) was determined for two samples (3 analyses) from the East Kemptville deposit. All arsenopyrite analyzed has low trace-element contents, with only Co, Sb, Se and Pb occurring in concentrations greater than 100 ppm. Nickel, Cu, Zn, Ge, Sn, and Bi occur in concentrations ranging from 10 to 100 ppm, with other trace elements typically occurring in concentrations of 1 ppm or less (Fig. 4.6c.). LA-ICP-MS spectra of arsenopyrite are characterized by smooth signals for most elements, while Co, Pb, and Bi exhibit significant variability (noise), as illustrated by Co and Pb in Figure 4.7c; the counts for these three elements commonly co-vary (Fig. 4.7c). Manganese and Zn generally covary and commonly exhibit peaks in LA-ICP-MS spectra. Indium in all samples was below the limit of detection of (< 2 ppm).

4.2.4 Sphalerite

Sphalerite major- and minor-element chemistry was determined for sixty-two samples (379 analyses) from East Kemptville and four samples (40 analyses) from Duck Pond using EPMA. The results are provided in Electronic Appendix A.

The mole % Fe in sphalerite ranges from 12.5 to 18.7 (mean = 16.1; Fig 4.8a). Iron concentrations in the irregularly zoned sphalerite from the hydrothermal breccia shows more variability, with mole % Fe ranging from 3.3 to 16.0 (mean = 9.7), where lighter colored bands contain lower Fe concentrations. Iron concentrations in sphalerite from the Duck Pond deposit are more restricted and range from 11.8 to 16.1 mole % (mean = 15.0). Iron exhibits a negative correlation with Zn in all sphalerite (Fig. 4.8b). The concentration ranges of major- and minor-elements (i.e., Fe, Zn, Cu, Mn, Cd, In) in sphalerite from greisens and quartz-sulfide veins from the Main and Baby zone at East Kemptville are

similar (Fig 4.9a). Copper and Cd occur in 1000s of ppm, with Mn occurring in 100s to 1000s of ppm. Indium was detected in all sphalerite from East Kemptville, except for some crystals in the Baby Zone mineralized breccia. Indium concentrations in sphalerite from greisens and quartz-sulfide veins range from 700 to 12,300 ppm, with an average concentration of 2,200 ppm (Fig. 4.10a). Indium in sphalerite exhibits a positive correlation with Cu, with most data clustering around a molar In/Cu ratio of 1 (Fig. 4.10a). The sphalerite chemistry from the breccia consists of generally lower Mn, Cu, Cd, and higher Ag compared to the rest of the East Kemptville deposit. Sphalerite from the Duck Pond deposit in general contains lower concentrations of Cu, In, and Cd, and higher Mn concentrations compared to the East Kemptville deposit (Fig. 4.9a).

Trace- and minor-element chemistry of sphalerite (Fig. 4.9b) was determined by LA-ICP-MS for twenty-nine samples (80 analyses) from East Kemptville and two samples (7 analyses) from Duck Pond. Trace-element concentrations in sphalerite from greisen and quartz-sulfide veins from East Kemptville show low variability for a given element, and generally only vary within 1 order of magnitude. Sphalerite hosted in greisens and quartz-sulfide veins of the Main and Baby zones lack any significant differences in trace-element chemistry, with most elements exhibiting similar ranges and mean values (Fig. 4.9b). Cadmium and In occur in 1000s of ppm. Manganese and Cu range from 100s to 1000s of ppm, with Se occurring in 10s to 100s of ppm, and Co, Ag, Sn, Ga occurring in 1 to 10s of ppm. Nickel, Ge, As, Sb, Pb, and Bi typically occur in concentrations of less than 1 ppm.

Silver exhibits a positive correlation with Cu and In in sphalerite hosted by both greisens and quartz-sulfide veins (Fig. 4.10b). Whereas sphalerite from the greisens and quartz-sulfide veins are chemically similar, sphalerite from the hydrothermal breccia contains higher concentrations of Ga, Ge, As, Ag, Sn, Sb, and Pb, and lower concentrations of Co, Cu, Se, Cd, In, and Bi compared with sphalerite from greisens and veins (Fig. 4.10b). In zoned sphalerite from the hydrothermal breccia, the darker (Fe rich) zones contain higher concentrations of Co, Cu, Ga, Ge, As, Cd, Sn, and Sb compared with the lighter zones (Fe poor), with both types containing similar concentrations of Mn, Ni, Ag, In, Pb, and Bi. Trace- and minor-element chemistry of sphalerite from Duck Pond exhibits similar

variability and geochemical characteristics to sulfide minerals from greisens and quartz-sulfide veins from East Kemptville, although the average abundance of a given trace-element is typically lower (Fig. 4.10b). LA-ICP-MS spectra of indium-bearing sphalerite are characterized by smooth signals with low count variability for most elements. The exceptions are Sb, Pb, Bi, and, to a lesser extent, Sn and Ag, which are characterized by more significant variability (noise), as illustrated by Pb in Figure 4.11a; counts for these latter elements also commonly co-vary. Iron, Cu, Sn, and, to a lesser extent, Ag also exhibit peaks that commonly co-vary, as illustrated by Sn in Figure 4.11a.

4.2.5 Chalcopyrite

Chalcopyrite major- and minor-element chemistry was determined for fifty-five samples (179 analyses) from East Kemptville and one sample (5 analyses) from Duck Pond using EPMA. The results are provided in Appendix A. Chalcopyrite hosted in greisens and quartz-sulfide veins from both the Main and Baby zones at East Kemptville all have near stoichiometric major element compositions and similar ranges and mean values for most minor elements (i.e., Zn, In, Ag), except for Sn (Fig. 4.12a). Zinc concentrations range from 300 to 12,410 ppm, with an average concentration of 860 ppm. Tin concentrations range from below detection to 6,710 ppm, with an average concentration of 800 ppm. Tin concentrations in chalcopyrite from the Baby Zone exhibit a lower range and mean concentration compared with the Main Zone. Silver concentrations range from below detection to 1,220 ppm, with an average concentration of 400 ppm. Indium concentrations in chalcopyrite from greisens and quartz-sulfide veins from the East Kemptville deposit range from 100 to 1,400 ppm In, with an average concentration of 600 ppm. As with sphalerite, chalcopyrite from the hydrothermal breccia has a different chemistry compared to other samples. Crystals are compositionally zoned and are characterized by larger ranges and higher average concentrations of Sn and Zn, lower concentrations of Ag, and by no detectable indium by EPMA methods (Fig. 4.12a). Chalcopyrite from Duck Pond contains low concentrations of In and Ag compared to East Kemptville.

Trace- and minor-element chemistry of chalcopyrite (Fig. 4.12b) was determined by LA-ICP-MS from a total of nineteen samples (38 analyses) from the East Kemptville deposit. The concentrations of elements in chalcopyrite hosted in greisens and quartz-sulfide veins

from the East Kemptville deposit exhibit generally low variability (within 1 order of magnitude), with similar ranges and mean concentrations for a given trace element for both the Main and Baby Zone (Fig. 4.12b). Zinc, In, and Sn occur in concentrations generally greater than a 1000 ppm. Selenium concentrations range from 10s to 100s of ppm, with Mn, Cd, Pb ranging from several 1 to 10s of ppm, and Co, Ni, Ga, Ge, As, Sb, and Sb occur in concentrations of less than 1 ppm. One analysis of a chalcopyrite crystal from the hydrothermal breccia indicates similar concentrations of Co, Ni, Ge, As, Se, Sn, Bi, and Zn, but higher concentrations of Sb, Pb, and Mn, and lower concentrations of Ga, Ag, Cd, and In, compared to the rest of the East Kemptville samples (Fig. 4.12b). Cadmium and Zn in chalcopyrite from all analyses have a positive correlation (r = 0.8). Spectra from LA-ICP-MS analyses of chalcopyrite generally have smooth signals for most elements, with low count variability. The exceptions are Sb, Pb, and Bi, which have noisy spectra, as is illustrated by Pb in Figure 4.11b. Zinc, In, Sn, and, to a lesser extent, Cd, also exhibit peaks that commonly co-vary, as illustrated by Zn and Cd in Figure 4.11b.

4.2.6 Stannite

Stannite major- and minor-element chemistry was determined from a total of twelve samples (35 analyses) from the East Kemptville deposit using EPMA. Ideal stannite has the formula Cu_2FeSnS_4. Stannite from East Kemptville contains variable amounts of Zn (1,200-24,000 ppm), In (below detection-3300 ppm), and Ag (below detection-1990 ppm) (Fig. 4.14). Generally, indium and zinc are enriched in stannite that is associated with sphalerite, whereas indium in stannite associated with chalcopyrite or cassiterite is generally below detection. Stannite from quartz-sulfide veins contained lower concentrations of indium (max = 900 ppm) compared with stannite hosted by greisens. Indium concentrations in stannite are highest when associated with the unnamed Zn-In mineral.

4.2.7 Unnamed Zn-In Mineral

The chemistry of the unnamed Zn-In mineral was determined using EPMA, and contains ~18 wt.% indium, which is the highest concentration of any mineral at East Kemptville. The mineral is compositionally intermediate between sphalerite (ZnS) and roquesite ($CuInS_2$; Fig. 4.15). Assuming a sphalerite structure, the mineral formula can be expressed

as $Cu_{0.2}Zn_{0.4}In_{0.2}Fe_{0.2}S_{1.0}$. Indium exhibits a positive correlation with Cu, with a molar In/Cu ratio of 1. Concentrations of Cd and Fe are very similar to that of the associated sphalerite.

4.2.8 Pyrrhotite

Pyrrhotite has a consistent Fe concentration of ~60.3 wt.% ± 0.9 (1σ) as determined by EPMA and EDS analyses (Calculated = $Fe_{0.87}S$). Pyrrhotite trace-element chemistry was determined by LA-ICP-MS from twelve samples (17 analyses) from the East Kemptville deposit. Pyrrhotite from all analyses contains low concentrations of trace elements, with Mn, Co, Cu, and Zn ranging from 10s to 100s of ppm, and As, Ag, and Pb ranging from 1 to 10 ppm, with other trace elements typically occurring in concentrations of less than 1 ppm (Fig. 4.16a). Indium is present in very low concentrations in pyrrhotite, with a maximum concentration of 0.6 ppm. Pyrrhotite from the Main Zone contains lower Ni concentrations than the that from the Baby Zone and exhibits a greater variation in Co concentrations. (Fig. 4.16a) LA-ICP-MS spectra for most elements in pyrrhotite are characterized by smooth signals with low count variability, with the exception of Ag, Pb, Bi, and, to a lesser extent, Cu and Zn, which commonly co-vary, as is illustrated by Ag, Cu, Pb, and Zn in Figure 4.11c. Copper, and to a lesser extent Zn and Ag also exhibit peaks that commonly co-vary (Fig. 4.11c)

4.2.9 Pyrite

Pyrite major element chemistry, as determined by EDS and EPMA analyses, indicate near stoichiometric character (FeS_2). Pyrite trace-element chemistry was determined by LA-ICP-MS from a total of five samples (6 analyses) from East Kemptville and one sample (2 analyses) from Duck Pond. All pyrite analyzed has low trace-element contents, except for Co and Ni, which have concentrations of between 100 and 1000 ppm. Manganese, Cu, Se, and Pb occur in concentrations ranging from 1 to 10 ppm, with other trace elements typically occurring in concentrations of less than 1 ppm (Fig 4.16b). Indium concentrations in pyrite are very low (< 0.1 ppm; Fig. 3.15b). LA-ICP-MS spectra of pyrite are characterized by smooth signals with low count variability for most elements, except for Pb, Ag, Sn, Sb, and Bi, which exhibiting significant variability, as illustrated by Pb in

Figure 4.11d. Copper, Zn, and Sn also exhibit peaks that commonly co-vary, as illustrated by Cu and Zn in Figure 4.11d.

4.3 Sulfur Isotope Data

Sulfur isotopic analysis of sulfide mineral separates (hand-picked or micro-drilled) were performed on eighteen samples from the Main Zone, nineteen samples from the Baby Zone and four samples from the Duck Pond deposit. The sulfides analyzed were mainly from quartz-sulfide veins, with a minor number of greisen-hosted sulfides, and consisted of arsenopyrite (n = 3), pyrrhotite (n = 3), chalcopyrite (n = 6), sphalerite (n = 20), pyrite (n = 4), and galena (n = 1) (Fig. 4.17a). In situ (SIMS) sulfur isotopic analyses were performed on a total of four samples from the Main Zone, six samples from the Baby Zone, and one sample from the Duck Pond deposit. The sulfides analyzed by SIMS were mainly examples of greisen-hosted sulfide, with a minor number from quartz-sulfide veins. Multiple grains of each sulfide mineral (where present) were analyzed in a given sample to assess any within-sample variation (Fig. 4.17). Sulfides analyzed were: sphalerite (n = 37), chalcopyrite (n = 12), pyrrhotite (n = 7), and pyrite (n = 3) (Fig. 4.18b). All sulfur isotopic data (mineral separates and in situ) are provided in Appendices D and E, respectively. Summary statistics for in situ sulfur isotope analyses are provided in Table 4.2.

4.3.1 Mineral Separates

Most of the measured $\delta^{34}S$ values of sulfide minerals from the East Kemptville deposit span a relatively narrow range (4.9-7.0 ‰), with less than 1 ‰ variation in a given sample (Fig. 4.17a). An exception is the sulfides analyzed from the hydrothermal breccia, which exhibit a somewhat larger variation (3.1-7.4 ‰; Fig. 4.19a). The measured $\delta^{34}S$ of arsenopyrite ranges from 6.6 to 6.9 ‰ (mean = 6.8 ‰; Fig. 4.18a). Sphalerite displays a larger range of $\delta^{34}S$ values, from 5.2 to 7.4 ‰ (mean = 6.2 ‰; Fig. 4.18a). Chalcopyrite displays a narrow range of $\delta^{34}S$ values, from 4.9 to 5.9 ‰ (mean = 5.4 ‰; Fig. 4.18a). Pyrrhotite ranges from 5.5 to 5.6 ‰ (mean = 5.5 ‰; Fig. 4.18a). Pyrite ranges from 5.4 to 6.3 ‰ (mean = 5.9 ‰; Fig. 4.18a). The sulfide $\delta^{34}S$ values exhibit little variation between the Main and Baby zones (Fig. 4.19a). The $\delta^{34}S$ of sphalerite and pyrite from the Duck pond deposit are higher than any of the minerals from East Kemptville and exhibit a narrow range, from 7.5 to 8.5 ‰ (mean = 8.2 ‰; Fig. 4.19a).

4.3.2 In Situ Sulfur Isotopes

The $\delta^{34}S$ values obtained from SIMS analysis for the East Kemptville deposit extend to lower (0.7 ‰) to higher (9.8 ‰) values compared to those obtained from mineral separate analyses (Fig. 4.18b). In-sample variation of $\delta^{34}S$ values for a given mineral range from 0.3 to 6.9 ‰ (Table 4.2). For example, the $\delta^{34}S$ values of sphalerite from sample EK-4-153.2 extend over a range of 3.5 ‰ (2.5-6.0 ‰), which is larger than the range for all sphalerite mineral separates (2.2 ‰). Individual sphalerite grains also can exhibit large variations. For example, one sphalerite grain in sample EK-11-103.9 has $\delta^{34}S$ values that range over 6.9 ‰, Generally, for a given sample, however, $\delta^{34}S$ values of sphalerite vary less than 3.0 ‰, pyrrhotite varies less than 2.5 ‰, chalcopyrite varies less than 2.0 ‰, and pyrite varies less than 1.5 ‰ (Table 4.2). No systematic variations in $\delta^{34}S$ values were recognized at the grain scale (i.e. zoning). Greisen-hosted sulfides have the lowest $\delta^{34}S$ values measured (0.7 ‰), and quartz-sulfide veins have the highest $\delta^{34}S$ values measured (9.8 ‰), with the average sulfur-isotopic composition of sulfides from quartz-sulfide veins being slightly higher than those from greisens (~4.1 vs 5.4 per mil; Fig. 4.19b). A comparison of the SIMS and mineral separate results on sphalerite from five in samples indicates that there is much more within-sample variation in $\delta^{34}S$ than the mineral separate data indicate (Table 4.2). Generally, the average $\delta^{34}S$ of sphalerite from SIMS analysis are within 1.0 ‰ of the mineral separates value, except for one sample that had a difference of 3 ‰.

The $\delta^{34}S$ values of minerals from the Duck Pond deposit range from 4.6 to 9.8 ‰ (mean = 7.4 ‰), which, as with East Kemptville, is larger than the range determined from mineral separates (Fig. 4.19b). The $\delta^{34}S$ of sphalerite ranges from 8.0 to 9.8 ‰ (mean = 8.7 ‰), with duplicate analyses of individual grains exhibiting ≤ 0.5 ‰ variation. The measured $\delta^{34}S$ of pyrite ranges from 4.6 to 5.4 ‰ (mean = 5.1 ‰), which has a similar range but different mean $\delta^{34}S$ compared to mineral separates (8.4 ‰). The one pyrrhotite SIMS $\delta^{34}S$ value determined was 5.9 ‰.

4.3.2 Mineral Geothermometry

The partitioning of Fe and Zn between co-precipitating sphalerite and stannite is known to be temperature dependent (Nekrasov et al., 1979; Nakamuru & Shima, 1982). The

equations provided by Nakamuru & Shima (1982) were used to calculate formation temperatures from sphalerite-stannite pairs. Temperature estimates were calculated from analyses that contained no evidence of contamination from other minerals and that contained low concentrations of minor and trace elements (< 1.4 wt.%). For example, if Sn was detected in the analyses of sphalerite, likely the analyses was contaminated by nearby cassiterite. Stannite selected for thermometry occurred either as an overgrowth on (i.e., partial rim) or as an inclusion in sphalerite. Temperatures were calculated for eight sphalerite-stannite pairs from a total of five greisen-hosted samples (Main; n = 3, Baby; n = 2). Calculated temperatures from the Main Zone range from 232-275 ℃, and temperatures determined for the Baby Zone were 252 ℃ and 265 ℃ (Table. 4.3). Duplicate sphalerite-stannite pairs from a given sample are similar (within 20 ℃). Temperatures provided by overgrowth and inclusions pairs provide similar results.

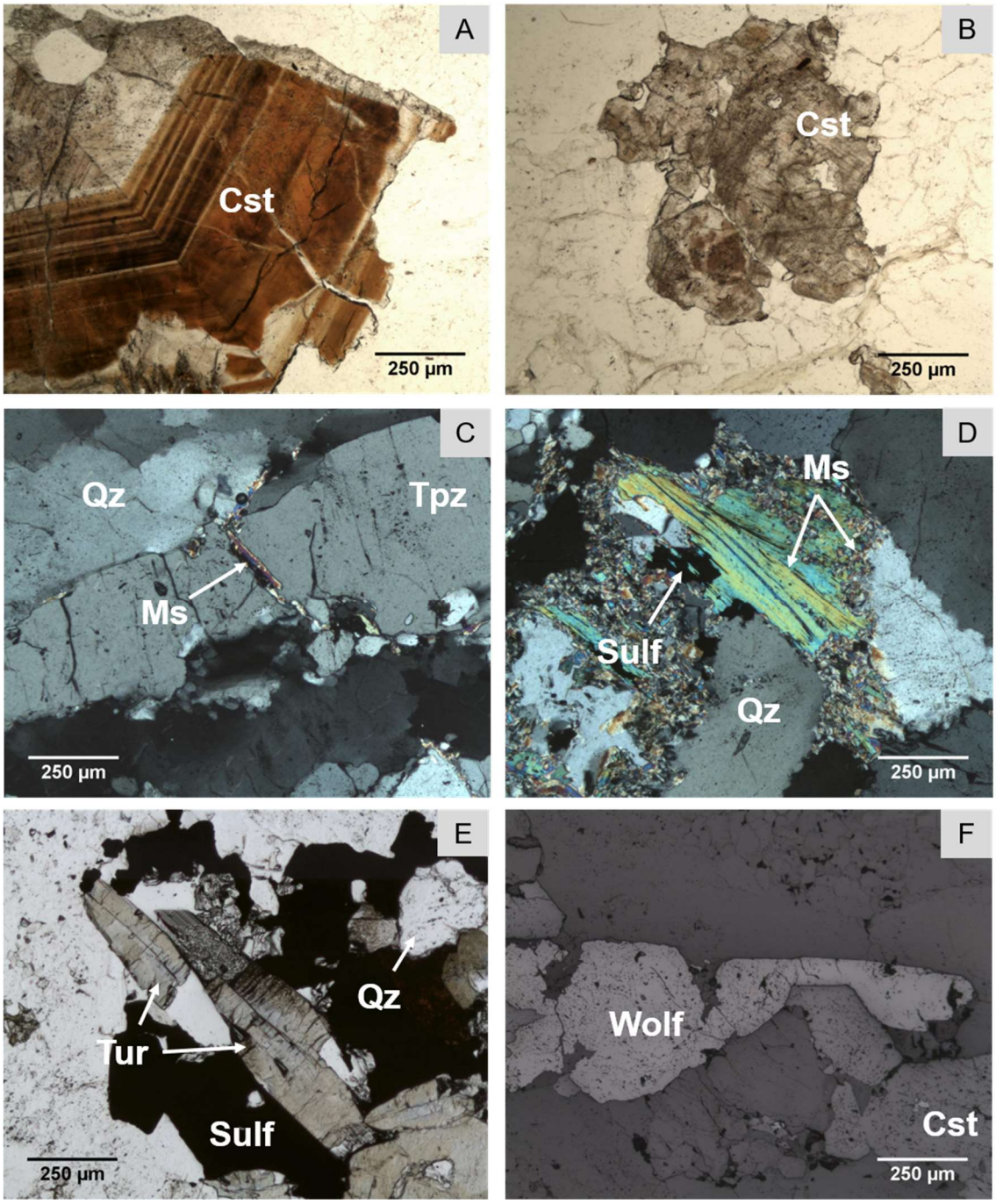

Figure 4.1 Plane-polarized and reflected-light images illustrating the textural characteristics of oxides in the East Kemptville deposit. (A) Euhedral cassiterite exhibiting oscillatory zoning in a greisen vein. (B) Subhedral cassiterite exhibiting weak zonation in a massive greisen. (C) Subhedral topaz and adjacent quartz, with muscovite alteration along a fracture in a topaz grain from a massive greisen. (D) Medium-grained muscovite that is replaced by minerals in a greisen selvage. (F) Wolframite and cassiterite exhibiting planar grain boundaries in a greisen selvage. Cst = cassiterite, Qz = quartz, Tpz = topaz, Ms = muscovite, Sulf = sulfide minerals, Tur = tourmaline, Wolf = wolframite.

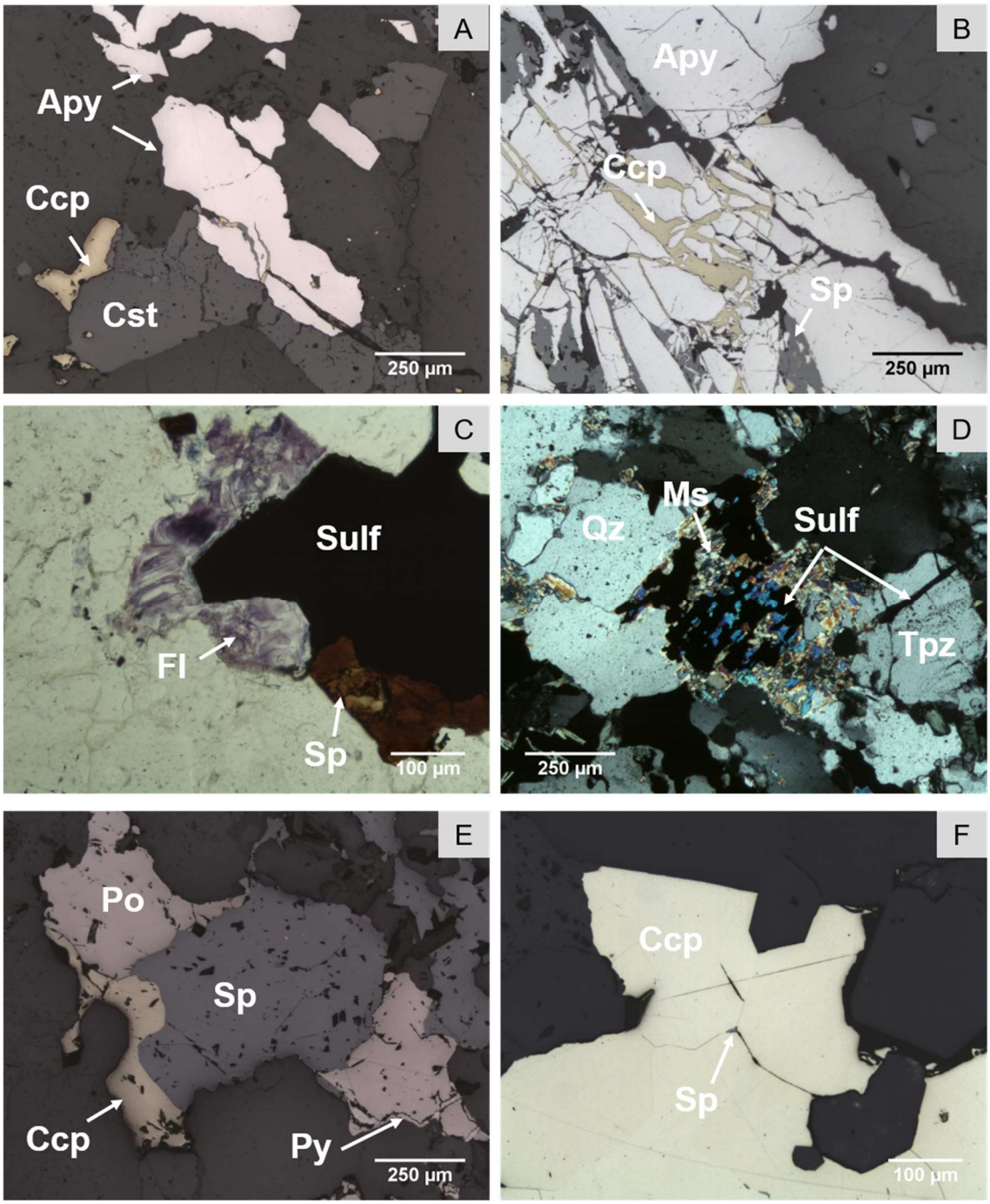

Figure 4.2 Plane-polarized and reflected-light images illustrating the textural characteristics of sulfide minerals in the East Kemptville deposit. (A) Discrete grains of arsenopyrite in a greisen vein. (B) Arsenopyrite with fractures filled by chalcopyrite, sphalerite, and quartz in a greisen vein. (C) Base-metal sulfides (i.e., sphalerite, chalcopyrite, pyrrhotite) that have filled a vug that also contains quartz and fluorite in a massive greisen. (D) Replacement of muscovite and fracture fill of topaz by pyrrhotite and

chalcopyrite in a massive greisen. (E) Pyrrhotite, sphalerite, and chalcopyrite exhibiting equilibrium boundaries in a massive greisen. Pyrrhotite is replaced by pyrite. (F) Euhedral chalcopyrite exhibiting a triple-junction in a greisen selvage. Sphalerite occurs along the grain boundaries. Cst= cassiterite, Apy = arsenopyrite, Ccp = chalcopyrite, Sp = sphalerite, Sulf = sulfide minerals, Fl = fluorite, Ms = muscovite, Qz = quartz, Tpz = topaz, Po = pyrrhotite, Py = pyrite.

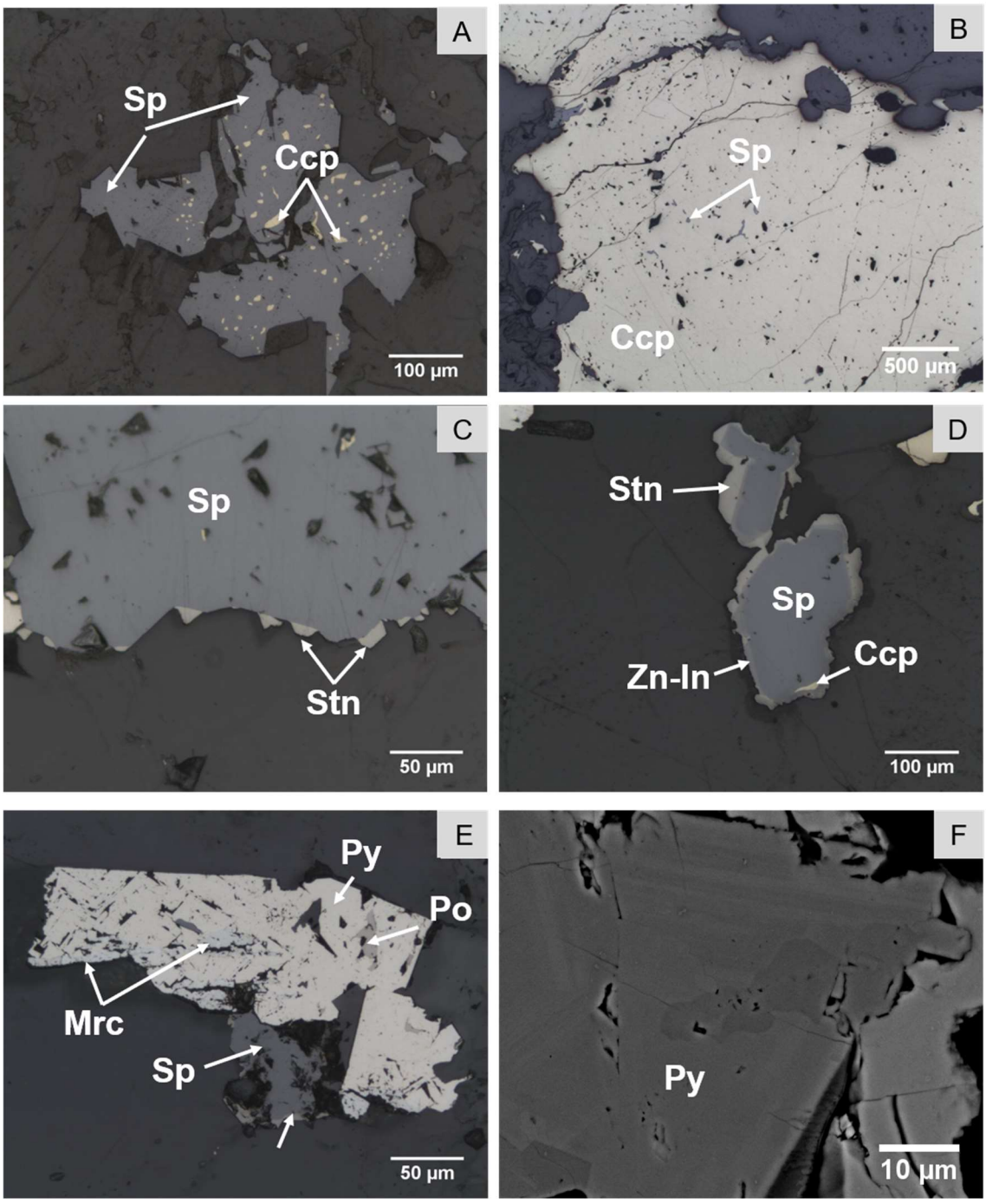

Figure 4.3 Reflected-light and BSE images illustrating the textural characteristics of sulfide minerals in the East Kemptville deposit. (A) Sphalerite with inclusions of chalcopyrite (i.e., 'chalcopyrite disease') in a greisen vein. (B) Chalcopyrite with inclusions of sphalerite in a greisen vein (C) euhedral overgrowth of stannite on sphalerite in a massive greisen. (D) Sphalerite rimmed by the unnamed Zn-In mineral and stannite in a greisen selvage. (E) Pyrite with cuspate inclusions of pyrrhotite and marcasite alteration along grain boundaries in a greisen selvage (F) Euhedral pyrite, exhibiting growth zonation

in a greisen selvage. Sp = sphalerite, Ccp = chalcopyrite, Stn = stannite, Zn-In = unnamed Zn-In mineral, Po = pyrrhotite, Py = pyrite, Mrc = Marcasite.

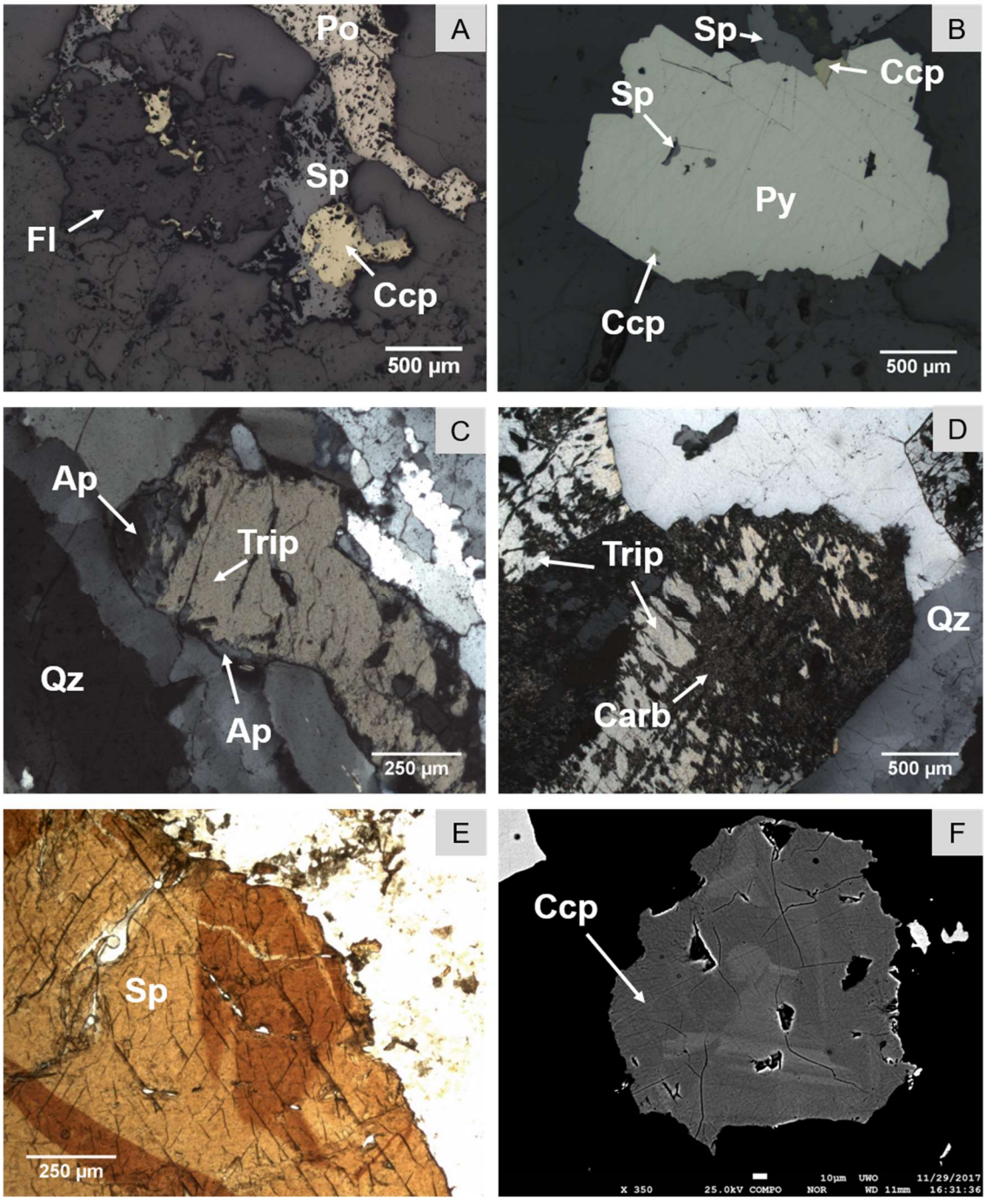

Figure 4.4 Reflected-light, plane-polarized, and BSE images illustrating the textural characteristics of sulfide minerals in the East Kemptville deposit. (A) Sphalerite, chalcopyrite, and pyrrhotite intergrown with fluorite in a quartz-sulfide vein. (B) Pyrite with inclusions of sphalerite and chalcopyrite in a quartz-sulfide vein. (C) Apatite exhibiting incipient replacement of triplite in a quartz-sulfide vein. (D) Carbonate that has replaced triplite in a quartz-sulfide vein. (E) Compositionally zoned sphalerite in the Baby Zone breccia. (F) Compositionally zoned chalcopyrite in the Baby Zone breccia. Sp =

sphalerite, Ccp = chalcopyrite, Po = pyrrhotite, Fl = fluorite, Py = pyrite, Qz = quartz, Trip = triplite, Ap = apatite, Carb = carbonate minerals.

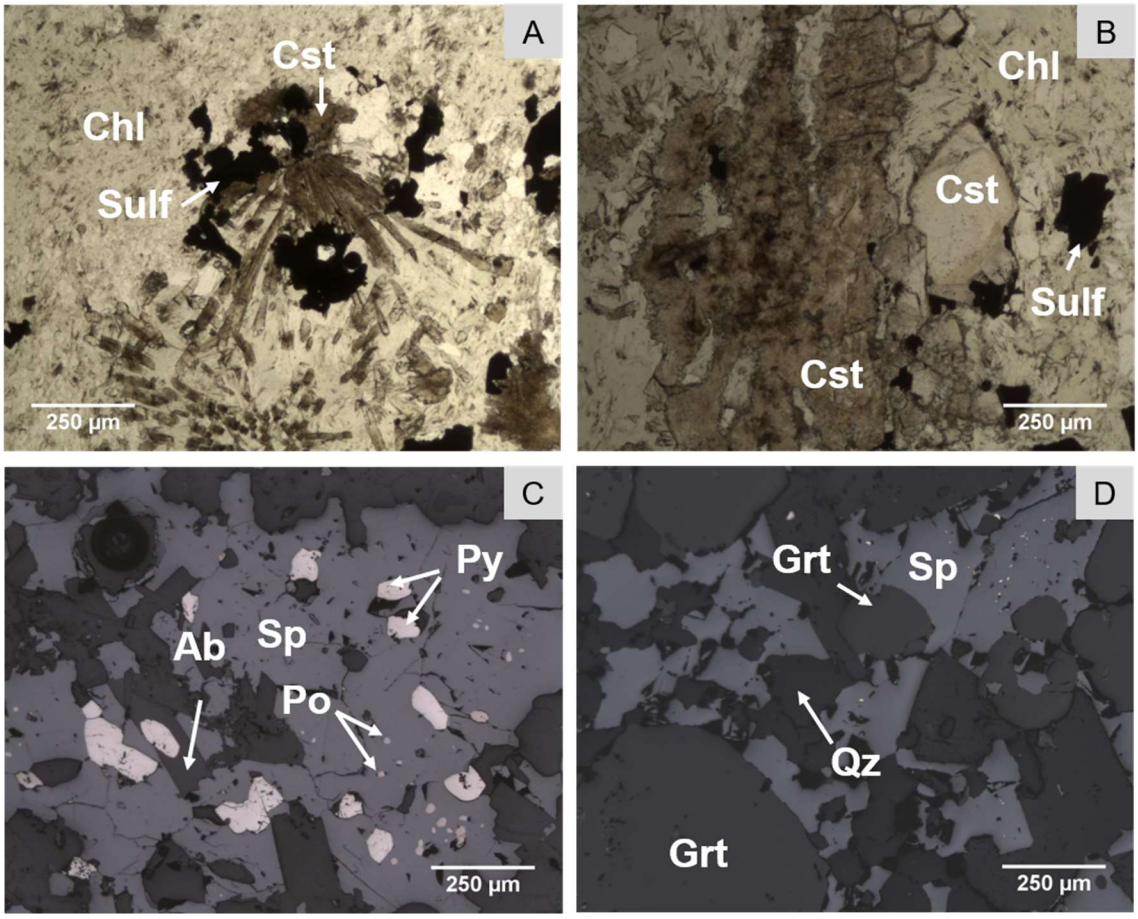

Figure 4.5 Plane-polarized and reflected-light images illustrating the textural characteristics of oxide and sulfide minerals of the Duck Pond deposit. (A) acicular crystals of cassiterite in a chlorite matrix. (B) Equant crystals and aggregates of cassiterite in a chlorite matrix. (C) Sphalerite and pyrite intergrown with albite. (D) Sphalerite that has replaced the matrix around garnet and quartz. Cst = cassiterite, Chl = chlorite, Sulf = sulfide minerals, Sp = sphalerite, Po = pyrrhotite, Py = pyrite, Ab = albite, Grt = garnet, Qz = quartz.

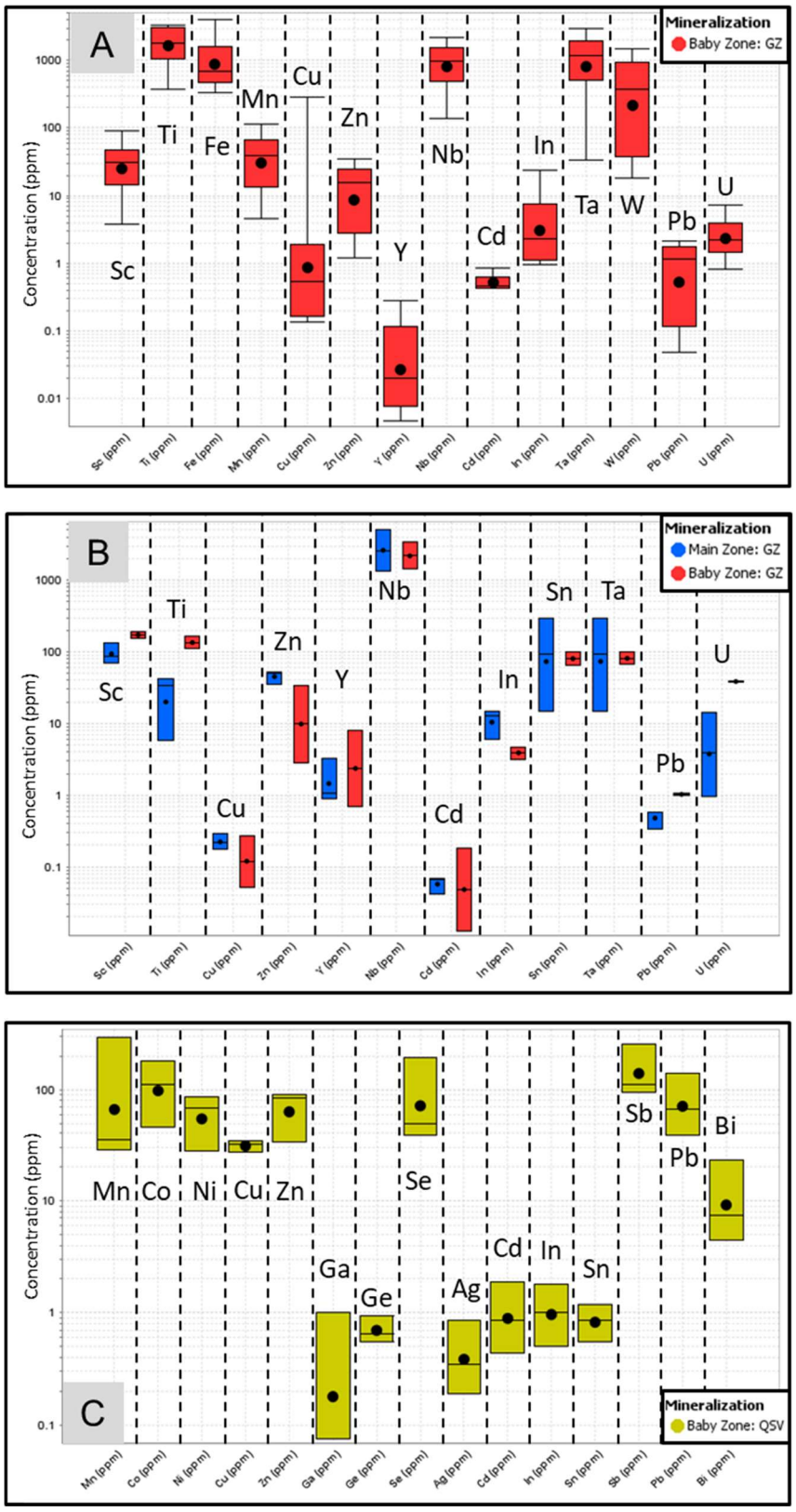

Figure 4.6 Box-whisker diagrams comparing the mineral minor and trace-element chemistry determined by LA-ICP-MS for (A) cassiterite, (B) wolframite, and (C)

arsenopyrite. Note the logarithmic scale for the concentrations. The whiskers represent the 10th and 90th percentile, the lower end and upper end of the box represent the 25th and 75th percentile, the line inside the box represents the median, the black circle represents the mean, and open circles represent data below the 10th and above the 90th percentile. GZ = greisen-hosted, QSV = quartz-sulfide vein.

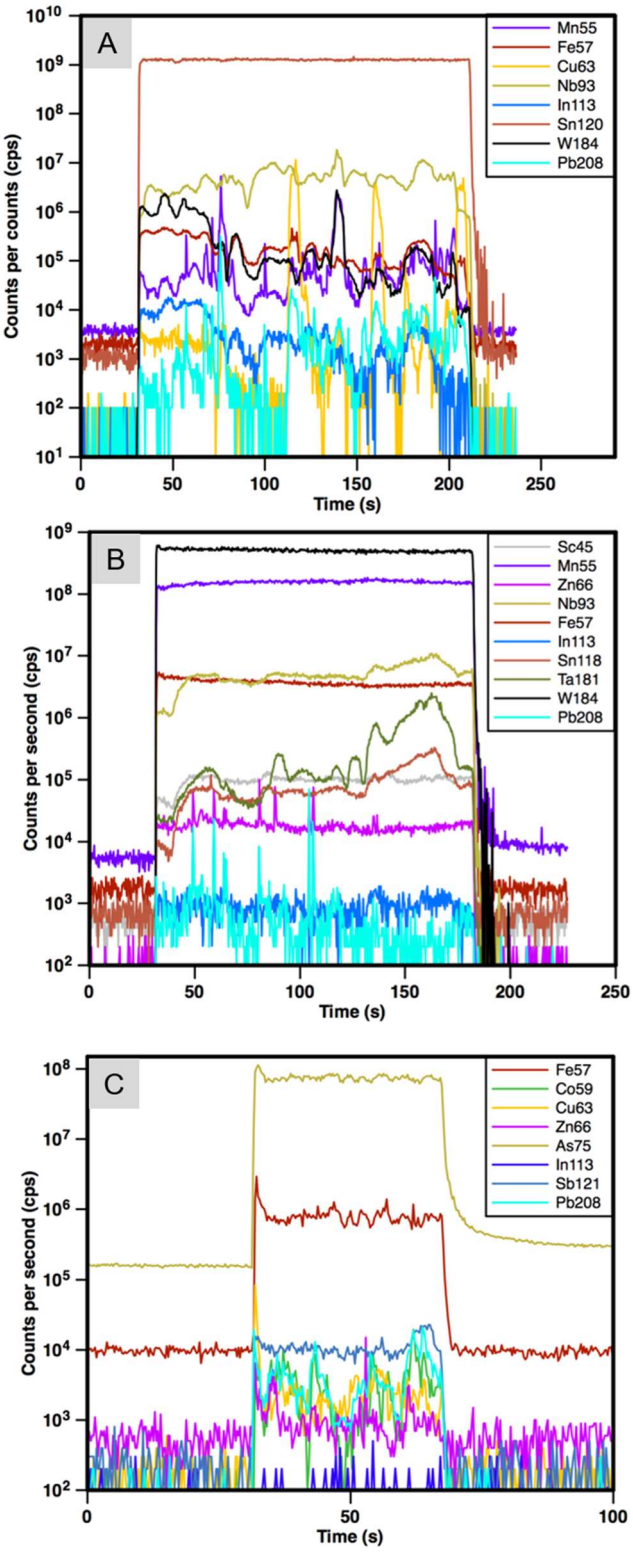

Figure 4.7 Representative time-resolved LA-ICP-MS spectra for (A) cassiterite, (B) wolframite, and (C) arsenopyrite. Note the logarithmic scale on the counts per second axis (cps).

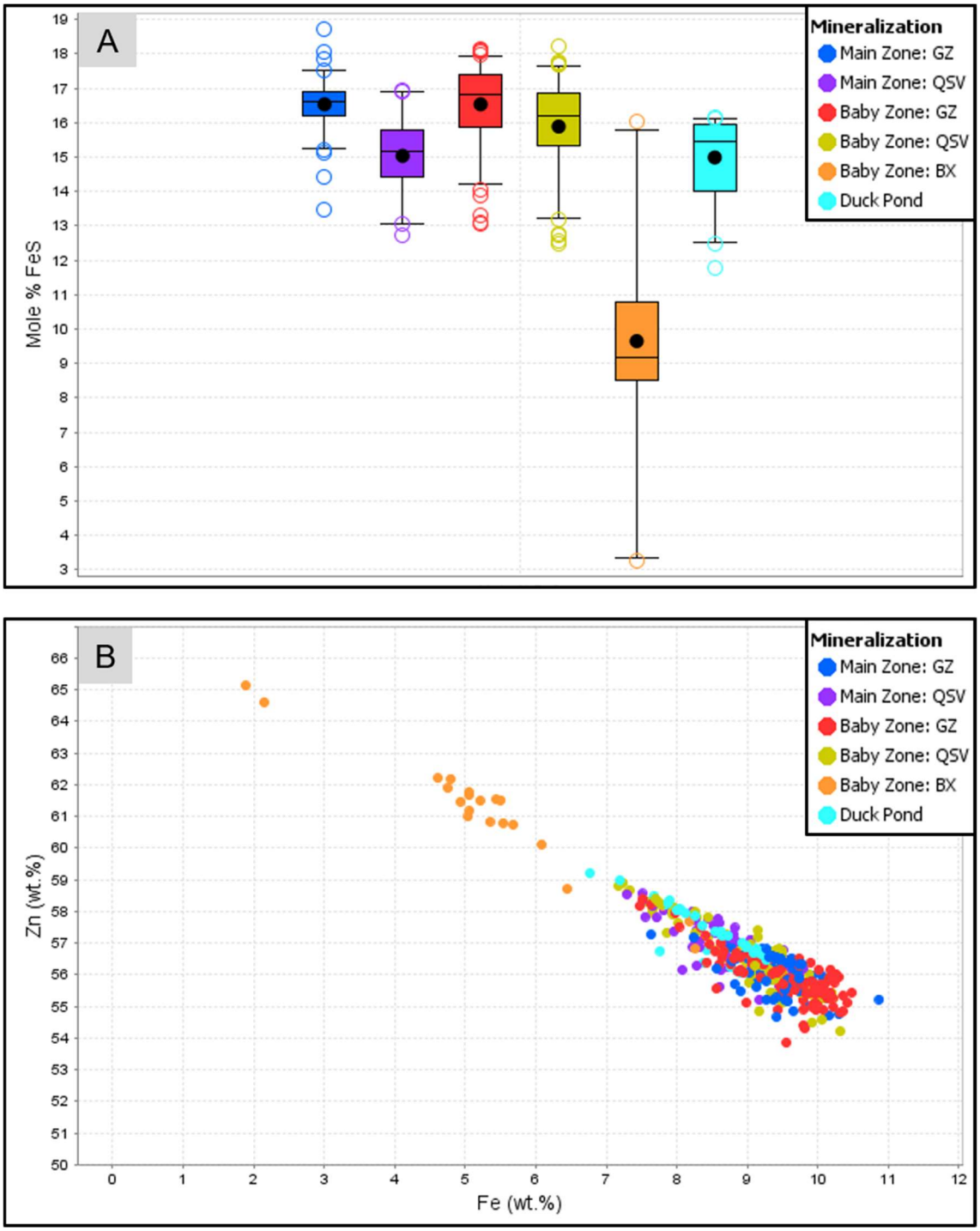

Figure 4.8 Bivariate plots illustrating the major-element composition of sphalerite from the East Kemptville and Duck Pond deposits. (A) Box-whisker diagram illustrating the mole % of FeS in sphalerite from different types of mineralization, (B) A bivariate plot of Fe vs Zn, illustrating covariation between the two elements. GZ = greisen-hosted, QSV = quartz-sulfide vein, BX = breccia.

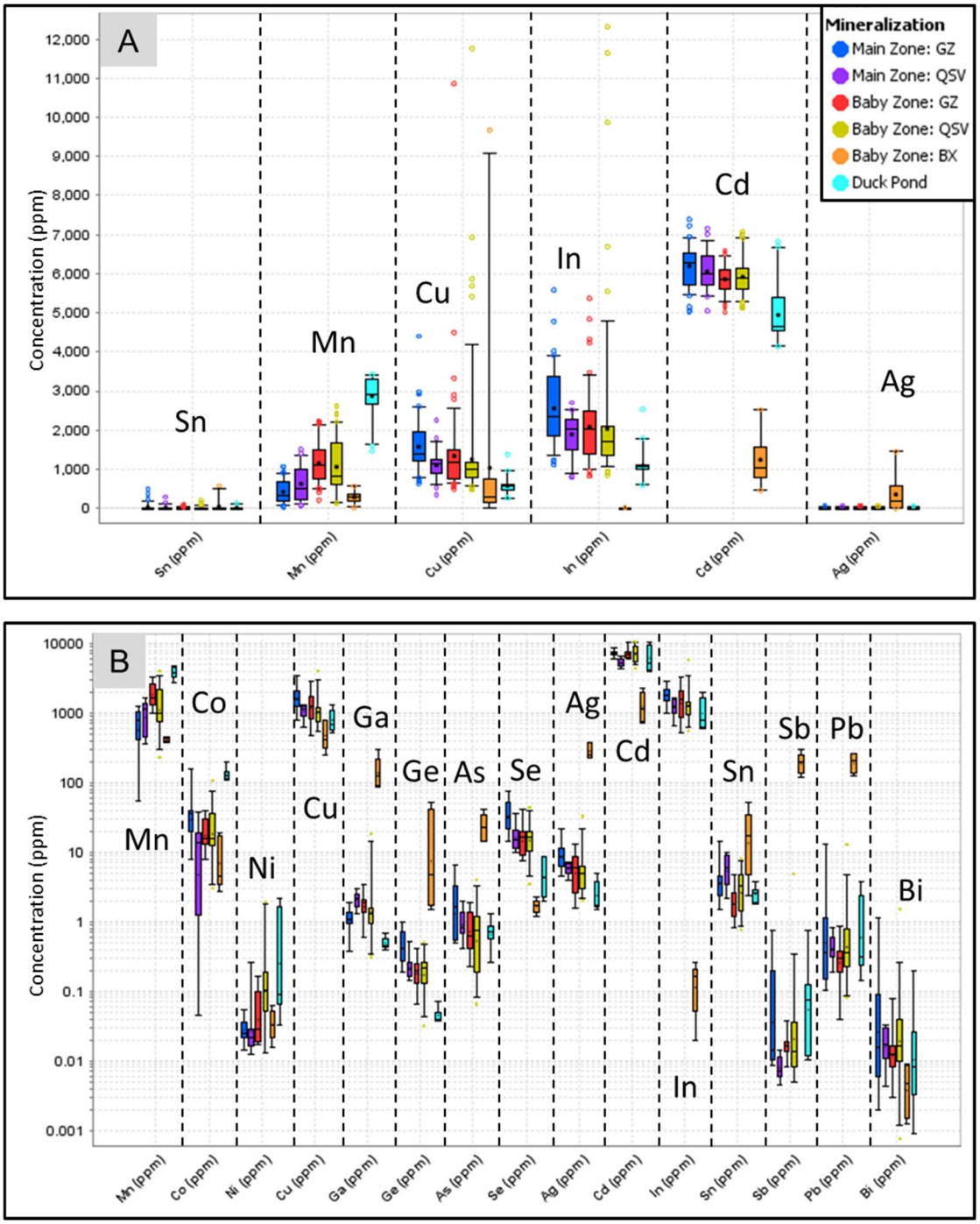

Figure 4.9 Box-whisker diagrams illustrating the chemical composition of sphalerite (A) major- and minor-element concentrations determined by EPMA (B) Minor- and trace-element concentrations determined by LA-ICP-MS; note the logarithmic scale for the concentrations in B. GZ = greisen-hosted, QSV = quartz-sulfide vein, BX = breccia.

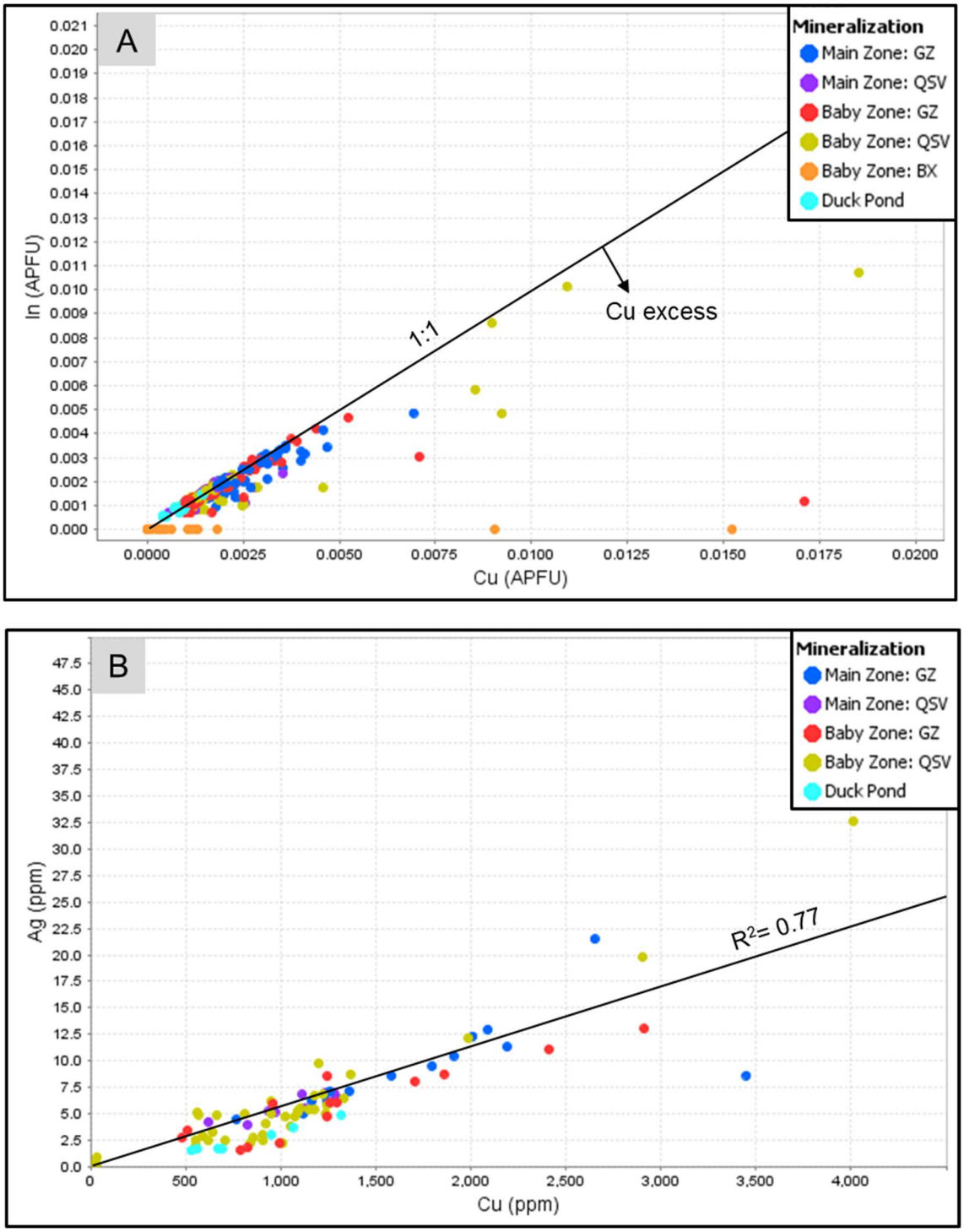

Figure 4.10 Bivariate diagrams illustrating the correlation of (A) Cu vs In, with a reference line indicating 1:1 Cu/In, and (B) Ag vs Cu in sphalerite with a positive linear correlation ($R^2 = 0.77$), GZ = greisen-hosted, QSV = quartz-sulfide vein, BX = breccia.

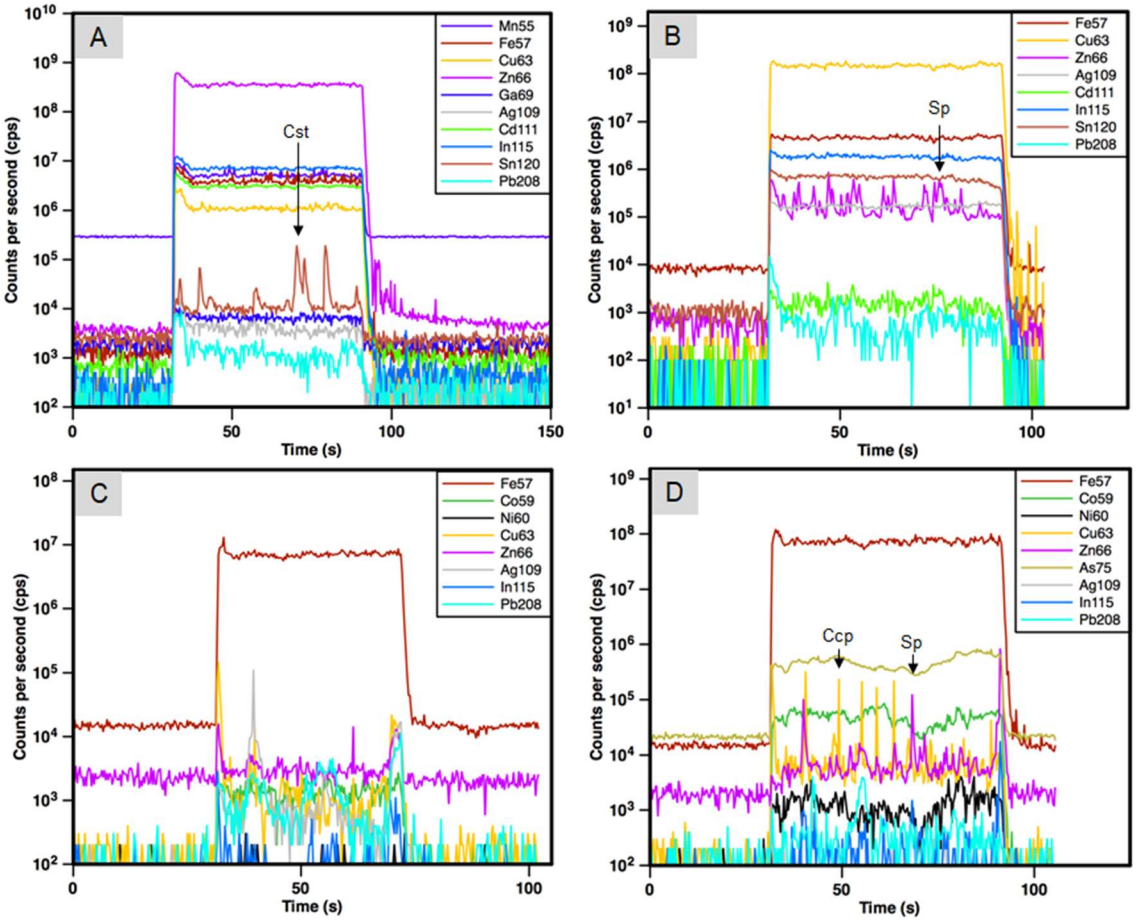

Figure 4.11 Representative time-resolved LA-ICP-MS spectra for sulfide minerals (A) sphalerite, (B) chalcopyrite, (C) pyrrhotite, and (D) pyrite. Note the logarithmic scale for the counts per second (cps). Cst = cassiterite, Sp = sphalerite, Ccp = chalcopyrite.

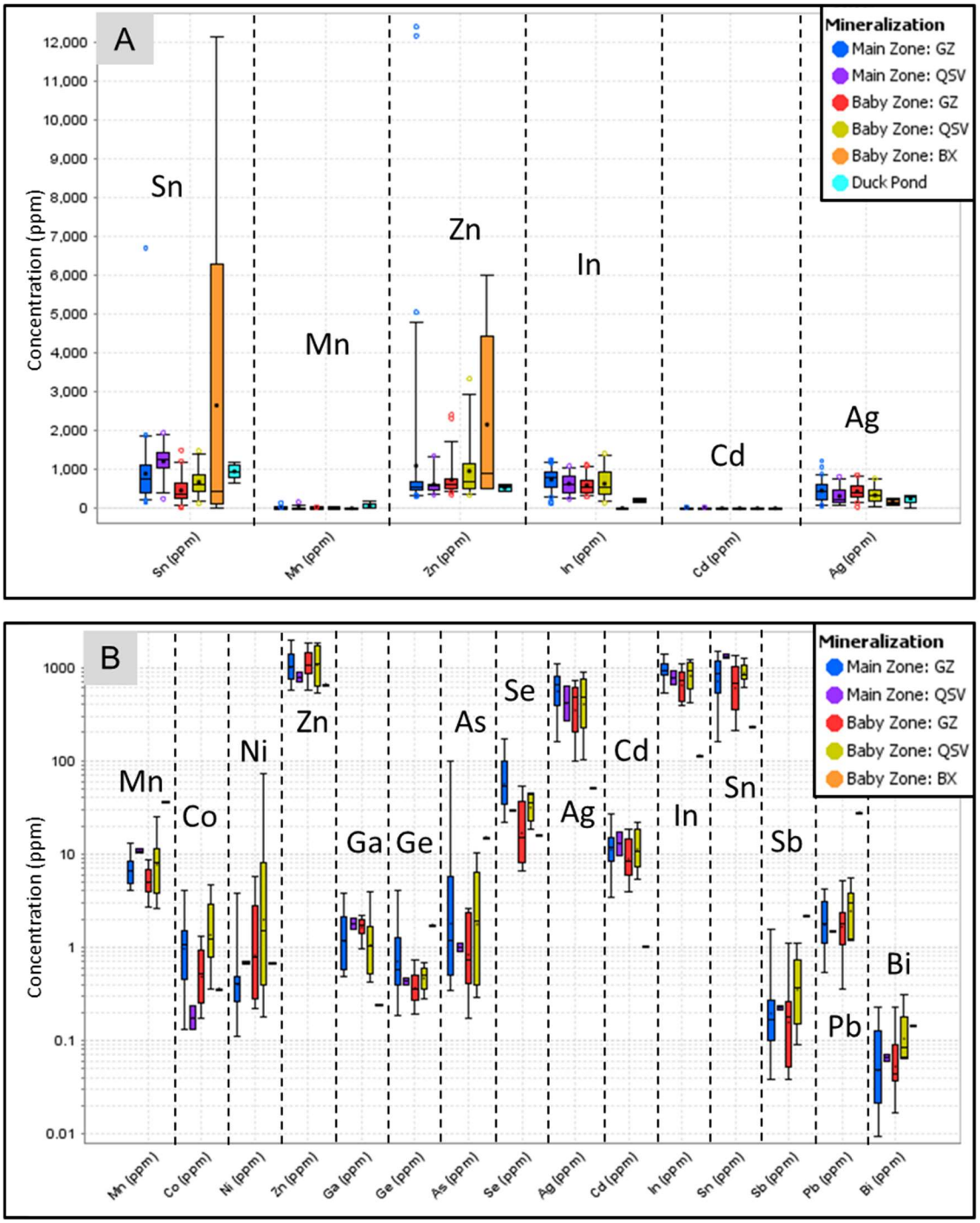

Figure 4.12 Box-whisker diagrams illustrating the chemical composition of chalcopyrite. (A) Major- and minor-element concentrations determined by EPMA. (B) Minor- and trace-element concentrations determined by LA-ICP-MS; note the logarithmic scale for the concentrations in B. GZ = greisen-hosted, QSV = quartz-sulfide vein, BX = breccia.

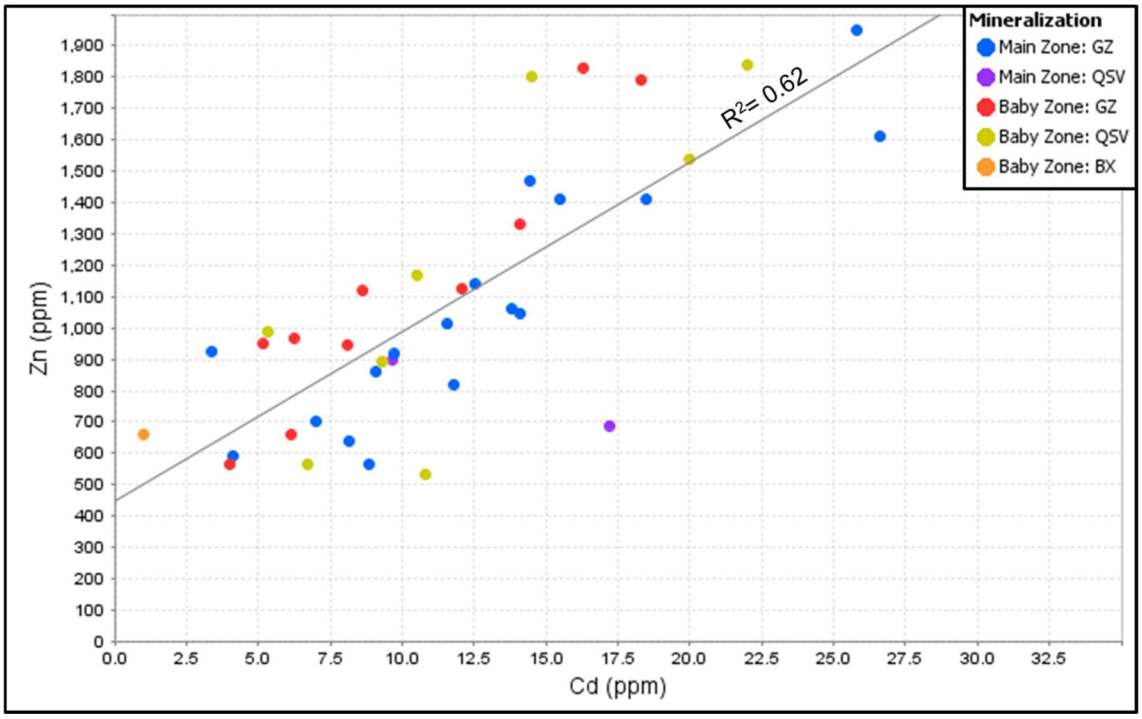

Figure 4.13 Bivariate diagrams illustrating the correlation of Cd vs Zn in chalcopyrite from the East Kemptville deposit. Note the positive linear correlation ($R^2 = 0.62$) for all the East Kemptville samples. GZ = greisen-hosted, QSV = quartz-sulfide vein, BX = breccia.

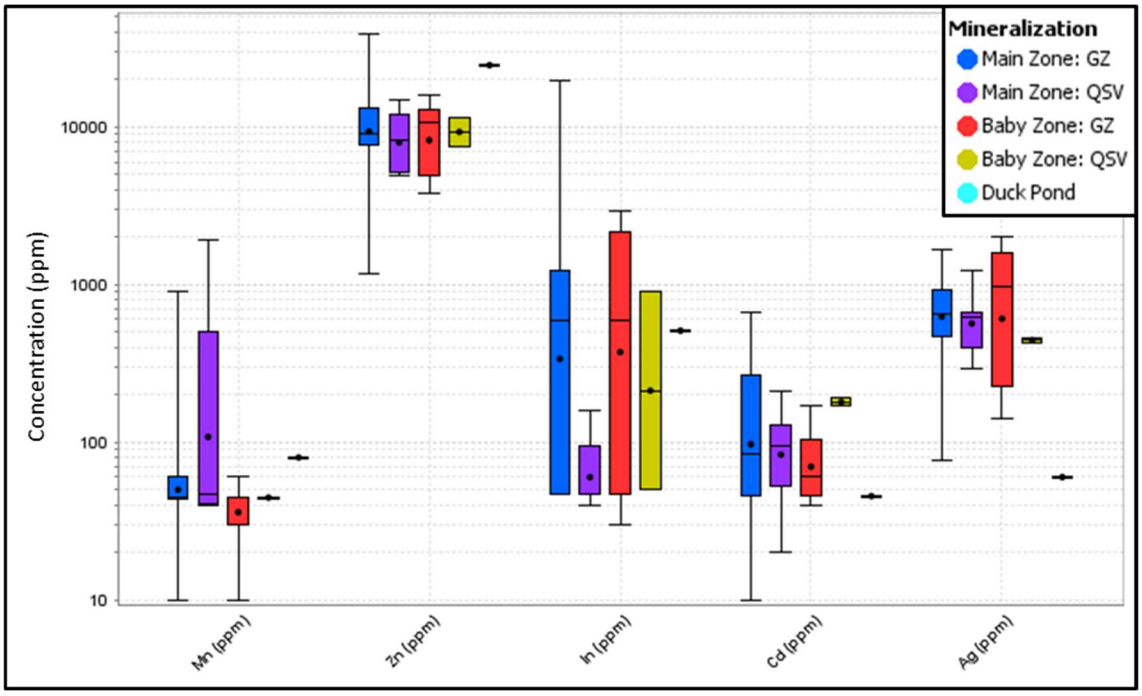

Figure 4.14 Box-whisker diagram illustrating the minor- and trace-chemical concentrations in stannite determined by EPMA. GZ = greisen-hosted, QSV = quartz-sulfide vein, BX = breccia.

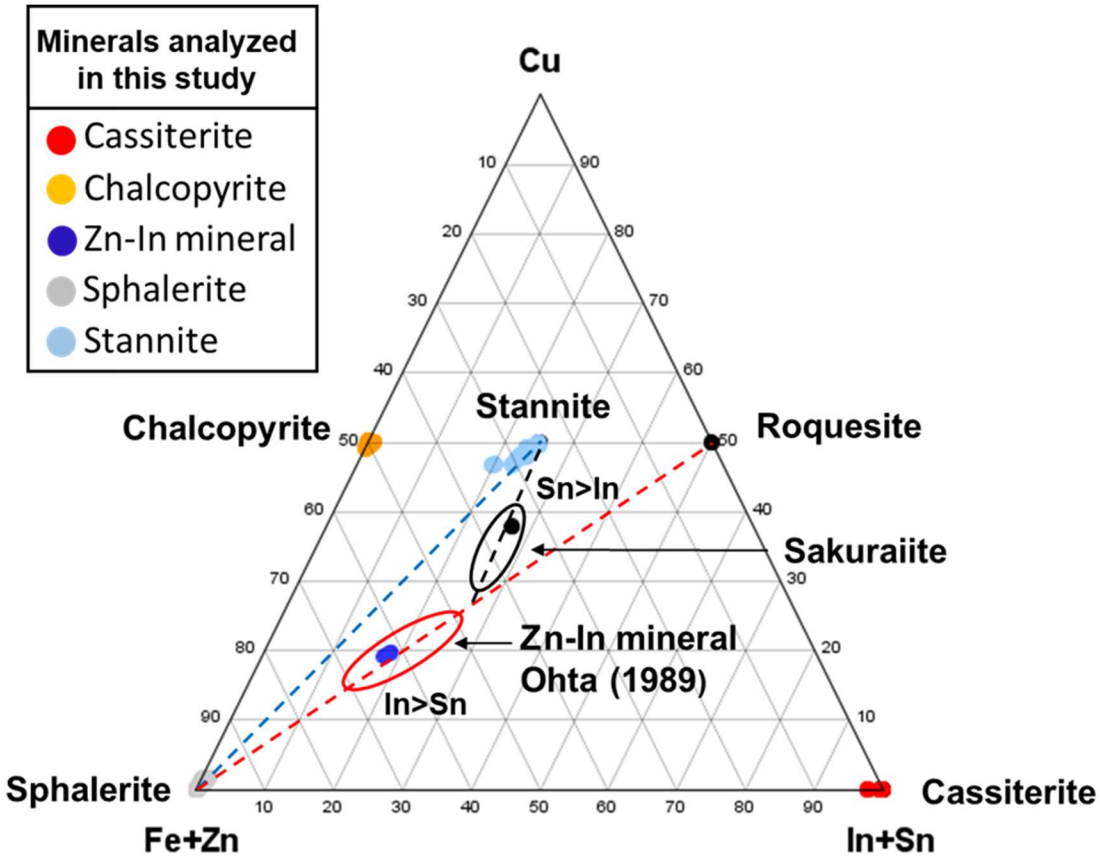

Figure 4.15 Molar proportions of Cu, (Fe+Zn), and (In+Sn) in indium-bearing minerals from the East Kemptville deposit. The red tie-line between sphalerite and roquesite represents the solid solution series defined by the coupled substitution of (Cu + In) ↔ 2 (Zn+Fe). The red circle along the red tie-line indicates the compositional range of the unnamed Zn-In mineral as reported by Ohta (1989). The blue tie-line between sphalerite and stannite-group minerals represents a solid solution series defined by the coupled substitution of (Cu_2Sn) ↔ 2(Zn, Fe). The black tie-line between stannite and the sphalerite-roquesite solid solution represents the couple substitution of (Zn,Fe)In ↔ (CuSn), along which sakuraiite is defined (Shimizu et al., 1986). The black dots indicate the ideal mineral composition for sakuraiite and roquesite.

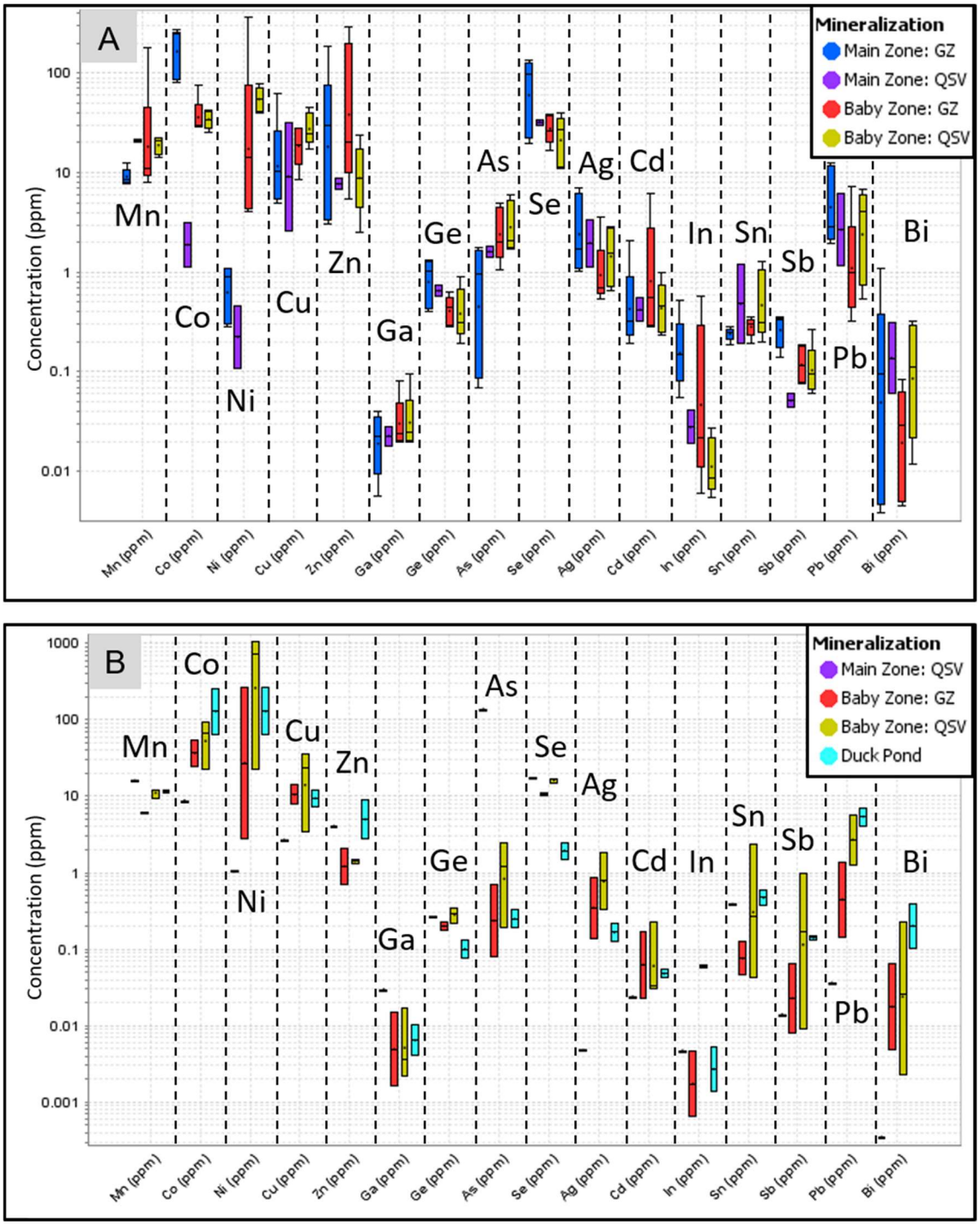

Figure 4.16 Box-whisker diagrams illustrating the minor- and trace-element concentrations determined by LA-ICP-MS for (A) pyrrhotite (B) pyrite. Note the logarithmic scale for the concentrations. GZ = greisen-hosted, QSV = quartz-sulfide vein, BX = breccia.

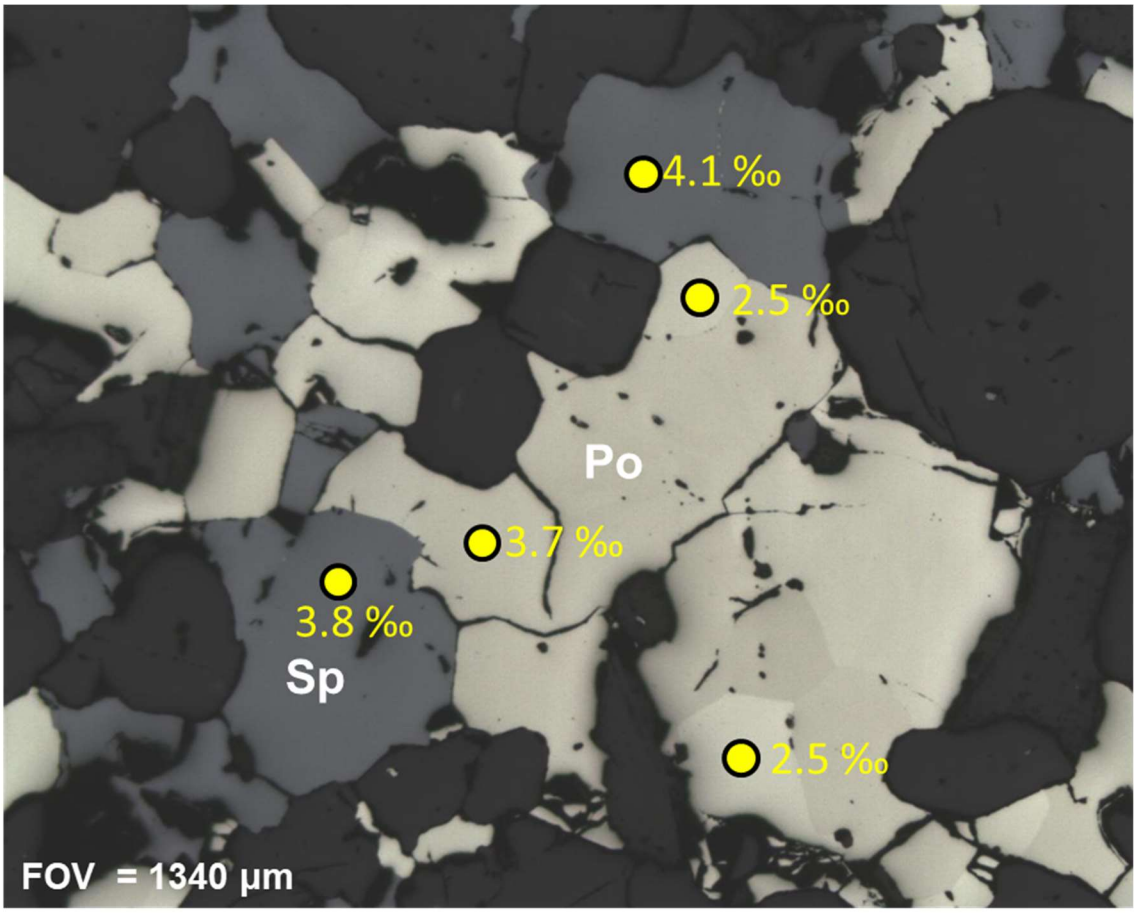

Figure 4.17 In situ sulfur isotopic spot analysis by SIMS of a typical sulfide assemblage from the East Kemptville deposit. Yellow circles show the location of an analysis; numbers show the corresponding $\delta^{34}S$ value. FOV = field of view, Sp = sphalerite, Po = pyrrhotite.

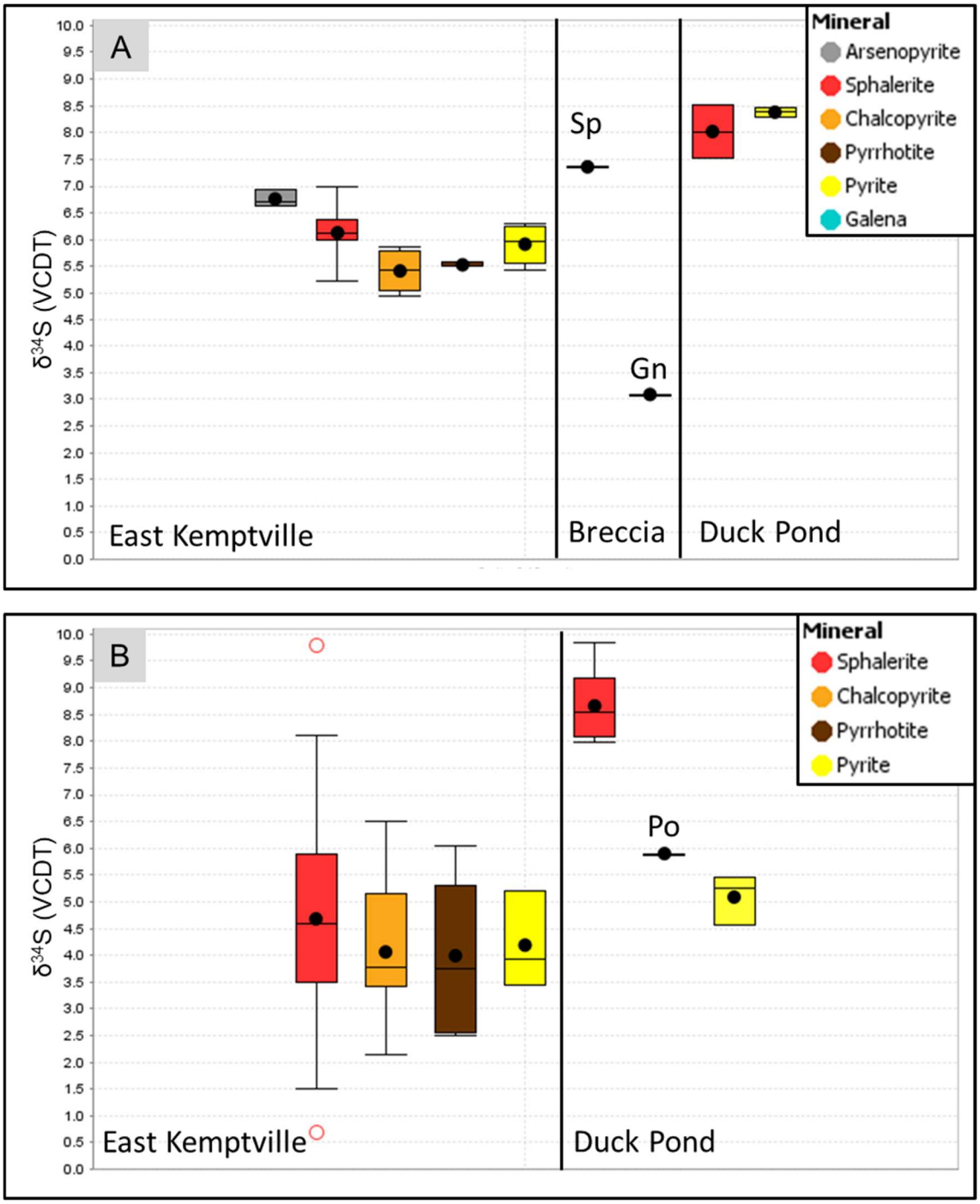

Figure 4.18 Box-whisker diagrams illustrating the sulfur isotopic composition ($\delta^{34}S$) of sulfide minerals from the East Kemptville and Duck Pond deposits. (A) Data from mineral separates and (B) Data from SIMS. Note that all sulfur isotopic values are reported in standard delta notation (per mil) relative to the Vienna Canyon Diablo Troilite (V-CDT) standard. EK = East Kemptville, DP = Duck Pond, BX = Breccia, Sp = sphalerite, Gn = Galena, Po = pyrrhotite.

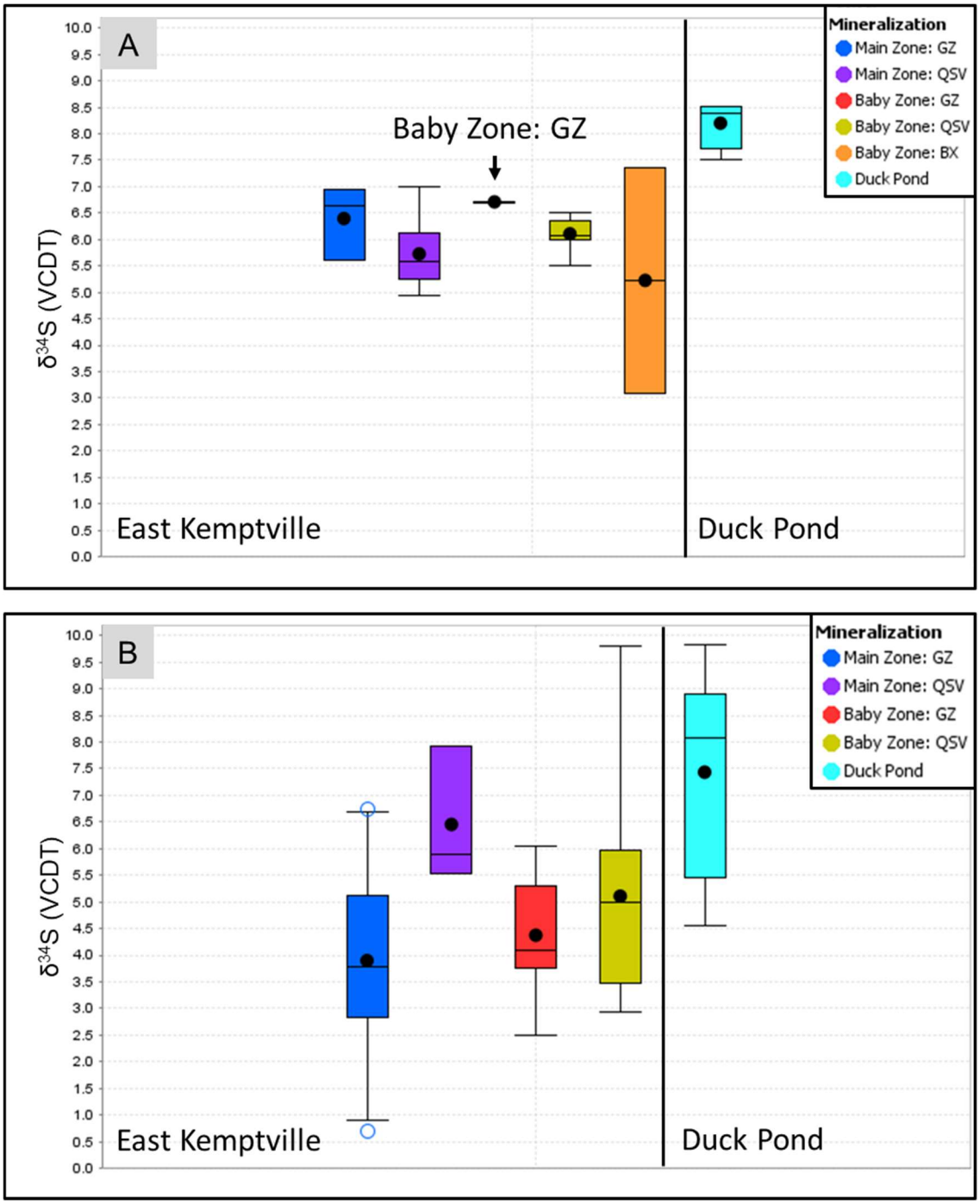

Figure 4.19 Box-whisker diagrams illustrating the sulfur isotopic composition ($\delta^{34}S$) of sulfides from the East Kemptville and Duck Pond deposits for the different mineralization styles. (A) Data from mineral separates and (B) Data from SIMS. Note that all sulfur isotopic values are reported in standard delta notation (per mil) relative to the Vienna Canyon Diablo Troilite (V-CDT) standard. GZ = greisen-hosted, QSV = quartz-sulfide vein, BX = breccia.

Table 4.1 Mass % of minerals, determined by QEMSCAN®, for selected samples (thin sections) from the East Kemptville deposit.

Sample		EK-11-88.9	EK-11-102.9	EK-25-115.5	EK-16-83.1	EK-2-135.5	EK-19-165.3	EK-15-183.8	EK-28-76.6	EK-9-139	EK-26-196.5	EK-28-181.7	EK-28-226.7	EK-11-38.1	EK-4-153.2
Zone		Baby	Baby	Main	Main	Baby	Main	Baby	Main	Baby	Main	Main	Main	Baby	Baby
Sample type		Greisen	Greisen	Greisen	Greisen	Greisen	Greisen	Greisen	Greisen	Greisen	Greisen	Greisen	Greisen	Breccia	Greisen
Alteration		Quartz-Topaz	Quartz-Topaz	Quartz-Topaz	Quartz-Topaz	Quartz-Muscovite	Quartz-Muscovite	Muscovite	Muscovite	Topaz	Topaz	Zoned Greisen	Zoned Greisen		Quartz-Topaz
Calculated ESD Particle Size		21660	22501	17862	22078	23368	22827	22997	23396	22181	16019	22966	22474	15869	20806
Mineral Mass (%)	Pyrite	1.71	0.75	8.39	1.26	0.33	0.23	0.49	2.12	1.06	0.76	0.87	0.38	0.09	0.60
	Chalcopyrite	0.34	0.28	0.44	4.34	0.58	2.06	0.54	4.39	0.54	14.6	3.53	0.47	0.06	0.02
	Cassiterite	0.07	0.02	8.10	0.04	0.00	0.03	0.00	52.4	0.15	13.8	7.50	0.01	0.00	0.05
	Sphalerite	1.87	2.04	1.25	7.52	2.18	0.09	1.23	0.64	4.14	0.04	0.57	0.02	9.34	10.2
	Pyrrhotite	5.22	8.04	0.04	0.03	4.08	1.36	8.81	1.02	7.24	3.15	0.00	7.77	0.00	14.9
	Other Sulphides	0.04	0.01	0.07	0.05	0.01	0.01	0.03	0.11	0.01	0.18	0.05	0.01	0.81	0.02
	Quartz	55.4	61.7	50.3	48.0	69.6	56.5	9.66	1.55	37.9	4.02	55.1	43.1	68.0	22.3
	K-Feldspar	0.26	0.01	0.01	0.00	0.05	0.01	0.06	0.00	0.01	0.00	0.12	2.69	0.54	0.01
	Plagioclase	0.16	0.07	0.09	0.03	0.39	0.07	0.00	0.00	0.05	0.02	0.21	5.14	0.09	0.06
	Topaz	25.9	17.2	27.3	25.5	0.10	10.4	0.02	0.00	40.9	60.0	6.76	13.4	0.04	37.6
	Micas	7.71	8.93	2.72	11.7	22.4	27.9	76.2	33.7	7.12	0.29	24.2	26.2	10.6	13.2
	Clays	0.03	0.03	0.05	0.01	0.00	0.01	0.00	0.00	0.02	0.02	0.04	0.01	0.01	0.04
	Chlorites	0.04	0.18	0.09	0.07	0.07	0.09	0.05	0.01	0.04	1.91	0.03	0.04	2.24	0.02
	Other Silicates	0.02	0.04	0.08	0.03	0.00	0.05	0.01	0.01	0.03	0.02	0.04	0.07	0.29	0.02
	Oxides	0.01	0.01	0.25	0.01	0.00	0.00	0.03	0.00	0.00	0.05	0.00	0.00	0.25	0.02
	Carbonates	0.07	0.03	0.02	0.01	0.02	0.04	0.10	0.00	0.01	0.01	0.00	0.00	0.08	0.01
	Fluorite	0.73	0.20	0.18	0.12	0.18	0.31	1.35	0.06	0.22	0.10	0.14	0.00	7.48	0.08
	Apatite	0.41	0.44	0.62	1.18	0.01	0.80	1.45	1.05	0.56	0.69	0.83	0.71	0.04	0.87
	Wolframite	0.00	0.00	0.00	0.00	0.00	0.01	0.00	2.94	0.00	0.38	0.00	0.01	0.00	0.00
	Other	0.01	0.00	0.01	0.00	0.00	0.00	0.00	0.00	0.01	0.01	0.00	0.00	0.00	0.01
	Total	100.0	100.0	100.0	100.0	100.0	100.0	100.0	100.0	100.0	100.0	100.0	100.0	100.0	100.0

Table 4.2 Summary statistics for $\delta^{34}S$ SIMS values (‰) for the East Kemptville and Duck Pond deposits. EK = East Kemptville, DP = Duck Pond, GZ = greisen, QSV = quartz-sulfide vein.

			Mineralization	Mineral									Bulk δ34
Sample ID	Deposit	Zone	Type	analyzed	n =	Min.	Max.	Range	Mean	Median	SD	CV	Value by EA-IRMS
EK-4-153.2	EK	Baby	GZ	Sphalerite	5	3.3	6.0	2.8	4.6	4.1	1.21	26	
				Pyrrhotite	4	2.5	4.1	1.6	3.2	3.1	0.81	25	
EK-11-88.9	EK	Baby	GZ	Sphalerite	7	3.9	5.8	1.8	4.6	4.6	0.65	14	
				Pyrrhotite	3	3.8	6.1	2.3	5.0	5.3	1.17	23	
EK-16-83.1	EK	Main	GZ	Sphalerite	6	0.7	4.9	4.3	2.4	2.3	1.44	59	
				Chalcopyrite	3	3.4	3.7	0.3	3.5	3.6	0.16	4.4	
				Pyrite	1	3.4	3.4						
EK-25-115.5	EK	Main	GZ	Sphalerite	3	4.4	6.7	2.3	5.8	6.4	1.3	21	
				Chalcopyrite	3	5.5	6.5	1.0	5.8	5.5	0.59	10	
				Pyrite	2	3.9	5.2	1.3					
EK-26-196.5	EK	Main	GZ	Chalcopyrite	6	2.1	4.2	2.0	3.4	3.8	0.76	22	
EK-2-115.6	EK	Baby	QSV	Sphalerite	3	3.3	4.59	1.3	3.7	3.3	0.74	20	6.3
EK-10-104.2	EK	Baby	QSV	Sphalerite	2	5.9	6.03	0.1	6.0	6.0	0.11	1.8	6.2
EK-11-103.9	EK	Baby	QSV	Sphalerite	7	2.9	9.8	6.9	5.6	5.3	2.2	40	6.1
EK-25-121.6	EK	Main	QSV	Sphalerite	3	5.5	7.9	2.4	6.5	5.9	1.3	20	6.1
DP-24-137.8	DP			Sphalerite	7	8	9.8	1.9	8.7	8.5	0.69	7.9	
				Pyrite	3	4.6	5.4	0.9	5.1	5.3	0.5	9.3	
				Pyrrhotite	1	5.9	5.9						

Table 4.3 Composition of sphalerite-stannite mineral pairs and equilibrium temperatures. Calculations were based on the geothermometer of Nakamura and Shima (1982).

Sample	Zone	Sample type	Mineral	Fe (wt%)	Zn (wt)	X_{Fe}/X_{Zn}	Kd	Log Kd	T (°C)
EK-3-93.2-1	Baby	Greisen	Sphalerite	9.80	55.68	0.2	0.01	-1.84	252
EK-3-93.2-1			Stannite	13.14	1.09	12.1			
EK-3-93.2-2	Baby	Greisen	Sphalerite	9.83	55.41	0.2	0.02	-1.70	265
EK-3-93.2-2			Stannite	12.94	1.45	8.9			
EK-11-88.9	Baby	Greisen	Sphalerite	9.92	54.91	0.2	0.02	-1.75	260
EK-11-88.9			Stannite	13.10	1.28	10.3			
EK-25-115.5-1	Main	Greisen	Sphalerite	8.82	55.71	0.2	0.01	-1.95	241
EK-25-115.5-1			Stannite	12.95	0.93	14.0			
EK-25-115.5-2	Main	Greisen	Sphalerite	8.90	55.48	0.2	0.02	-1.82	253
EK-25-115.5-2			Stannite	12.98	1.23	10.6			
EK-26-196.5-1	Main	Greisen	Sphalerite	10.82	54.84	0.2	0.01	-1.84	251
EK-26-196.5-1			Stannite	14.58	1.07	13.7			
EK-26-196.5-2	Main	Greisen	Sphalerite	9.78	54.64	0.2	0.01	-2.04	232
EK-26-196.5-2			Stannite	15.45	0.79	19.6			
EK-28-168.8	Main	Greisen	Sphalerite	7.63	57.27	0.1	0.02	-1.60	275
EK-28-168.8			Stannite	12.88	2.40	5.4			

Chapter 5

Discussion

5.1 The Character and Genesis of Indium Mineralization at East Kemptville

5.1.1 Textures and Mineralogy

Indium accumulated in the East Kemptville deposit over the entire temporal range of mineral deposition, from the early deposition of tin mineralization to the later base-metal sulfides. This enrichment occurred both in greisen-hosted mineralization and quartz-sulfide veins. Texturally, the sulfide mineral assemblage of the greisens and quartz-sulfide veins are very similar, however, they differ in the nature of the associated gangue minerals. The common presence of fluorite and albite in veins that cross-cut greisens and albitites, respectively (Results: section 4.1), indicates that gangue mineralogy in part reflects the surrounding wallrock, such that the late fluids associated with the base-metal sulfides equilibrated with the surrounding wallrocks (i.e., the system was partially rock buffered). This is also true with respect to phosphate minerals, which are more common in the Main Zone than in the Baby Zone, which reflects higher phosphorus concentrations in the EKLG in the Main Zone compared with the Baby Zone (Halter et al., 1995; Bickerton et al., 2017). The lack of alteration selvages and the similarity of oxygen isotopic signatures between the quartz-sulfide veins (quartz) and from the EKLG and greisens (whole rock) (Kontak, 1994), further indicate that the late fluids were rock-buffered. Chemical equilibrium between the quartz-sulfide veins and their host-rock has also been previously suggest by Kontak (1994), based on the similar REE chemistry of albite from quartz-sulfide veins and from pegmatites in the EKLG. The interpretation that the gangue minerals hosted in quartz-sulfide veins were influenced by the surrounding wallrock differs from previous interpretations, which suggested that differences in the gangue mineralogy of quartz-sulfide veins were related to different paragenetic events (i.e., fluids) (Richardson, 1988; Kontak, 1994).

The fluids responsible for greisen formation differ from that of quartz-sulfide veins in that the fluids were in disequilibrium with the host EKLG (Halter et al., 1996). However, the sulfide minerals present in the greisens were generally either precipitated in open-space or they occur in veinlets that cross-cut earlier greisen-related minerals (i.e., cassiterite and

topaz), and there is a general lack of textures that suggest replacement of aluminosilicate minerals (i.e., topaz, muscovite, albite) by sulfides. These textural relationships between the greisen-related minerals and sulfides suggests that the sulfides were precipitated after greisen formation and that the fluid(s) responsible for sulfide formation infiltrated the system later than those that formed the greisens. The lack of replacement textures could be due to slow kinetics for replacement reactions, or that the fluids responsible for sulfide precipitation in the greisens were also in equilibrium with the greisen assemblage. Overall, the evidence for a wallrock control on gangue mineralogy of the veins and the similarity of sulfide assemblages in the greisens and veins indicates that, during the quartz-sulfide stage, the fluids permeated the wallrocks and equilibrated with them, such that the system was rock-buffered.

5.1.2 Mineral Chemistry

The mineral chemistry data are consistent with the conclusions made above from textural observations in that the compositions of the sulfide minerals in the greisens and in the quartz-sulfide veins are generally indistinguishable (see Results: section 4.2). Both the greisen-hosted sulfides and quartz-sulfide veins are enriched in indium and exhibit similar element concentration ranges and means. This contrasts with data from most other Sn-polymetallic deposits, which exhibit a wide range of indium concentrations in sulfides (e.g., Mount Pleasant, Toyoha; Sinclair et al., 2006; Murkamai & Ishihara, 2012). For the most part, individual sulfide grains have a homogeneous distribution of indium concentrations. Variations in concentration from grain to grain within a given sample are, however, of a similar magnitude to the variations seen between samples and even between the Main and Baby zones. There is no correlation between the indium concentrations in sulfides with host lithology, vein assemblage, or alteration type. The proportions of indium-bearing sulfides do, however, vary between the mineralized zones: the Main zone contains more chalcopyrite than the Baby Zone, which is also represented in assay data from the deposit, and the Zn-In mineral only is observed in the Main Zone. Despite its low abundance, the high indium content and fine grain size of the Zn-In mineral means that it could contribute a significant proportion of the indium in a given rock and, as such, be analogous to platinum-group minerals in many platinum-group element deposits.

The chemistry of a mineral is controlled by the initial physicochemical conditions during precipitation (P-T-fO_2-fS_2, fluid composition), and by any post-depositional re-equilibration. Elements can be either incorporated into the mineral structure or occur as micro- or nano-scale mineral inclusions. Only elements incorporated into the mineral structure in solid solution can be used to directly infer fluid conditions (i.e., fluid-mineral partitioning) during mineral deposition, or to characterize post-depositional re-equilibration (i.e., mineral-fluid and mineral-mineral interdiffusion). The presence of a smooth time-domain signal, both for counts and concentration, for a given element in LA-ICP-MS spectra suggests that the element occurs in solid solution, and the associated time-resolved data indicates how these elements are distributed within the crystal. Elements that exhibit irregular (noisy, spikey) profiles in LA-ICP-MS spectra are commonly interpreted as micro-inclusions, potentially in addition to being present in solid solution. Inclusions that are greater than 100s of nanometers in size are generally considered to be resolvable in LA-ICP-MS spectra (Cook et al., 2016). The concentration of elements associated with inclusions reflects the mineralogy, size, and density of the inclusions. If such inclusions are the result of mineral exsolution, then the entire LA-ICP-MS spectrum represents the bulk chemistry of the mineral when it was precipitated and can be used to infer fluid-mineral partitioning. However, if the inclusions were not the result of exsolution, but rather resulted from, for example, replacement, then the bulk chemistry cannot be used to infer fluid chemistry.

LA-ICP-MS profiles for indium-bearing sphalerite indicate that Fe, Mn, Co, Cu, Ga, Ge, Cd, In, and, to a lesser extent, Ag are in solid solution and homogeneously distributed through grains. The direct substitution of divalent cations for Zn^{2+} is documented for Fe^{2+} (see Figure 3.8b) and is well known for Mn^{2+}, Cd^{2+}, and Co^{2+} (Cook et al., 2009; Johan, 1988). Trivalent In is incorporated via a coupled substitution with monovalent ions (e.g., Cu^{1+}, Ag^{1+}) for Zn^{2+} and/or Fe^{2+}, which is demonstrated by the positive correlations between Cu, Ag, and In (see Figure 4.9).

$$(Cu^{1+}, Ag^{1+}) + In^{3+} \Leftrightarrow 2(Zn,Fe)^{2+} \qquad (1)$$

The substitution mechanism for Ge is less well understood, however, it is thought to occur as a coupled substitution involving two monovalent cations (e.g., Cu^{1+}) and one Ge^{4+} for 3

Zn^{2+} or as a substitution of Ge^{4+} for 2 Zn^{2+}, in which case a vacancy is created (Bellisont et al., 2016).

$$2Cu^{1+} + Ge^{4+} \Leftrightarrow 3Zn^{2+} \qquad (2)$$

$$Ge^{4+} + \square \Leftrightarrow 2Zn^{2+} \qquad (3)$$

The substitution of Ga is also not well understood, but it is expected that Ga^{3+} is likely incorporated by a coupled substitution with a monovalent cation (Cook et al., 2009). The heterogeneous distribution of Pb, Sb, and Bi in sphalerite demonstrates that these elements are present as mineral inclusions of sulfide, sulfosalt, and/or native metal. Of all the elements analyzed in sphalerite, only Fe, Mn, Cd, and Co are thought to reflect a direct substitution into sphalerite at East Kemptville, and thus these elements are the most reflective of changes in the fluid conditions during precipitation or post-depositional diffusion processes.

Diffusion readily occurs in minerals at high temperatures in the presence of an element concentration gradient. A concentration gradient might have existed if the crystal were initially zoned or if the crystal was in contact with a phase (i.e., fluid or mineral) with a higher or lower concentration of a given element than that in the mineral in question. Unless complete re-equilibration occurred, diffusion will have induced concentration (diffusion) gradients in a crystal. The LA-ICP-MS spectra, however, do not indicate the presence of diffusion gradients such that there is no increase or decrease in concentration for a given element from the center towards the rim of a given crystal (see Figure 4.11a). This indicates that diffusion would have to had completely re-homogenized the crystal. The East Kemptville deposit underwent a tectono-thermal disturbance, which is recorded by the partial to complete resetting of the Ar^{40}/Ar^{39} and Rb-Sr systems at approximately 300 Ma (Kontak & Cormier, 1991; Kontak et al., 1995), post-dating sphalerite deposition. This tectono-thermal disturbance consisted of temperatures higher than 250-300 ℃ (Kontak et al., 1995), which could have provided the elevated temperatures necessary for diffusion. However, experimentally determined diffusivities of Fe in sphalerite by Mizuta (1988) indicate that sphalerite of several centimeters in diameter, like those in the quartz-sulfide veins at East Kemptville, would require higher temperatures (> 500 ℃) and slow cooling

to completely homogenize the Fe in sphalerite for the assumed conditions of thermo-tectonism present at East Kemptville. Also, the presence of compositionally zoned sphalerite and chalcopyrite in the breccia further indicates that sphalerite did not re-equilibrate, but rather reflects the primary depositional conditions (see Figure 4.4e). It would also be expected that systematic variation in elements would exist between different mineral pairs (i.e., mineral-mineral partitioning), which also was not observed.

There is uncertainty in how elements are incorporated into chalcopyrite, partly because there is no consensus regarding the oxidation states of Cu and Fe in chalcopyrite. The valences could be either $Cu^{1+}Fe^{3+}S_2$ or $Cu^{2+}Fe^{2+}S_2$ (Todd et al., 2003; Mikhlin et al., 2005; Pearce et al., 2006; Klekovkina et al., 2014). It is generally believed that an intermediate covalent configuration between both oxidation configurations occurs (George et al., 2018). Only Zn, Ag, In, Sn, and Se are commonly thought to occur in solid solution in chalcopyrite, and it is uncertain if As, Sb, Mn, and Ga occur in solid solution or as inclusions (Huston et al., 1995; George et al., 2018). Indium-bearing chalcopyrite is only enriched in Zn, Ag, and Sn at East Kemptville, with most other trace-elements generally occurring in concentrations less than 10 ppm. The trace-element characteristics of chalcopyrite at East Kemptville are consistent with the observations of George et al. (2018) for several different deposit types, who reported that only Zn, Se, Ag, In, and Sn are found in chalcopyrite in concentrations greater than 100 ppm. LA-ICP-MS analysis of indium-bearing chalcopyrite at East Kemptville indicate that Zn, Ag, In, and Sn occur in both solid solution and as nano-inclusions of sphalerite, pyrrhotite, and stannite, which are also visible under high-magnification reflected light and BSE imaging. It is possible that the signal for the mineral host is solely due to the presence of finely dispersed nano-scale inclusions, but this cannot be determined given the resolution of LA-ICP-MS. It is therefore difficult to use these trace elements in chalcopyrite confidently to infer fluid conditions, until the question of solid solution versus nano inclusions and the substitution mechanism are further constrained. The heterogeneous distribution of Pb, Sb, and Bi in a crystal is similar to that seen in sphalerite and indicates that these elements are also present as inclusions in chalcopyrite.

The recent study by George et al. (2018) proposed that the Zn:Cd ratio in chalcopyrite can be used to infer variations in physicochemical conditions during precipitation. Furthermore, they suggested that if the Zn:Cd ratios of chalcopyrite and sphalerite are both constant and similar in value, then they formed from a similar fluid source under constant physiochemical conditions. If the Zn:Cd ratios of chalcopyrite and sphalerite are both relatively constant, but have different values, then it suggests that these minerals either formed at different times or from different fluid sources (George et al., 2018). The positive correlation between Zn and Cd in indium-bearing chalcopyrite (i.e., they have a constant ratio) is also exhibited at East Kemptville (Table 5.1), and the general ratio of Zn:Cd exhibited from indium-bearing chalcopyrite (0.011 ± 0.004) is the same as the average Zn:Cd ratio of co-genetic sphalerite (0.011 ± 0.001). There are minor differences between the Cd:Zn ratio of sulfides from greisens and quartz-sulfide veins, and between chalcopyrite from the Main and Baby zones (Table 5.1). These minor variations in the Cd:Zn ratios may indicate differences in precipitation temperature, where higher Zn:Cd ratios are generally interpreted to be related to higher temperatures (George et al., 2018). The Zn:Cd ratio of the single chalcopyrite measured from the breccia is 0.002, suggesting that it formed under quite different physicochemical conditions compared with indium-bearing chalcopyrite from the Main and Baby zones; the lower value suggests a lower formation temperature.

The relatively constant and similar Zn:Cd ratios for sphalerite and chalcopyrite at East Kemptville is interpreted to reflect relatively constant physiochemical conditions and precipitation from the same ore-forming fluid. This is consistent with mineral textures that indicate these minerals formed at the same time and with the relatively homogenous mineral chemistry for indium-bearing sphalerite and chalcopyrite. However, the interpretation of Zn:Cd ratios in chalcopyrite are generally dependent on the assumption that the Zn:Cd ratio in chalcopyrite is due to mineral substitution and not inclusions. The incorporation of Zn and Cd via substitution was suggested by George et al. (2018) because Zn and Cd were positively correlated in chalcopyrite from both deposits that contained chalcopyrite with co-existing sphalerite and deposits that contained only chalcopyrite.

Regardless of the oxidation states of the cations in chalcopyrite, it could be expected that Zn^{2+} and Cd^{2+} could have substituted for Cu^{1+} and Fe^{3+} in a coupled substitution or have been incorporated as a simple substitution for divalent Cu and Fe. However, Cd concentrations in chalcopyrite are quite low (1-30 ppm), whereas Zn commonly exceeds 1000 ppm. The similarities in Zn:Cd ratio between sphalerite and chalcopyrite also would be expected if this ratio reflects the presence of sphalerite inclusions, as sphalerite at East Kemptville has a relatively constant Zn:Cd ratio (Table 5.1). However, if the Zn:Cd ratio is related to sphalerite inclusions, the similar ratio preserved in chalcopyrite indicates that the conditions that formed sphalerite were relatively constant and that the co-precipitation of these two phases would, by extension, imply that physiochemical conditions were similar and relatively constant. These observations indicate that further work is required to determine the substitution mechanism for these elements, which would allow assessment of the application of Zn:Cd ratios in chalcopyrite to understanding timing relationships and variations in physicochemical conditions.

The chemistry of both sphalerite and chalcopyrite further supports the textural observations that indicate that both greisen-hosted and vein-hosted indium-bearing sulfides formed from the same fluids. This indicates that the sulfide forming fluids must have been chemically similar, and that any variation in physicochemical conditions or source resulted in subtle chemical changes that could not be determined with the data collected for this study.

5.1.3 Thermometry

The range of temperature estimates for the greisen-hosted sulfides provided by the sphalerite-stannite geothermometer (232 to 275 °C) are somewhat lower than the range for the quartz-sulfide veins based on fluid inclusion homogenization temperatures (> 280-317 °C) and sulfur isotope thermometry (344 ± 45 °C) (Table 4.2) (Kontak, 1990a; Kontak, 1994; Bickerton et al, 2017). These differences in temperature estimates were also recognized by Shimizu & Shikazono (1985) in other deposits, who compared the sphalerite-stannite geothermometer from several deposits with other thermometry techniques. Shimizu & Shikazono, (1985) reported that temperatures based on the sphalerite-stannite geothermometer were typically ±35 °C of those provided by other techniques. For East Kemptville, the maximum value for the sphalerite-stannite

geothermometer is between 5 and 25°C lower than the minimum value for the other estimates; the median values are 45 to 90°C lower (Table 4.2). The differences between the sphalerite-stannite and isotope-based estimates are larger than for the fluid inclusion estimates. As discussed in section 5.1.2., it is possible that the lower temperature estimates reflect re-equilibration by diffusion, however, as discussed above, diffusion is not thought to have affected mineral chemistry. Also, a narrow range in temperature estimates (possibly < 10 °C) would be expected if re-equilibration had occurred, as is observed in temperatures based on the sphalerite-stannite geothermometer for the metamorphosed Sinancha Sn-W porphyry deposit (Dobrovol'skaya et al., 2008).

The previously determined fluid inclusion homogenization temperatures of Kontak (1994) and Bickerton et al. (2017) were determined for gangue minerals (i.e., quartz, triplite) in quartz-sulfide veins, and it is not certain if these minerals were co-precipitated with sphalerite and stannite. The fluid inclusion temperature estimates only provide the minimum formation temperature and require pressure corrections to determine formation temperatures. If these minerals are representative of the formation temperatures of sphalerite, then the results of the sphalerite-stannite geothermometer would be invalid, as they are lower than the minimum formation temperature provided by fluid inclusions. However, it has not been demonstrated that the fluid inclusions in the gangue minerals are related to sphalerite formation. Previously determined temperature estimates by sulfur isotope thermometry were based on a single sphalerite-galena mineral pair using mineral separates and provide a large uncertainty (± 45 °C). For the sulfur isotopic thermometry to be valid, it is necessary that both minerals formed at the same time and were in equilibrium, and that the sulfur isotopic compositions of the two minerals were not later modified (Campbell & Larson, 1999). It is possible that sphalerite and galena did not co-precipitate but had similar timing, such that the resulting sulfur isotope thermometry would differ from the actual formation temperature. As discussed above, only the sphalerite-stannite geothermometer is thought to provide an adequate temperature estimate for sphalerite formation, indicating that sphalerite associated with co-genetic stannite formed at 232-275 °C.

5.1.4 Sulfur Isotopes

The sulfur isotopic composition of sulfide minerals is related to: i) the physicochemical conditions at the time of precipitation (fO_2-pH-temperature), and ii) the bulk isotopic composition of the sulfur in the fluid. Sulfide mineral deposition from the fluid could also have modified the fluid sulfur isotopic composition if precipitation occurred in an open system (i.e., Rayleigh fractionation occurred). Textural observations indicate that indium-bearing sulfides formed in an assemblage with pyrrhotite and Fe-rich sphalerite; This constrains the fS_2 and fO_2 to reducing conditions, where reduced sulfur species (i.e., H_2S) are dominant (Ohmoto & Goldharber, 1998). Under conditions where H_2S is the dominant sulfur species, isotopic fractionation between fluids and sulfide minerals is negligible (< 0.5 ‰) and any variation in the sulfur isotopic character of sulfides can be directly related to the bulk sulfur isotopic composition of the fluid or to Rayleigh fractionation effects (Ohmoto & Rye, 1979).

In situ sulfur isotope (SIMS) analyses of indium-bearing sulfides from East Kemptville indicate a larger range of $\delta^{34}S$ values compared with the range determined from analysis of mineral separates provided in both this study and in previous work by Kontak (1990a; 1993; Fig. 5.1). Data from both in situ and separates analyses have similar average isotopic compositions for indium-bearing sulfides (~4.5 and 6 ‰, respectively), however, the larger variation in isotopic values provided by SIMS indicates that the mineral separate data is not representative of the sulfur isotopic variations of indium-bearing sulfides at East Kemptville. The variability in $\delta^{34}S$ of most sphalerite determined by SIMS is generally small (coefficient of variation < 20%), and only a few samples have sphalerite crystals that have highly variable $\delta^{34}S$ values (coefficient of variation >40%). It is uncertain if this variation is the result of instrumental bias, which is known to occur in sphalerite of different crystal orientations or if the variation is real (Kozdon et al., 2010). To reduce the effects of instrumental bias, analyses comprised shallow pits, as suggested by Kozdon et al. (2010). Even if the samples with high variability are excluded from consideration, however, the range of in situ $\delta^{34}S$ would still be larger than that determined by mineral separates (in situ = 2.1-7.9‰; mineral separates = 4.9-7.0 ‰). This suggest that previous interpretations of the sulfur isotope systematics at East Kemptville need to be reconsidered. Accordingly,

interpretations made here will be primarily based on the sulfur isotopic composition obtained by SIMS.

Greisen-hosted sulfides have the lowest value measured (0.7 ‰), whereas the quartz-sulfide veins have the highest value measured (9.8 ‰); the average sulfur isotopic composition of all quartz-sulfide veins are slightly higher than that of greisens (4.1 vs 5.4 ‰). This relationship is also true when the two ore zones are considered individually (Fig. 4.18b). The large range in $\delta^{34}S$ indicates that the bulk sulfur isotopic composition of the fluid related to indium mineralization varied significantly during deposition. Four processes could have influenced mineral isotopic compositions under the conditions determined for indium-bearing sulfides and cause the large measured variation: i) Rayleigh fractionation, ii) variations at source (in the magmatic fluids), iii) water-rock interaction with the metasedimentary country rocks that surround the EKLG, or iv) mixing with an external fluid source containing isotopically different sulfur.

Rayleigh fractionation processes were modelled for East Kemptville to determine if the range in observed mineral sulfur isotopic compositions could be explained solely by this process and to assess the magnitude of such variations. The isotopic composition of arsenopyrite was initially taken to represent the composition of the earliest fluids. Arsenopyrite is the paragenetically earliest sulfide to have formed at East Kemptville and is considered to be part of the greisen assemblage and co-precipitated with cassiterite and associated minerals. The pyrite-H_2S fractionation equation provided by Ohmoto & Rye (1979) was used as a proxy for the arsenopyrite-H_2S fractionation, since first-principles calculations for isotope fractionation between arsenopyrite-H_2S and pyrite-H_2S indicate near identical fractionation at the temperatures purposed for arsenopyrite formation (Liu et al., 2016). The highest $\delta^{34}S$ value provided by arsenopyrite (6.9 ‰) was used in the isotope fractionation equation, using an initial temperature of 450 °C, which is consistent with the temperatures determined for co-genetic cassiterite (Halter et al., 1996). Results of this modelling indicate that most of the range of sulfur isotopic compositions exhibited in the deposit can be explained by Rayleigh fractionation (Fig. 5.2). However, *f* values (fraction of sulfur remaining after precipitation) of 0.14 are required to explain the average $\delta^{34}S$ values of the deposit (4.5 ‰), and values of 0.001 are required to explain the lowest $\delta^{34}S$

values (0.7 ‰). It is assumed that the fluids (and their contained sulfur) responsible for arsenopyrite formation were genetically related to the fluids responsible for the later base-metal sulfides. Given that assumption, the large amount of fractionation (precipitation) required to explain the observed $\delta^{34}S$ values of indium-bearing sulfides is quite significant and does not seem very probable. Also, the greisen-hosted sulfides, excluding the early arsenopyrite, consist of lower values compared with the equivalent vein-hosted sulfides, which would imply that greisen-hosted sulfides formed from a fluid containing sulfur that underwent greater fractionation. This would also imply that the greisen-hosted sulfides in general, formed later than the quartz-sulfide veins. It is possible that the fluids that precipitated arsenopyrite (i.e., the greisenizing fluids) were not genetically related to the fluids responsible for the later, indium-bearing sulfide formation, and that the initial sulfur isotopic composition of the fluid is incorrect. However, the highest $\delta^{34}S$ values for vein sulfides is somewhat higher than the arsenopyrite values and given that Rayleigh fractionation will result in a decrease in mineral $\delta^{34}S$ values, the same conclusion is reached if we start with a $\delta^{34}S_{fluid}$ values based on the heaviest vein sulfides. In conclusion, although a simple Rayleigh fractionation model cannot account for the entire range of values, this process could account some of the observed sulfur isotopic variation.

The sulfur isotopic compositions of magmatic fluids are almost identical to the magma from which they are derived for magma compositions applicable to the SMB and EKLG (i.e., S-type magma, P_{H20} > ~100 bars, low fO_2), and, given such magma compositions, H_2S would be the dominant sulfur species in the magma (Ohmoto & Goldhaber, 1997). Under these conditions, the fractionation factor between H_2S and other sulfur species in the melt (e.g., S_2) is small (<0.5 ‰), such that the $\Sigma\delta^{34}S$ values of magmatic fluids would have been nearly identical to those of the magma (Ohmoto & Goldhaber, 1997). Therefore, any changes in the sulfur isotopic composition of the magma will result in changes in the sulfur isotopic composition of the magmatic fluid. If the range exhibited by the sulfur isotopic composition of sulfide minerals at East Kemptville was related to source variations, multiple magma sources for the fluids with different $\Sigma\delta^{34}S$ values would have been required. Differences in REE and immobile element characteristics of the EKLG have been taken to indicate that different pulses of magmas may have formed the granites in the Main and Baby zones (Halter et al., 1996; Stanley & Willson, 2016; Bickerton et al., 2017).

However, the similarity in sulfur isotopic values in the two zones does not support a model in which the mineralization in the two zones formed from different magmas and thus different magmatic fluids. There is also limited evidence that the mineralization at East Kemptville was the result of multiple magmatic fluid pulses, suggesting that the observed variation in sulfur isotopes of the sulfides were not likely due to difference in magma sources.

Variations in the sulfur isotopic signature of a magmatic-derived fluid could occur by leaching of sulfur from the surrounding Meguma metasedimentary country rocks. The degree to which addition of country rock sulfur would have affected the sulfur isotopic composition of the magmatic fluid would depend on the amount of sulfur added, with the resulting sulfur isotopic composition being proportional to the amounts of sulfur contributed by the two reservoirs. It is difficult to constrain the initial magma sulfur isotopic compositions for the EKLG, as it is likely that the magma was modified by the assimilation of metasedimentary sulfur (Poulson et al., 1991). Magmas that have derived their sulfur from the mantle have $\delta^{34}S$ values of around 1 ‰, but magmas that have assimilated significant amounts of sedimentary rocks can have values that deviate significantly from this (Seal, 2006). The majority of Meguma metasedimentary rocks have positive $\delta^{34}S$ values that range from 8 to 30 ‰, although values as low as -5 ‰ (Goldenville Group) to -9 ‰ (Halifax Group) have been measured (Poulson et al., 1991; Sangster, 1992). The low values, however, are a minor component of these sequences, and therefore it is reasonable to postulate that assimilation would have principally involved $\delta^{34}S$ values greater than ~ 5 to 10 ‰, which would have raised the $\delta^{34}S$ values above mantle values. These data also indicate that it is very unlikely that the low $\delta^{34}S$ values in the East Kemptville sulfides (as low as 0.7 ‰) did not result from leaching sulfur from the Meguma rocks or, as discussed above, by Rayleigh fractionation. Such low values therefore point to the involvement of magmatic sulfur that has mantle-like values, and which provides a reasonable end-member for the magmatic fluids in the system. The leaching of metasedimentary sulfur could occur either from direct interaction of the magmatic fluid with the metasedimentary rocks or leaching by an external fluid that later mixed with the magmatic fluids. There is limited evidence for the interaction of magmatic fluids with the wallrocks above the EKLG, indicating that this process would have had to occur at depth

or that external fluids interacted with the surrounding metasedimentary country rocks (Kontak, 1994). Sulfur addition could have occurred through fluid interaction with metasedimentary enclaves in the EKLG below the level of the deposit. Such enclaves have been documented in the SMB (Erdmann, 2006) and have also been recognized in the Baby Zone (Halter et al., 1996). In addition, it has been proposed that the formation of granitic plutons resulted from the intrusion of discrete pulses of magma as sill-like bodies (Menand, 2009). If this is the case, then these 'sills' could be separated by septa of metasedimentary rocks, which could have resulted in the reaction of fluids with variable amounts of metasedimentary rocks at depth.

The sulfur isotopic composition of the Meguma metasedimentary rocks around East Kemptville is unknown. However, in other parts of Nova Scotia, as described above, these rocks exhibit $\delta^{34}S$ values that mostly range from 8 to 30 ‰ and are rarely observed to have $\delta^{34}S$ values less than 1 ‰ (Kontak & Smith, 1989; Sangster, 1992). Sulfides in the nearby Duck Pond deposit, which is hosted in the Meguma metasedimentary rocks are characterized by relatively heavy $\delta^{34}S$ values (4.6-9.8 ‰), which suggests that the sulfur in the metasedimentary rocks surrounding the East Kemptville deposit is characterized by relatively high $\delta^{34}S$ values. It is likely that magmatic fluids interacted with the metasedimentary country rocks because the observed sulfur isotopic compositions at East Kemptville lie between a typical magmatic value and the expected value of the Meguma metasedimentary rocks. The higher $\delta^{34}S$ values for arsenopyrite compared with that of the later indium-bearing sulfides would be consistent with this model because the arsenopyrite is paragentically earlier. However, the generally heavier $\delta^{34}S$ values of the quartz-sulfide veins compared to the greisen-hosted sulfides would suggest that the fluids responsible for the quartz-sulfide veins contain more metasedimentary sulfur. This would suggest that the pathways for fluids responsible for the sulfide veins were different from those responsible for the greisen-hosted sulfides. Both mineralization styles, however, are structurally controlled by the EKEDFZ, suggesting that large variations in fluid-pathways likely did not exist. This overall model can explain the variation in sulfur isotopic composition at East Kemptville, however, it is difficult to explain the differences in isotope values between the greisen-hosted sulfides and the quartz-sulfide veins.

The sulfur isotopic composition of a magmatic fluid could have been modified by simple fluid-mixing with an externally derived fluid. Fluid inclusion and oxygen isotope studies have shown that temperature, salinity, and $\delta^{18}O_{fluid}$ decrease during the temporal progression from tin mineralization to sulfide mineralization at East Kemptville (Kontak, 1994; Bickerton et al., 2017). This relationship is consistent with other Sn-W deposits and is widely interpreted to represent increasing degrees of fluid mixing of early magmatic-derived fluids with an externally-derived fluid (i.e., meteoric or metamorphic) (Heinrich, 2007). This externally-derived fluid would have been heated by the intrusion and circulated in the upper parts of the granite intrusion and the adjacent country rock (Audetat et al., 2000). This externally derived fluid also could have leached sulfur from the metasedimentary country rocks as the external fluid interacted with the country rock. This model has been proposed for the Mole granite, a Sn district that hosted genetically similar (i.e., greisen) deposits (Heinrich & Ryan, 1992). This model is analogous to a magmatic fluid interacting directly with the metasedimentary country rocks, except that country rock sulfur would have been provided by an external fluid rather than the magmatic fluid. It might be expected that the upper and lower range of sulfur isotopic values would reflect the general character of these two reservoirs, with the average composition reflecting the degree of fluid mixing. However, the lower and upper values exhibited by the sulfides would not necessarily reflect the end-member compositions of the fluid reservoirs, as they may represent the end-members with minor amounts of mixing. In this scenario, the magmatic fluid would have to represent a lighter sulfur reservoir (e.g., 0-2 ‰), and the external reservoir would be enriched in heavy sulfur (> 8 ‰), which is consistent with the likely sulfur isotopic composition of the Meguma metasedimentary rocks surrounding the East Kemptville deposit.

It is possible to model the effects of simple mixing between two putative sulfur reservoirs, although it is difficult to constrain the end member compositions. If it is assumed that the surrounding Meguma metasedimentary rocks and the external fluids are enriched in heavy sulfur ($\delta^{34}S$ = 20-30 ‰), and that this external fluid mixed with a magmatic fluid ($\delta^{34}S$ = 0 ‰), the observed sulfur isotopic compositions can be easily explained, and would suggest that the magmatic reservoir was mixed with 30-50 % externally derived sulfur on a molar basis (Fig. 5.3). This indicates that fluid mixing could explain the observed sulfur isotopic

compositions of the sulfides present at East Kemptville. This model would require that the greisen-hosted sulfides reflect a fluid with a higher magmatic fluid content (lower $\delta^{34}S$ values) than the vein-hosted sulfides, which is consistent with the mineralogy of the two assemblages. Comparison of the sulfur isotopic composition of the sulfides with their major- and minor-element mineral chemistry does not reveal any clear correlations that could be related to fluid mixing processes (Fig. 5.4). A similar decoupling of mineral chemistry and sulfur isotopic composition has been documented in other hydrothermal deposits (e.g., Tanner et al., 2016; Belissont et al., 2014), however, the reason for this decoupling is not well understood. It would suggest that the processes responsible for the variation in sulfur isotopic composition did not influence mineral chemistry (i.e., mineral-fluid partitioning) or vice-versa. However, the Sr isotopic characteristics of gangue minerals (i.e., fluorite, triplite, and apatite) associated with quartz-sulfide veins are thought to reflect fluid mixing of a magmatic fluid with a fluid modified by the metasedimentary country rocks (Richardson et al., 1990). Richardson et al. (1990), also proposed that the degree of fluid-rock interaction decreased with time and was associated with cooling, which is reflected in a decrease in $^{87}Sr/^{86}Sr$ ratios.

It is difficult to explain the high $\delta^{34}S$ values of arsenopyrite using a simple fluid-mixing model, as it would suggest that mixing of a magmatic fluid (0 ‰) with an externally derived heavy sulfur reservoir occurred early in the system, during greisen formation. This is inconstant with fluid inclusion and oxygen isotopic data for greisen minerals (i.e., cassiterite, topaz), which indicate that minimal fluid mixing occurred during the deposition of these minerals (Kontak, 1994). These values can, however, be explained in terms of water-rock interaction, where high $\delta^{34}S$ values could reflect minimal fluid mixing if the early externally derived fluids leached larger amounts of sulfur from the surrounding Meguma metasedimentary country rocks than later fluids. Early in the development of the system, more sulfur would have been available for leaching in the metasedimentary country rocks. As time progressed, this reservoir would have been depleted of sulfur, such that later fluids would have lower sulfur concentrations. Thus, the early fluids would have had a greater influence on the sulfur isotopic composition of a mixed fluid, such that the fluids that precipitated arsenopyrite could have had relatively high $\delta^{34}S$ values. This model is also consistent with the model proposed by Richardson et al. (1990) to explain the Sr isotopic

systematics of gangue minerals associated with quartz-sulfide veins. However, much like the previous model purposed, the difference in sulfur isotopic values between greisen-hosted sulfides and vein-hosted sulfides would imply variations in fluid-pathways amongst both mineralization styles

The differences in sulfur isotopic values between earlier formed arsenopyrite, greisen-hosted sulfides, and vein-hosted sulfides under the defined physiochemical conditions indicate that either the isotopic characteristics of the magmatic fluid or the magmatic source must have varied. However, there is limited evidence at the level of exposure of the deposit that supports multiple mineralizing events due to different magma sources. The observed sulfur isotopic compositions are more likely to be the result of a magmatic fluid that has been influenced by the Meguma metasedimentary country rocks, which would explain the higher $\delta^{34}S$ values for arsenopyrite. The two models that incorporate sulfur addition by the metasedimentary country rocks best explain the observed sulfur isotopic characteristics at East Kemptville. Fluid-mixing by an external fluid is further supported by fluid inclusion and isotopic data, suggesting it is a better constrained model. However, this model is only valid under the assumption that the earlier externally derived fluid consisted of higher $\delta^{34}S$ values compared with the later fluid. The decoupling of sulfur isotopes and mineral chemistry also indicates that the changes in the sulfur source did not influence mineral chemistry. The reason for this is uncertain and requires further investigation.

5.2 Comparison with the Indium-Depleted Breccia and the Nearby Duck Pond Deposit

The breccia zone at East Kemptville is characterized by a very similar mineralogy to the indium-bearing sulfide assemblage in the greisens and veins, however, it is distinguished by containing abundant galena and by base-metal sulfide minerals with compositional zoning and very low indium contents. Sphalerite chemistry is distinctly different to the indium-bearing assemblage and is enrichment in an entirely different suite of elements (e.g., Ge, Ga, Ag). These elements are generally consistent with lower formation temperatures compared with the indium-bearing assemblage (Frezel et al., 2016). The presence of compositionally zoned, Sn-rich chalcopyrite is unusual, but has also been documented at the Toyoha Sn-polymetallic indium deposit (Kase, 1987). The

physicochemical conditions during breccia formation are poorly defined, however, a single temperature estimate using sphalerite-galena sulfur isotope geothermometry provides a formation temperature estimate of 154 ± 30°C using the isotope fractionation equation of Kiyosu (1973). This temperature is consistent with the Ge, Ga, and Ag enrichment of sphalerite, however, the validity of this estimate requires further confirmation using an independent thermometry technique (e.g., fluid inclusion homogenization temperatures). The difference in the mineral assemblages between the breccia and indium-bearing sulfides can be related to differences in physicochemical conditions or a different fluid, where it is likely that the breccia mineralization reflects lower formation temperatures. The relative timing of the breccia with respect to the indium-bearing sulfide assemblage is poorly defined, however, if the sulfides in the breccia did form under lower temperature conditions and from the same fluid source, it can be inferred that the breccia formed later, once the system had cooled sufficiently. The differences in paragenetic and physicochemical conditions between the indium-bearing sulfide assemblage and the breccia indicate a different genesis for the two assemblages and requires further work.

The nature of the indium mineralization at East Kemptville is very similar to that of the nearby Duck Pond deposit. Indium enrichment at Duck Pond is confined to a distinct event related to the deposition of base-metal sulfides that occur as stratabond disseminated mineralization and in quartz-sulfide veins (see Results: section 4.1.2). As with East Kemptville, the primary host for indium is sphalerite. The sulfide assemblage, however, is different, with sulfides of higher sulfidation state being more commonly observed in the Duck Pond deposit (pyrite, bornite), whereas stannite is rare, and no primary indium-rich phases have been recognized. This difference in mineralogy indicates that the physicochemical conditions must have been different from the East Kemptville deposit, and represent higher fS_2 and fO_2 (Pitre & Richardson, 1989). The chemistry of sphalerite from the Duck Pond deposit is characterized by similar element enrichments as the East Kemptville deposit, however, the elements generally occur in lower concentrations. The exceptions are Mn and Co, which occur in higher concentrations than at East Kemptville. The enrichment of Mn is reflective of the host rock, in that the Duck Pond deposit is hosted by manganiferous metasedimentary rocks (Pitre & Richardson, 1989). The $\delta^{34}S$ values are higher than East Kemptville, with a narrow range for indium-bearing sphalerite (7.5-9.8

‰). This suggests a homogenous sulfur reservoir compared with East Kemptville, and the higher $\delta^{34}S$ values are consistent with a fluid that had equilibrated with the surrounding Meguma metasedimentary rocks, which would also explain the elevated Mn concentrations in sphalerite compared with sphalerite from East Kemptville.

It is difficult to ascertain if the fluid source at Duck Pond is the same as East Kemptville, as proposed by Pitre & Richardson (1989). However, as previously discussed by Pitre & Richardson (1989), the conditions of formation of the two deposits were different. The generally similarities in sphalerite chemistry suggests a similar ore fluid, however, a common source with East Kemptville cannot be precluded.

5.3 Implications for the Formation of Indium Mineralization at East Kemptville

The similarities in mineral assemblages and chemistry of greisen-hosted sulfides and quartz-sulfide veins are consistent with a model in which the fluids that formed the two assemblages had the same source. Indium-bearing sulfides are proposed to be penecontemporaneous between veins and greisens, whereas differences in fluid-rock interactions for the fluids responsible for greisen-hosted and vein-hosted sulfides resulted in different gangue minerals and sulfur isotopic compositions. This is a less-complex evolution for sulfide mineralization at the East Kemptville deposit than proposed in earlier studies (Richardson, 1988; Kontak, 1994). Initial greisen formation was focused along parallel fault structures within the EKEFZ, where orthomagmatic fluids infiltrated along structural pathways. The later fluids responsible for the indium-bearing sulfides moved through interconnected pore space (i.e., micro-fractures) that developed prior to sulfide mineral deposition, and through larger fractures that resulted in quartz-sulfide veins (cf. Halter et al., 1996). These veins likely formed when fluid overpressuring occurred, where fluid pressure exceeded the total confining pressures (Kontak, 1994). The differences exhibited in gangue mineralogy and sulfur isotopic composition can be attributed to the variable interaction of the ore-bearing fluid as a result of wallrock interactions and/or interaction with externally derived fluids. The fluid-fluid interactions (mixing) appear to have been more common in the Main Zone, compared with the Baby Zone, which is likely due to the more extensive deformation that is apparent in the Main Zone, allowing for more accessible fluid pathways. These interactions do not appear to have modified the element

chemistry of the ore-bearing fluid(s), such that differences in sulfide mineral chemistry between the Main and Baby Zone were not significant.

The formation of the breccia appears to have occurred at lower temperatures, suggesting that it occurred after the deposition of the main indium-bearing sulfides. The textures of the breccia suggest localized fluid buildup and consequent overpressurization. This event likely occurred near the end of base-metal deposition. A detailed investigation of the genetic association of the nearby Duck Pond deposit is beyond the scope of this study, however, similarities in mineral chemistry suggest a similar ore-bearing fluid to those at East Kemptville, where the difference in host rocks caused a somewhat different sulfur isotopic signature.

5.4 Comparison with Other Indium-Bearing Sn-Polymetallic Deposits

Sn-polymetallic deposits consist of several different deposit sub-types, including: greisen, Sn-polymetallic vein, Sn-W porphyry, stratabound, and skarn deposits. Indium mineralization in Sn-polymetallic vein deposits is generally characterized by heterogeneous mineral concentrations of indium, whereas stratabound and skarn deposits are generally characterized by homogenous concentrations of indium (Murakami & Ishihara, 2012). In all deposits, however, the indium-bearing ore-assemblages are generally similar and typically consist of sphalerite, chalcopyrite, and stannite-group minerals, with sphalerite generally containing the highest concentrations of indium and is typically the most abundant indium-bearing phase.

A comparison of sphalerite trace-element chemistry from several Sn-polymetallic deposits indicates a large variation in composition (Table 5.3). Sphalerite from Sn-polymetallic vein deposits is generally characterized by lower Fe, Mn, Cd and higher Zn, Ga, Ag, Sn, Sb, and Pb than sphalerite from other types of Sn-polymetallic deposits. Also, Sn-polymetallic vein deposits generally exhibit larger variations in these elements compared with other types of Sn-polymetallic deposits. Murakami & Ishihara (2012) proposed that the variation exhibited in these trace-elements are in part the result of different substitution mechanisms that are inter-related to Cu and In. In the polymetallic vein deposits the following substitution mechanisms have been proposed: $2Zn^{2+} \leftrightarrow ((Cu^{1+}, Ag^{1+}) + In^{3+})$, $3Zn^{2+} \leftrightarrow (2Cu^{+} + Sn^{4+})$, $3Zn^{2+} \leftrightarrow ((Cu^{+}, Ag^{+}) + Sn^{4+})$), and $2Zn^{2+} \leftrightarrow (Cu^{1+} + Ga^{3+})$. In stratabound

and skarn deposits the proposed substitution: $2Zn^{2+} \leftrightarrow ((Cu^{1+}$ or $Ag^{1+}) + In^{3+})$ has been proposed, where sphalerite also exhibits low Ag and Sn concentrations. The composition of sphalerite at East Kemptville is consistent with the proposed mechanisms for stratabound and skarn deposits. Generally, it appears that complex substitution mechanisms occur in sphalerite where heterogeneous indium concentrations characterize the sphalerite, compared with sphalerite from deposits with homogenous indium concentrations. The differences in trace-element chemistry and substitution mechanism indicate that different physicochemical conditions and/or fluid sources must characterize the different deposit types.

5.4.1 Physicochemical Conditions

5.4.1.1 Temperature

A comparison of temperature estimates for the indium-bearing sulfide assemblage for several Sn-polymetallic deposits indicate that indium concentration occurs between 230 and 405 °C, based on several different thermometric techniques (Table 5.2). Published homogenization temperatures for indium-bearing sphalerite from Sn-polymetallic vein deposits range from 255 to 321 °C, which overlaps with the temperature range determined from sphalerite-stannite geothermometry in this study for the East Kemptville deposit (232-275 °C). Temperature estimates determined for chalcopyrite formation from other deposits using the chalcopyrite-stannite geothermometer indicate somewhat higher temperatures (300-400 °C) than that determined for sphalerite, however these estimates are few in number. A higher formation temperature for indium-bearing chalcopyrite has been suggested based on phase relationships (Cook et al., 2011; Ohta, 1989) and thermodynamic modelling (Heinrich & Ryan, 1992). Thermodynamic modelling of the Yankee Lode Sn-polymetallic deposit in Australia, which is similar in character to the East Kemptville deposit (i.e., a greisen-hosted deposit), indicated chalcopyrite precipitation to be favored (i.e. low mineral solubilities) from ~390-330 °C and 290-280 °C (Ryan et al., 1995). Higher temperatures for the precipitation of chalcopyrite is also a characteristic of granitoid-related copper porphyry deposits (Hezarkahani et al., 1999; Landtwing et al., 2005). Despite the lack of temperature estimates for chalcopyrite formation in Sn polymetallic deposits, empirical observations suggest that chalcopyrite generally precipitated at higher

temperatures than sphalerite. The overlapping ranges in temperatures for mineral precipitation between the different deposit styles indicates that the overall temperature for precipitation is very similar for indium concentration in Sn-polymetallic deposits. This similar range in temperatures and contrasting mineral concentrations of indium between deposits indicates that indium concentration is not directly related to the temperature of formation. However, there appears to be temperature controls on the formation of certain indium-bearing phases (i.e., chalcopyrite versus sphalerite).

5.4.1.2 Fluid Composition

The only available fluid composition data for indium-bearing Sn polymetallic deposits consist of microthermometric determination of salinity, and only limited data are available from fluid inclusions that have been demonstrated to be genetically related to indium mineralization. The available salinity estimates determined for the Pinguino and Freiberg Sn-polymetallic vein deposits consist of fluids with low to moderate salinity (0.5-8.8 wt. % $NaCl_{equiv.}$; Jovic et al., 2011; Bauer et al., 2018), whereas the salinity of the East Kemptville fluids are moderate to high (10-23.0 wt.% $NaCl_{equiv}$; Bickerton et al., 2017). It is difficult to draw any meaningful conclusions from this limited data set, however, the differences in salinities may suggest that different fluid sources are responsible for polymetallic vein type and other types of Sn-polymetallic deposits. Further studies are required to determine the minor and trace-element chemistry of indium-bearing fluids to better understand the compositional variations between deposit types. The lack of detailed fluid-chemistry makes it impossible to assess the variation in source fluid, however, the limited control of temperature suggests that fluid-chemistry and/or fluid source and evolution (i.e., water-rock interactions) is an important control on indium mineralization.

5.4.1.3 Depth of Formation

Sn-polymetallic deposits are thought to have formed over a range of depths, from sub-volcanic to deep plutonic environments. Generally, mineral deposits in the sub-volcanic environments are characterized by heterogeneous indium concentrations, whereas deposits that occur in deeper plutonic environments consist of more homogenous indium concentrations (Murakami & Ishihara, 2012). In addition, deposits that formed in shallow environments also contain higher concentrations of Ag and Sb with higher Ag contents in

sphalerite compared with those from greater depths (> 2 km) (Ishihara et al., 2011; Murakami & Ishihara, 2012). This is consistent with the observations at East Kemptville, where indium-bearing sphalerite contains lower Ag concentrations (< 30 ppm) and is thought to have formed at significant depths (> 14 km; Kontak et al., 2001). The differences in depth of formation for these deposits and the differences in the nature of ore suggests that the depth of ore emplacement is an important control on the nature of indium mineralization. The reason for these differences is not known, however, it would be expected that the fluid dynamics and architecture of shallow and deep deposits would be different, where shallower environments are more susceptible to interactions with surface-derived waters and to pressure and temperature fluctuations. The textural characteristics of sphalerite from sub-volcanic polymetallic vein-type deposits suggest rapid changes in fluid composition during growth (i.e., colloform, dendritic, rhythmic zoning), which has been attributed to complex fluid mixing with meteoric fluids (Pattrick et al.,1993; Shimuzu & Morishita, 2012). It is possible that the different characteristics of indium mineralization between Sn-polymetallic deposits are the result of different fluid dynamics that occur at shallow and deep levels.

5.4.2 Source of Indium

Sn-polymetallic deposits are thought to be associated with a diverse range of felsic source magma compositions, including A-type (e.g., Mount Pleasant, Sarvlaxviken; Inverno & Hutchinson, 2006; Valkama et al., 2015), S-type (e.g., East Kemptville, Dulong, Dachang ; Dostal et al., 2004; Ishihara et al., 2011; Xu et al, 2015), and I-type (e.g., Toyoha, Ashio; Ishihara et al., 2006). The large variability in magma type and related tectonic environment suggests that indium mineralization is largely not controlled by the affinity of the felsic magma. Recent experimental studies indicate that the formation of hydrothermal indium mineralization associated with felsic melts requires that limited crystallization of ferromagnesian minerals (i.e., biotite and amphibole) occur, as indium is compatible in these phases and subsequent fractionation of these phases will limit the availability of indium to the magmatic fluid (Gion et al., 2018). Alternatively, it has been proposed that indium could be introduced into the hydrothermal fluids from carbonaceous sedimentary wallrocks, as several Sn-polymetallic deposits occur in sedimentary country rocks (Ohta, 1995; Ishihara et al., 2009; Ishihara et al., 2011). Generally, the sulfur isotope composition

of indium-bearing ores from polymetallic veins from Japan (e.g., Toyoha), are thought to reflect a strong contribution of sulfur from the surrounding country rocks (Murakami & Ishihara, 2012), which is similar to that proposed for East Kemptville in this study. The source of indium at East Kemptville is not known, and analysis of the surrounding metasedimentary rocks would be required to assess if these rocks could have been a potential source, or if the indium was provided solely by magmatic hydrothermal fluids.

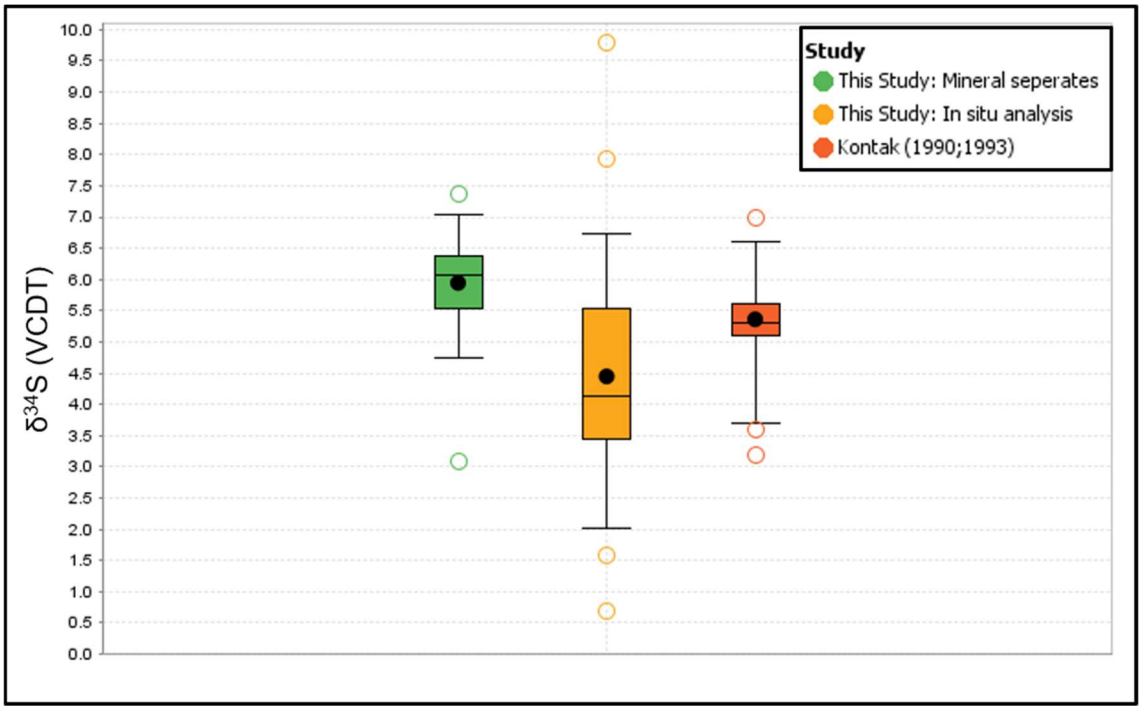

Figure 5.1 Box-whisker diagram comparing the sulfur isotopic composition of sulfides from this study with the mineral separates results of Kontak (1990;1993).

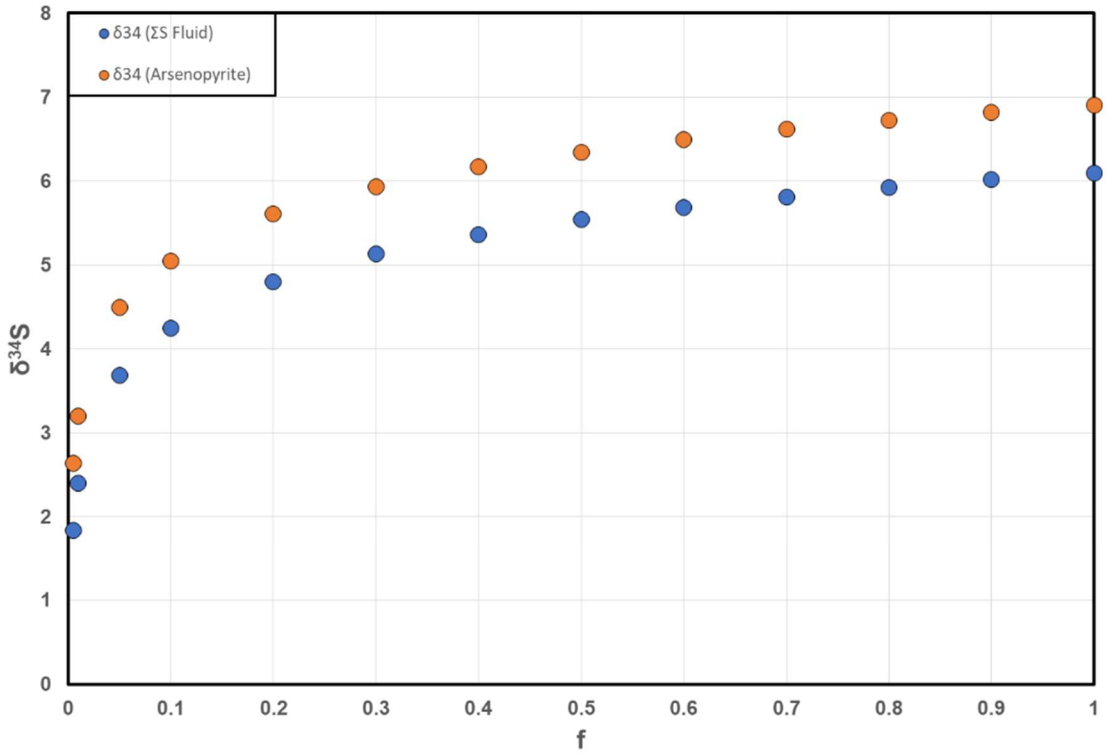

Figure 5.2 Calculated $\delta^{34}S$ values of dissolved H_2S and precipitated arsenopyrite using the Rayleigh fractionation model as a function of the proportion of sulfur remaining in the fluid reservoir (f) as precipitation proceeds (from f = 1 to f = 0). The initial $\delta^{34}S$ (fluid) = 6.1 ‰.

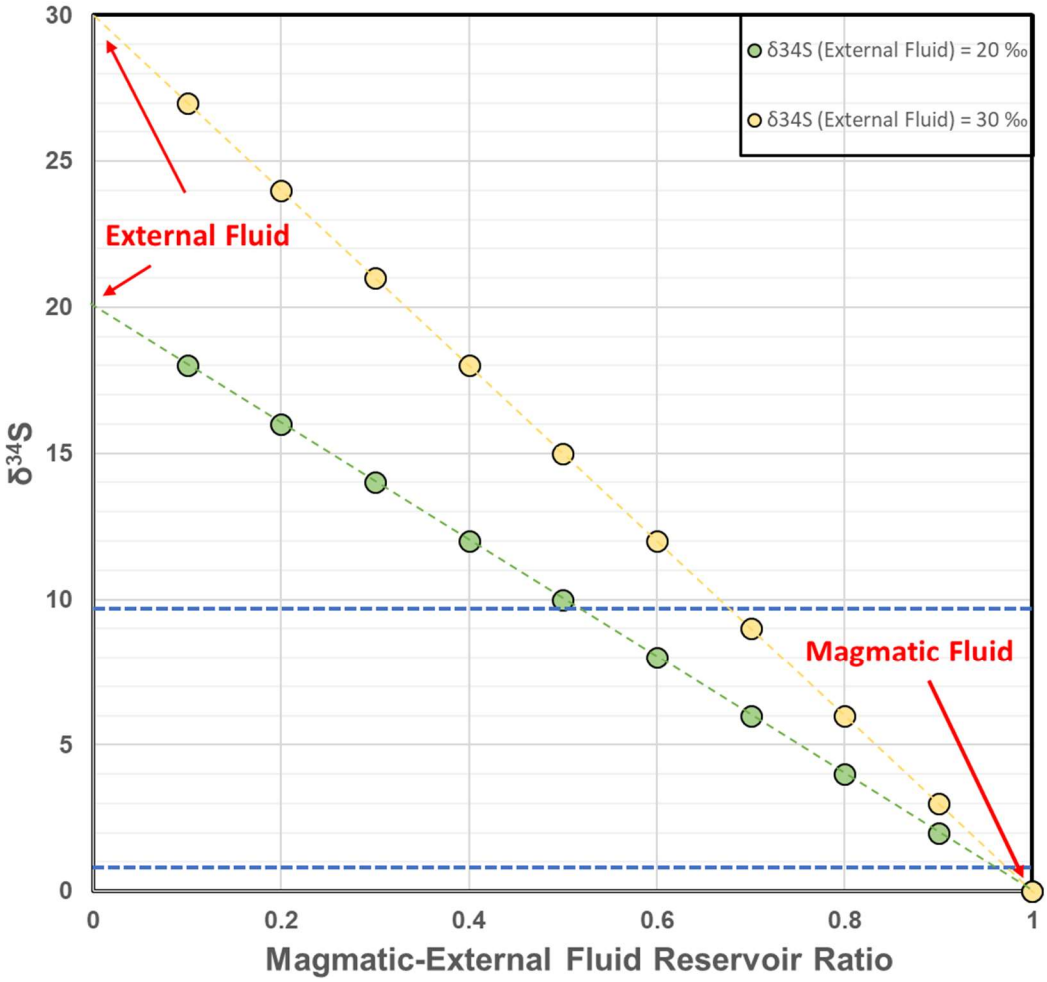

Figure 5.3 Modelled $\delta^{34}S$ values for simple fluid mixing of a magmatic and external fluid. The green line represents mixing with an external fluid with a $\delta^{34}S$ value of 20 ‰, and the yellow line represents mixing with an external fluid with a $\delta^{34}S$ value of 30 ‰. The solid blue line represents the average in situ $\delta^{34}S$ value, and the dashed blue lines represent the range of $\delta^{34}S$ values for the East Kemptville deposit.

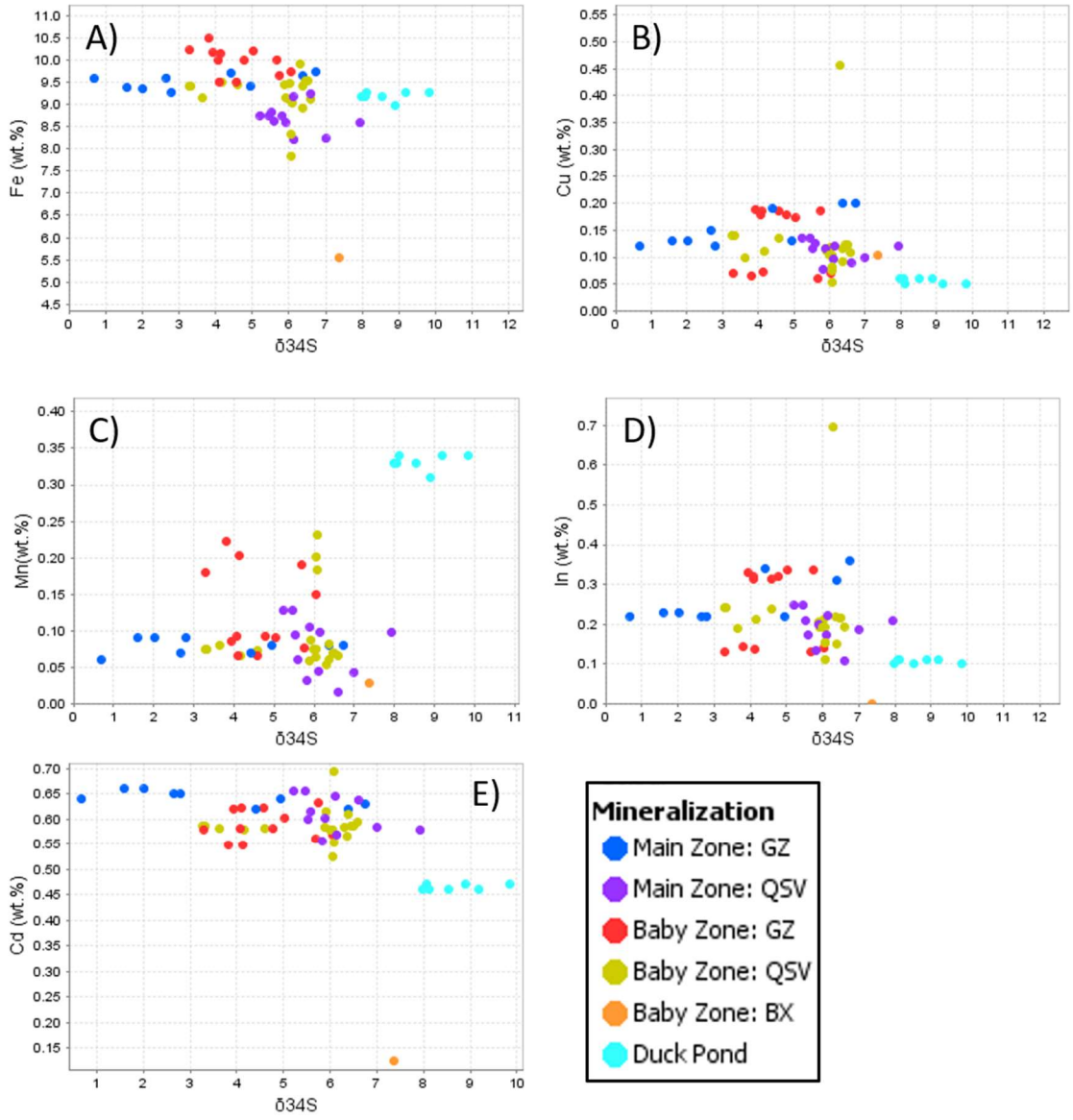

Figure 5.4 Bivariate plots comparing major- and minor-element mineral chemistry with the sulfur isotopic composition of sphalerite from the East Kemptville and Duck Pond deposits. (A) Fe vs $\delta^{34}S$, (B) Cu vs $\delta^{34}S$, (C) Mn vs $\delta^{34}S$, (D) In vs $\delta^{34}S$, (E) Cd vs $\delta^{34}S$.

Table 5.1 The Cd:Zn ratio of chalcopyrite from different mineralization types from the East Kemptville deposit.

Zone	Main Zone		Baby Zone		
Mineralization Style	Greisen	Quartz-Sulfide Veins	Greisen	Quartz-Sulfide Veins	Breccia
n, analyses =	17	2	10	8	1
Average Cd:Zn	0.012	0.018	0.008	0.011	0.002
Standard Deviation	0.003	0.010	0.002	0.004	

Table 5.2 Temperature estimates for the East Kemptville deposit and other indium-bearing Sn-polymetallic deposits. Note that homogenization temperatures are not corrected for pressure. F.I. = Fluid inclusions.

Deposit	Location	Method	Minimum (°C)	Maximum (°C)	Range (°C)	Reference
East Kemptville	Canada	Sphalerite-stannite geothermometer	232	275	43	This study
		Sulfur isotopic thermometery (Galena-Sphalerite)	299	389	90	Kontak, 1990
		F.I. microthermometry (quartz)	280	317	37	Bickerton et al., 2017; Kontak, 1994
Pinguino	Argentina	F.I. microthermometry (quartz)	308	327	19	Jovic et al. 2011
		F.I. microthermometry (sphalerite)	255	312	57	
Mount Pleasant (North Zone)	Canada	Sphlerite-stannite geothermometer	305	387	82	Sinclair et al., 2006
Changpo	China	Sphlerite-stannite geothermometer	310	340	30	Lattanzi et al., 1989
Dachang	China	F.I. microthermometry (quartz)	310	340	`	Fu et al., 1993
Freiberg (KB veins)	Germany	F.I. microthermometry (quartz)	298	341	43	Bauer et al., 2018
		F.I. microthermometry (sphalerite)	285	321	36	
Toyoha	Japan	F.I. microthermometry (sphalerite)	270	290	20	Shimizu & Morishita, 2012
		Chalcopyrite-stannite geothermometer	350	400	50	Ohta, 1989
Nakakoshi	Japan	Chalcopyrite-stannite geothermometer	300	-		Tsushimi et al. 1999
Akenobe	Japan	F.I. microthermometry (quartz)	285	310	25	Shimizu & Kato, 1991

Table 5.3 Average concentrations of minor and trace elements in sphalerite from selected deposits determined by LA-ICP-MS analysis.

Deposit	Mineralization type	Sample	1000(In/Zn)			Zn	Fe	Cu	Mn	Ga	Ag	Cd	In	Sn	Sb	Pb	Bi
			Ore	Sphalerite		%	%	µg/g	µg/g	µg/g	µg/g	µg/g	µg/g	µg/g	µg/g	µg/g	µg/g
					LOD	0.01	0.01	7	4	2	3	7	1	4	4	2	1
Toyoha	Tin polymetallic vein	TYHZn (23)	2.1	0.4	A.V.	63.7	1.7	1940	109	137	406	2670	263	1260	86	168	
Murakami & Ishihara, (2013)					S.D.	1.5	0.8	2680	104	368	1010	1890	507	1410	80	159	< 1
Ashio (Kajika)	Tin polymetallic vein	ASK3 (32)	1.5	0.7	A.V.	53.6	7.7	3160	54	126	26	4030	356	2150	< 4	< 2	< 1
Murakami & Ishihara, (2013)					S.D.	0.9	0.5	5600	23	71	42	640	603	4530			
Akenobe	Tin polymetallic vein	AK2307 (26)	0.5	0.3	A.V.	66.4	0.2	432	19	< 2	14	3710	219	< 4	< 4	8	< 1
Murakami & Ishihara, (2013)					S.D.	0.3	0	254	6	< 2	11	180	36	< 4		9	
Potosi	Tin polymetallic vein	98110509 (46)	1.4	0.7	A.V.	60.4	1.5	9850	17	85	223	1500	430	6780	< 4	367	< 1
Murakami & Ishihara, (2013)					S.D.	2.3	0.6	5730	10	72	200	900	853	4090		496	
Huari Huari	Tin polymetallic vein	HUC (60)	11	6.1	A.V.	56.1	5.6	3100	101	116	125	2840	3450	699	22	9	< 1
Murakami & Ishihara, (2013)					S.D.	2.2	1.3	2560	106	87	129	550	2910	1160	68	13	
Bolivar	Tin polymetallic vein	B1905 (31)	7.4	4	A.V.	57.8	4.2	2450	78	249	156	6660	2290	671	88	13	< 1
Murakami & Ishihara, (2013)					S.D.	1.6	0.8	1320	54	111	186	260	1220	487	154	7	
Porco	Tin polymetallic vein	98110401 (15)	0.3	0	A.V.	55.1	5.2	755	375	35	36	1680	20	618	< 4	< 2	< 1
Murakami & Ishihara, (2013)					S.D.	3.1	1.9	939	226	17	57	460	30	881			
Freiberg district (KB veins)	Tin polymetallic vein	4 samples (205	NA	1.1	A.V.	52.4	9.5	3888	3082	12.6	30	5966	560	256	1.6	423	
					S.D.	2.2	1.4	10037	3531	24.0	62	1085	491	655	5.4	5946	
Dulong	Stratabound and Skarn	1122A2 (34)	2.2	2.6	A.V.	53.9	6	3810	1760	< 2	14	2000	1380	11	< 4	7	20
Murakami & Ishihara, (2013)					S.D.	1.3	0.2	4060	280	< 2	9	120	460	0		5	20
Dachang	Stratabound	8111907 (32)	3.3	1.9	A.V.	53.4	5.7	5250	2260	32	54	4100	1020	3640	< 4	< 2	< 1
Murakami & Ishihara, (2013)					S.D.	1.2	0.5	5630	650	15	67	190	240	4810		< 2	< 1
Duck Pond	Stratabound	2 Samples (7)	2.5	1.9	A.V.	56.8	8.9	826.1	3850	0.5	2.6	6548	1085	2.6	0.3	1.1	0.0
This study					S.D.	1.1	0.5	294.4	684	0.1	1.3	2753	563	0.7	0.3	1.4	0.1
East Kemptville	Greisen	28 Samples (80	4	2.7	A.V.	56.2	9.3	1267	1313	1.9	6.6	6979	1513	3.5	0.5	0.9	0.1
This study					S.D.	1.0	0.7	670	913	2.7	4.7	1602	770	2.5	1.2	2.3	0.2
Mount Pleasant (FTZ)	Sn-W porphyry	SYA82B (2)	NA	0.3	A.V.	62.3	2.8	151	1162	7.5	0.7	1338	207	2.4	< 0.03	7.2	0.0
Unpublished data					S.D.	6.3	0.3	25	205	10.3	0.2	124	93	1.5		8.0	0.0

Data for Toyoha, Ashio, Akenobe, Potosi, Huari Huari, Bolivar, Porco, Dulong, and Dachang provided by Murakami & Ishihara (2013). Data for the Freiberg district provided by Bauer et al., (2018). LOD = Limit of Detection, FTZ = Fire Tower Zone

Chapter 6

Conclusions

6.1 Conclusions

The main objectives of this thesis were to characterize the mineralogical distribution of indium at East Kemptville, assess if any spatial and temporal variation in indium mineralization existed, characterize the fluid source, physiochemical conditions, and chemical evolution of the hydrothermal fluids responsible for indium mineralization, and compare the observations of East Kemptville with other indium-bearing Sn-polymetallic deposits. The conclusions of this study are as follows:

- Temporal variations in indium mineralization exist at East Kemptville, with increasing indium enrichment from the earlier Sn mineralization to the later base-metal sulfides. Indium is hosted in cassiterite, and to a lesser extent wolframite, in the early Sn greisen event. Most indium resides in sphalerite and chalcopyrite in the East Kemptville deposit, which postdate Sn mineralization. The Zn-In mineral contains the highest concentrations of indium, and where present could contribute significant indium to the grade.
- All indium-bearing sulfides from greisen-hosted and quartz-sulfide veins were precipitated from a penecontemporaneous event.
- There are no spatial variations in the distribution of indium mineralization at East Kemptville.
- Gangue mineralogy of quartz-sulfide veins are in part the result of fluid-wall rock equilibration.
- Sulfides in greisens and in quartz-sulfide veins formed from the same fluids under similar physicochemical conditions.
- Indium-bearing sphalerite was precipitated between 232 and 275 ℃
- Sulfur isotopic data, particularly those from SIMS, suggest that sulfur was in part derived from the metasedimentary country rocks. This required either magmatic fluid interaction with the metasedimentary country rocks directly likely below the

deposit, or by mixing between magmatic fluids and external fluids that had interacted with the country rocks.

- The characteristics of indium mineralization at the nearby Duck Pond deposit are similar to those of East Kemptville, suggesting a similar genesis.
- Magma source and temperature do not largely control the nature of indium mineralization in Sn-polymetallic deposits. Rather, differences in depth of formation and fluid composition are more likely the key parameters.

6.2 Suggestions for Future Work

There are five recommendations for further work.

- Determine if the Zn and Cd concentrations observed in chalcopyrite from East Kemptville and other deposits are related to micro-inclusion or if they are they represent solid-solution. This is required to determine if the application of Zn:Cd ratios are valid in determining the physicochemical conditions of chalcopyrite-bearing ores. This could be done by utilizing focused ion beam-scanning electron microscopy (FIB-SEM) or transmission electron microscopy (TEM).
- To better constrain the sulfur isotope systematics at East Kemptville, whole-rock sulfur isotopes should be completed on the surrounding metasedimentary country rocks.
- A detailed fluid chemistry study that determines the minor and trace-element chemistry of the fluids using single inclusion techniques (e.g., LA-ICP-MS) is required to better understand the fluids responsible for indium mineralization.
- Further investigation of the fluid composition and physicochemical characteristics of the breccia zone is required to better understand the evolution of the East Kemptville deposit.
- Cassiterite dating would be useful to better determine the genetic relationship between the Duck Pond and East Kemptville deposit.

References

Andersen, J. C. Ø., Stickland, R. J., Rollinson, G. K., and Shail, R. K., 2016, Indium mineralisation in SW England: Host parageneses and mineralogical relations: Ore Geology Reviews, v. 78, p. 213–238.

Audétat, A., Günther, D., and Heinrich, C. A., 2000, Causes for Large-Scale Metal Zonation around Mineralized Plutons: Fluid Inclusion LA-ICP-MS Evidence from the Mole Granite, Australia: Economic Geology, v. 95, p. 1563–1581.

Bauer, M. E., Seifert, T., Burisch, M., Krause, J., Richter, N., and Gutzmer, J., 2017, Indium-bearing sulfides from the Hämmerlein skarn deposit, Erzgebirge, Germany: evidence for late-stage diffusion of indium into sphalerite: Mineralium Deposita, v. 54, p. 175–192.

Bauer, M. E., Burisch, M., Ostendorf, J., Krause, J., Frenzel, M., Seifert, T., and Gutzmer, J., 2019, Trace element geochemistry of sphalerite in contrasting hydrothermal fluid systems of the Freiberg district, Germany: insights from LA-ICP-MS analysis, near-infrared light microthermometry of sphalerite-hosted fluid inclusions, and sulfur isotope geochemistry: Mineralium Deposita, v. 54, p. 237–262.

Belissont, R., Boiron, M.-C., Luais, B., and Cathelineau, M., 2014, LA-ICP-MS analyses of minor and trace elements and bulk Ge isotopes in zoned Ge-rich sphalerites from the Noailhac – Saint-Salvy deposit (France): Insights into incorporation mechanisms and ore deposition processes: Geochimica et Cosmochimica Acta, v. 126, p. 518–540.

Belissont, R., Muñoz, M., Boiron, M.-C., Luais, B., and Mathon, O., 2016, Distribution and oxidation state of Ge, Cu and Fe in sphalerite by μ-XRF and K-edge μ-XANES: insights into Ge incorporation, partitioning and isotopic fractionation: Geochimica et Cosmochimica Acta, v. 177, p. 298–314.

Bickerton, L., Kontak, D. J., Samson, I. M., and Murphy, J. B., 2016, A mesothermal greisen-hosted Sn-Zn-Cu-Ag-In deposit at East Kemptville, Nova Scotia, Canada.: SGA Quebec 2017 – 14th Biennial Meeting: Quebec City, Quebec, Canada, Proceedings, v. 4, p. 1273–1276.

Bodnar, R. J., Lecumberri-Sanchez, P., Moncada, D., and Steele-MacInnis, M., 2014, Fluid Inclusions in Hydrothermal Ore Deposits, in Treatise on Geochemistry: Elsevier, p. 119–142.

Cameron, B. I., and Zentilli, M., 1997, Geochemical characterization of the mineralized transition between the Goldenville and Halifax formations and the interaction with adjacent granitoid intrusions of the Liscomb Complex, Nova Scotia: Atlantic Geology, v. 33, p. 143–155.

Campbell, A. R., and Larson, P. B., 1998, Introduction to Stable Isotope Applications in Hydrothermal Systems: In: Richards, J.P., Larson, P.B. (Ed.), Introduction to Stable Isotope Applications in Hydrothermal Systems "Geochemistry of Hydrothermal Ore Deposits Geology," Society of Economic Geology.

Chatterjee, A. K., 1983, Metallogenic map of Nova Scotia.: Nova Scotia Department of Mines and Energy, Nova Scotia, Map MCR 37, Scale 1:500,000.

Chatterjee, A. K., and Cormier, R. F., 1991, A Rb-Sr geochronological study of the Davis Lake pluton, South Mountain batholith, southern Nova Scotia: evidence of a 374 Ma time of emplacement: D.R. MacDonald (ed). Nova Scotia Department of Mines and Energy Resources, Report 91-A, p. 19

Cook, N. J., Ciobanu, C. L., Pring, A., Skinner, W., Shimizu, M., Danyushevsky, L., Saini-Eidukat, B., and Melcher, F., 2009, Trace and minor elements in sphalerite: A LA-ICPMS study: Geochimica et Cosmochimica Acta, v. 73, p. 4761–4791.

Cook, N. J., Sundblad, K., Valkama, M., Nygård, R., Ciobanu, C. L., and Danyushevsky, L., 2011, Indium mineralisation in A-type granites in southeastern Finland: Insights into mineralogy and partitioning between coexisting minerals: Chemical Geology, v. 284, p. 62–73.

Dill, H. G., Garrido, M. M., Melcher, F., Gomez, M. C., Weber, B., Luna, L. I., and Bahr, A., 2013, Sulfidic and non-sulfidic indium mineralization of the epithermal Au–Cu–Zn–Pb–Ag deposit San Roque (Provincia Rio Negro, SE Argentina) — with special

reference to the “indium window” in zinc sulfide: Ore Geology Reviews, v. 51, p. 103–128.

Dobrovol’skaya, M. G., Genkin, A. D., Bortnikov, N. S., and Golovanova, T. I., 2008, Unusual sphalerite, chalcopyrite, and stannite intergrowths at tin deposits: Geology of Ore Deposits, v. 50, p. 75–85.

Dostal, J., and Chatterjee, A. K., 1995, Origin of topaz-bearing and related peraluminous granites of the Late Devonian Davis Lake pluton, Nova Scotia, Canada: crystal versus fluid fractionation: Chemical Geology, v. 123, p. 67–88.

Franchini, M., McFarlane, C., Maydagán, L., Reich, M., Lentz, D. R., Meinert, L., and Bouhier, V., 2015, Trace metals in pyrite and marcasite from the Agua Rica porphyry-high sulfidation epithermal deposit, Catamarca, Argentina: Textural features and metal zoning at the porphyry to epithermal transition: Ore Geology Reviews, v. 66, p. 366–387.

Frenzel, M., Hirsch, T., and Gutzmer, J., 2016, Gallium, germanium, indium, and other trace and minor elements in sphalerite as a function of deposit type — A meta-analysis: Ore Geology Reviews, v. 76, p. 52–78.

Fu, M., Kwak, T. A. P., and Mernagh, T. P., 1993, Fluid inclusion studies of zoning in the Dachang tin-polymetallic ore field, People’s Republic of China: Economic Geology, v. 88, p. 283–300.

Gagnevin, D., Menuge, J. F., Kronz, A., Barrie, C., and Boyce, A. J., 2014, Minor Elements in Layered Sphalerite as a Record of Fluid Origin, Mixing, and Crystallization in the Navan Zn-Pb Ore Deposit, Ireland: Economic Geology, v. 109, p. 1513–1528.

George, L. L., Cook, N. J., Crowe, B. B. P., and Ciobanu, C. L., 2018, Trace elements in hydrothermal chalcopyrite: Mineralogical Magazine, v. 82, p. 59–88.

Gion, A. M., Piccoli, P. M., and Candela, P. A., 2018, Partitioning of indium between ferromagnesian minerals and a silicate melt: Chemical Geology, v. 500, p. 30–45.

Gowans, R., Jacobs, C., Anderson, D., Spooner, J., Mercer, W., Hains, D.H., Smith, R., 2018, The East Kemptville Tin Production and Site Remediation Project Preliminary Economic Assessment Nova Scotia, Canada. NI-43-101 Report, p. 1-277.

Halter, W. E., Williams-Jones, A. E., and Kontak, D. J., 1995, Origin and evolution of the greisenizing fluid at the East Kemptville tin deposit, Nova Scotia, Canada: Economic Geology, v. 93, p. 1026–1051.

Halter, W. E., Williams-Jones, A. E., and Kontak, D. J., 1996, The role of greisenization in cassiterite precipitation at the East Kemptville tin deposit, Nova Scotia: Economic Geology, v. 91, p. 368–385.

Halter, W. E., Williams-Jones, A. E., and Kontak, D. J., 1998, Modeling fluid–rock interaction during greisenization at the East Kemptville tin deposit: implications for mineralization: Chemical Geology, v. 150, p. 1–17.

Heinrich, C. A., 2007, Fluid-Fluid Interactions in Magmatic-Hydrothermal Ore Formation: Reviews in Mineralogy and Geochemistry, v. 65, p. 363–387.

Heinrich, C. A., and Ryan, C. G., 1992, Mineral paragenesis and regional zonation of granite-related Sn-As-Cu-Pb-Zn deposits: A chemical model for the Mole Granite district (Australia) based on PIXE fluid inclusion analyses In: Fluid-Rock Interaction. Kharaka YK, Maest AS (eds) Balkema, p. 1583–1587.

Hezarkhani, A., Williams-Jones, A. E., and Gammons, C. H., 1999, Factors controlling copper solubility and chalcopyrite deposition in the Sungun porphyry copper deposit, Iran: Mineralium Deposita, v. 34, p. 770–783.

Horne, R. J., MacDonald, M. A., Corey, M. C., and Ham, L. J., 1992, Structure and emplacement of the South Mountain Batholith, southwestern Nova Scotia: Atlantic Geology, v. 28, p. 29–50.

Horne, R. J., King, M. S., Kontak, D. J., O'Reilly, G. A., and Black, D., 2006, The Kemptville shear zone: Regional shear related to emplacement and mineralization.: In

Mines and Minerals Branch Report of Activities 2005. D.R. MacDonald (ed). Nova Scotia Department of Natural Resources, Report 2006-1, p. 19–37.

Huston, D. L., Sie, S. H., Suter, G. F., Cooke, D. R., and Booth, R. A., 1995, Trace Elements in Sulfide Minerals from Eastern Australian Volcanic-Hosted Massive Sulfide Deposits: Part 1. Proton Microprobe Analyses of Pyrite, Chalcopyrite, and Sphalerite, and Part 2. Selenium Levels in Pyrite: Comparison of 34 S values and Implications for the Source of Sulfur in Volcanogenic Hydrothermal Systems: Economic Geology, v. 90, p. 1167–1196.

Inverno, C. M. C., and Hutchinson, R. W., 2004, The endogranitic tin zone, Mount Pleasant, New Brunswick, Canada and its metallogenesis: Applied Earth Science, v. 113, p. 261–288.

Ishihara, S., Hoshino, K., Murakami, H., and Endo, Y., 2006, Resource Evaluation and Some Genetic Aspects of Indium in the Japanese Ore Deposits: Resource Geology, v. 56, p. 347–364.

Ishihara, S., Murakami, H., and Marquez-Zavalia, M. F., 2011, Inferred Indium Resources of the Bolivian Tin-Polymetallic Deposits: Indium resources in Bolivian deposits: Resource Geology, v. 61, p. 174–191.

Ishihara, S., Ishiyama, D., Sato, H., and Murakami, H., 2009, Indium contents of some sedimentary and igneous rocks in the In-mineralized areas in China, Japan and Bolivia (abs in English).: Shigen-Chishitsu, v. 59, p. 219–222.

Jiménez-Franco, A., Alfonso, P., Canet, C., and Trujillo, J. E., 2018, Mineral chemistry of In-bearing minerals in the Santa Fe mining district, Bolivia: Andean Geology, v. 45, p. 410–432.

Klekovkina, V.V., Gainov, R.R., Vagizov, F.G., Dooglav, A.V., Golovanevskiy, V.A., and Pen'kov, I.N., 2014, Oxidation and Magnetic States of Chalcopyrite $CuFeS_2$: A First Principles Calculation[1]: Optics and Spectroscopy, v. 116, p. 885–888.

Johan, Z., 1988, Indium and germanium in the structure of sphalerite: an example of coupled substitution with Copper: Mineralogy and Petrology, v. 39, p. 211–229.

John, T., 1983, Tin, East Kemptville, Yarmouth County, Nova Scotia. Geology and Ore Reserves Section from the East Kemptville Tin Project Feasibility Study, v.1, Property Report ME 1983-006, p. 1-79

Jonsson, E., Högdahl, K., Majka, J., and Lindeberg, T., 2013, Roquesite and Associated Indium-bearing sulfides from a Paleoproterozoic Carbonate-hosted Mineralization: Lindbom's Prospect, Bergslagen, Sweden.: The Canadian Mineralogist, v. 51, p. 629–641.

Jovic, S. M., Guido, D. M., Schalamuk, I. B., Ríos, F. J., Tassinari, C. C. G., and Recio, C., 2011a, Pingüino In-bearing polymetallic vein deposit, Deseado Massif, Patagonia, Argentina: characteristics of mineralization and ore-forming fluids: Mineralium Deposita, v. 46, p. 257–271.

Jovic, S. M., Guido, D. M., Melgarejo, J. C., Paez, G. N., Ruiz, R., and Schalamuk, I. B., 2011b, The Indium-Bearing Minerals of the Pingüino Polymetallic Vein System, Desado Massif, Patagonia, Argentina.: The Canadian Mineralogist, v. 49, p. 931–946.

Kase, K., 1987, Tin-Bearing Chalcopyrite from the Izumo Vein, Toyoha Mine, Hokkaido, Japan.: The Canadian Mineralogist, v. 25, p. 9–13.

Kiyosu, Y., 1973, Sulfur isotopic fractionation among sphalerite, galena and sulfide ions: Geochemical Journal, v. 7, p. 191–199.

Kontak, D. J., 1990a, A sulfur isotope study of main-stage tin and base metal mineralization at the East Kemptville tin deposit, Yarmouth County, Nova Scotia, Canada; evidence for magmatic origin of metals and sulfur: Economic Geology, v. 85, p. 399–407.

Kontak, D. J., 1990b, The East Kemptville Topaz-Muscovite Leucogranite, Nova Scotia 1. Geological Setting and Whole-Rock Geochemistry: The Canadian Mineralogist, v. 28, p. 787–825.

Kontak, D. J., 1993, 34 S enrichment in late-stage veins, East Kemptville tin and base metal deposit, Nova Scotia, Canada; evidence for late incursion of metasedimentary processed sulfur in a magmatic system: Economic Geology, v. 88, p. 203–207.

Kontak, D. J., 1994, Geological and Geochemical Studies of Alteration Processes in a Fluorine-Rich Environment: The East Kemptville Sn-(Zn-Cu-Ag) Deposit, Yarmouth County, Nova Scotia, Canada, In: Alteration and alteration processes associated with ore-forming systems.: Geological Association of Canada, p. 261–314.

Kontak, D. J., and Kyser, K., 2011, A fluid inclusion and isotopic study of an intrusion-related gold deposit (IRGD) setting in the 380 Ma South Mountain Batholith, Nova Scotia, Canada: evidence for multiple fluid reservoirs: Mineralium Deposita, v. 46, p. 337–363.

Kontak, D. J., and Smith, P. K., 1989, Sulphur isotopic composition of sulphides from the Beaver Dam and other Meguma-Group-hosted gold deposits, Nova Scotia: implications for genetic models: Canadian Journal of Earth Sciences, v. 26, p. 1617–1629.

Kontak, D. J., Farrar, E., McBride, S., and Martin, R. F., 1995, Mineral Chemistry and 40Ar/39Ar Dating of Muscovite from the East Kemptville Leucogranite, Southern Nova Scotia: Evidence for Localized Resetting of 40Ar/39Ar systematics in a Shear Zone: Canadian Mineralogist, v. 33, p. 1237–1253.

Kontak, D. J., Ansdell, K., Dostal, J., Halter, W. E., Martin, R., and Williams-Jones, A. E., 2001, The nature and origin of pegmatites in a Fluorine-rich leucogranite, East Kemptville Tin Deposit, Nova Scotia, Canada: Geochimica et Cosmochimica Acta, v. 46, p. 115.

Kontak, D. J., Horne, R. J., Creaser, R. A., Petrus, J. A., and Archibald, D., 2013, A petrological and geochronological study of a 360 Ma metallogenic event in Maritime Canada with implications for lithophile-metal mineralization in the Canadian Appalachians: Canadian Journal of Earth Sciences, v. 50, p. 1147–1163.

Kozdon, R., Kita, N. T., Huberty, J. M., Fournelle, J. H., Johnson, C. A., and Valley, J. W., 2010, In situ sulfur isotope analysis of sulfide minerals by SIMS: Precision and accuracy, with application to thermometry of ~3.5Ga Pilbara cherts: Chemical Geology, v. 275, p. 243–253.

Landtwing, M. R., Furrer, C., Redmond, P. B., Pettke, T., Guillong, M., and Heinrich, C. A., 2010, The Bingham Canyon Porphyry Cu-Mo-Au Deposit. III. Zoned Copper-Gold Ore Deposition by Magmatic Vapor Expansion: Economic Geology, v. 105, p. 91–118.

Lattanzi, P., Corazza, M., Corsini, F., and Tanelli, G., 1989, Sulfide mineralogy in the polymetallic cassiterite deposits of Dachang, P.R. China: Mineralium Deposita, v. 24, p. 141–147.

Li, R., Chen, H., Xia, X., Yang, Q., Li, L., Xu, J., Huang, C., and Danyushevsky, L. V., 2017, Ore fluid evolution in the giant Marcona Fe-(Cu) deposit, Perú: Evidence from in-situ sulfur isotope and trace element geochemistry of sulfides: Ore Geology Reviews, v. 86, p. 624–638.

Liu, S., Li, Y., Gong, H., Chen, C., Liu, J., and Shi, Y., 2016, First-principles calculations of sulphur isotope fractionation in MX2 minerals, with M= Fe, Co, Ni and X2= AsS, SbS: Chemical Geology, v. 441, p. 204–211.

Longerich, H. P., Jackson, S. E., and Gunther, D., 1996, Laser Ablation Inductively Coupled Plasma Mass Spectrometric Transient Signal Data Acquisition and Analyte Concentration Calculation*: Analytical Atomic Spectrometry, v. 11, p. 899–904.

Lopez, L., Jovic, S. M., Guido, D. M., Permuy Vidal, C., Páez, G. N., and Ruiz, R., 2015, Geochemical distribution and supergene behavior of indium at the Pingüino epithermal polymetallic vein system, Patagonia, Argentina: Ore Geology Reviews, v. 64, p. 747–755.

Menand, T., 2011, Physical controls and depth of emplacement of igneous bodies: A review: Tectonophysics, v. 500, p. 11–19.

Mikhlin, Y., Tomashevich, Y., Tauson, V., Vyalikh, D., Molodtsov, S., and Szargan, R., 2005, A comparative X-ray absorption near-edge structure study of bornite, Cu5FeS4, and chalcopyrite, CuFeS2: Journal of Electron Spectroscopy and Related Phenomena, v. 142, p. 83–88.

Mizuta, T., 1988, Compositional Homogenization of Sphalerite in Hydrothermal Ore Deposits of Japan by Post-depositional Diffusion Processes: With Particular Reference to Metamorphosed Besshi-type Deposits: Mining Geology, v. 38, p. 263–278.

Murakami, H., and Ishihara, S., 2013, Trace elements of Indium-bearing sphalerite from tin-polymetallic deposits in Bolivia, China and Japan: A femto-second LA-ICPMS study: Ore Geology Reviews, v. 53, p. 223–243.

Nakamura, Y., and Shima, H., 1982, Fe and Zn partitioning between sphalerite and stannite (abstr.): Joint Meeting of Soc. Mining Geol. Japan, Assoc. Miner. Petr. Econ. Geol., and Miner. Soc. Japan, A-8.

Nekrasov, I. J., Sorokin, V. I., and Osadchii, E. G., 1979, Fe and Zn partitioning between stannite and sphalerite and its application in geothermometry. In: Origin and Distribution of the Elements.: Physics and chemistry of the Earth, v. 34, p. 739–742.

Ohmoto, H., and Goldhaber, M. B., 1997, Sulfur and carbon isotopes.: In: Barnes, H.L. (Ed.), Geochemistry of Hydrothermal Ore Deposits, New York, Wiley, p. 517–611

Ohmoto, H., and Rye, R. O., 1979, Isotopes of sulfur and Carbon.: In: Barnes, H.L. (Ed.), Geochemistry of Hydrothermal Ore Deposits, New York, Wiley, p. 509–567

Ohta, E., 1989, Occurrence and Chemistry of Indium-containing Minerals from the Toyoha Mine, Hokkaido, Japan: Mining Geology, v. 39, p. 355–372.

Ohta, E., 1991, Polymetallic Mineralization at the Toyoha Mine, Hokkaido, Japan: Mining Geology, v. 41, p. 279–295.

Ohta, E., 1995, Common features and genesis of tin-polymetallic veins, in Proceedings of the Sapporo International Conference on “Mineral Resource of the NW Pacific Rim”: Resource Geology Special Issue, p. 187–195.

Paton, C., Hellstrom, J., Paul, B., Woodhead, J., and Hergt, J., 2011, Iolite: Freeware for the visualisation and processing of mass spectrometric data: Journal of Analytical Atomic Spectrometry, v. 26, p. 2508.

Pattrick, R. A. D., Dorling, M., and Polya, D.A., 1993, TEM study of Indium- and Copper-bearing Growth-Banded Sphalerite: The Canadian Mineralogist, v. 31, p. 105–117.

Pavlova, G. G., Palessky, S. V., Borisenko, A. S., Vladimirov, A. G., Seifert, Th., and Phan, L. A., 2015, Indium in cassiterite and ores of tin deposits: Ore Geology Reviews, v. 66, p. 99–113.

Pearce, C. I., Pattrick, R. A. D., Vaughan, D. J., Henderson, C. M. B., and van der Laan, G., 2006, Copper oxidation state in chalcopyrite: Mixed Cu d9 and d10 characteristics: Geochimica et Cosmochimica Acta, v. 70, p. 4635–4642.

Pfaff, K., Koenig, A., Wenzel, T., Ridley, I., Hildebrandt, L. H., Leach, D. L., and Markl, G., 2011, Trace and minor element variations and sulfur isotopes in crystalline and colloform ZnS: Incorporation mechanisms and implications for their genesis: Chemical Geology, v. 286, p. 118–134.

Pitre, C. V., and Richardson, J. M., 1989, Paragenesis of veins of the Duck Pond tin prospect, Meguma Group, East Kemptville, Nova Scotia: Canadian Journal of Earth Sciences, v. 26, p. 2032–2043.

Reich, M., Deditius, A., Chryssoulis, S., Li, J.-W., Ma, C.-Q., Parada, M. A., Barra, F., and Mittermayr, F., 2013, Pyrite as a record of hydrothermal fluid evolution in a porphyry copper system: A SIMS/EMPA trace element study: Geochimica et Cosmochimica Acta, v. 104, p. 42–62.

Richardson, J., 1988, Genesis of the East Kemptville Greisen-hosted tin deposit, Davis Lake (PhD Dissertation): Carleton University, Ottawa, Ontario, Canada.

Richardson, J. M., Roberts, C.M., Grice, J.D., Ramik, R.A., 1988, Mcauslanite, a Supergene Hydrated Iron Aluminum Fluorophosphate from the East Kemptville Mine, Yarmouth County. Nova Scotia.: The Canadian Mineralogist, v. 26, p. 917–921.

Richardson, J. M., Blenkinsop, J., and Bell, K., 1990, Extreme variations in strontium initial ratios in ore-related fluids: Fluorite and phosphate minerals from the greisen-style East Kemptville tin mine, Nova Scotia, Canada: Contributions to Mineralogy and Petrology, v. 104, p. 516–529.

Rottier, B., Kouzmanov, K., Wälle, M., Bendezú, R., and Fontboté, L., 2016, Sulfide Replacement Processes Revealed by Textural and LA-ICP-MS Trace Element Analyses: Example from the Early Mineralization Stages at Cerro de Pasco, Peru: Economic Geology, v. 111, p. 1347–1367.

Schwarz-Schampera, U., and Herzig, P. M., 2002, Indium: geology, mineralogy, and economics: Berlin, Springer-Verlag, p. 1–257.

Seal, R. R., 2006, Sulfur Isotope Geochemistry of Sulfide Minerals: Reviews in Mineralogy and Geochemistry, v. 61, p. 633–677.

Sedge, C., Hanley, D. J., Kontak, D. D., and Mercer, D. B., 2015, Characterizing the mineral domains of Li-(Rb-Cs) enrichment at the East Kemptville Sn-(Cu-Zn-Ag) deposit, southwestern Nova Scotia: Knowledge Transfer Report to Avalon Rare Metal Inc., Saint Mary's University, Halifax, Nova Scotia, p. 1–34.

Seifert, T., and Sandmann, D., 2006, Mineralogy and geochemistry of indium-bearing polymetallic vein-type deposits: Implications for host minerals from the Freiberg district, Eastern Erzgebirge, Germany: Ore Geology Reviews, v. 28, p. 1–31.

Shimizu, M., and Kato, A., 1991, Roquesite-Bearing Tin Ores from the Omodani, Akenobe, Fukoku, and Ikuno Polymetallic Vein-type Deposits in the Inner Zone of Southwestern Japan: The Canadian Mineralogist, v. 29, p. 207–215.

Shimizu, M., and Shikazono, N., 1985, Iron and zinc partitioning between coexisting stannite and sphalerite: a possible indicator of temperature and sulfur fugacity: Mineralium Deposita, v. 20, p. 314–320.

Shimizu, M., Kato, A., Shiozawa, T., 1986, Sakuraiite: Chemical Composition and Extent of (Zn, Fe)In-For-CuSn Substitution: Canadian Mineralogist, v. 24, p. 405–409.

Shimizu, T., and Morishita, Y., 2012, Petrography, Chemistry, and Near-Infrared Microthermometry of Indium-Bearing Sphalerite from the Toyoha Polymetallic Deposit, Japan.: Economic Geology, v. 107, p. 723–735.

Poulson, S.R., Kubilius, W.P., and Ohmoto H., 1991, Geochemical behavior of sulfur in granitoids during intrusion of the South Mountain batholith, Nova Scotia, Canada: Geochimica et Cosmochimica Acta, v. 55, p. 3809–3830.

Sangster, A.L., 1992, Light stable-isotope evidence for a metamorphic origin for bedding-parallel, gold bearing veins in Cambrian flysch, Meguma Group, Nova Scotia. Exploration and Mining Geology, v. 1, pg. 69–79

Sinclair, W. D., Kooiman, G. J. A., Martin, D. A., and Kjarsgaard, I. M., 2006, Geology, geochemistry and mineralogy of indium resources at Mount Pleasant, New Brunswick, Canada: Ore Geology Reviews, v. 28, p. 123–145.

Stanley, C., and Willson, J., 2016, Recent investigations at the East Kemptville Sn deposit: Identifying lithologies, understanding hydrothermal alteration, constraining controls on mineralization, and estimating bulk densities using lithogeochemical data: AGS Colloqium-2016, Truro, Nova Scotia.

Tanner, D., Henley, R. W., Mavrogenes, J. A., and Holden, P., 2016, Sulfur isotope and trace element systematics of zoned pyrite crystals from the El Indio Au–Cu–Ag deposit, Chile: Contributions to Mineralogy and Petrology, v. 171, p. 1–17.

Todd, E. C., Sherman, D. M., and Purton, J. A., 2003, Surface oxidation of chalcopyrite (CuFeS2) under ambient atmospheric and aqueous (pH 2-10) conditions: Cu, Fe L- and O K-edge X-ray spectroscopy: Geochimica et Cosmochimica Acta, v. 67, p. 2137–2146.

Tsushima, N., Matsueda, H., and Ishihara, S., 1999, Polymetallic Mineralization at the Nakakoshi Copper Deposits, Central Hokkaido, Japan: Resource Geology, v. 49, p. 89–97.

Valkama, M., Sundblad, K., Nygård, R., and Cook, N., 2016, Mineralogy and geochemistry of indium-bearing polymetallic veins in the Sarvlaxviken area, Lovisa, Finland: Ore Geology Reviews, v. 75, p. 206–219.

Werner, T. T., Mudd, G. M., and Jowitt, S. M., 2017, The world's by-product and critical metal resources part III: A global assessment of indium: Ore Geology Reviews, v. 86, p. 939–956.

Wilson, S.A., Ridley, W.I., and Koenig, A.E, 2002, Development of sulfide calibration standards for the laser ablation: Journal of Analytical Atomic Spectrometry, v. 17, p. 406-409.

Xu, B., Jiang, S.-Y., Wang, R., Ma, L., Zhao, K., and Yan, X., 2015, Late Cretaceous granites from the giant Dulong Sn-polymetallic ore district in Yunnan Province, South China: Geochronology, geochemistry, mineral chemistry and Nd–Hf isotopic compositions: Lithos, v. 218–219, p. 54–72.

Vita Auctoris

Jason Willson was born in Alberta, Canada in 1989. He graduated from Acadia University in 2013, where he obtained a B.Sc. in Geology with Honours. After graduating, he moved to Grande Prairie, Alberta and worked in the energy sector. From there, he came to Windsor, where he started his M.Sc. degree at the University of Windsor. He has successfully defended his dissertation and will graduate at the Fall 2019 convocation.